# UNIVERSITY OF SOUTHAMPTON

FACULTY OF NATURAL AND ENVIRONMENTAL SCIENCES

Ocean and Earth Science,

National Oceanography Centre, University of Southampton

## Mean Transport and variability in the subpolar North Atlantic

by

Elizabeth Anne Comer

**Thesis for the degree of Master of Philosophy**

**August 2019**

UNIVERSITY OF SOUTHAMPTON

ABSTRACT

FACULTY OF NATURAL AND ENVIRONMENTAL SCIENCES

Ocean and Earth Sciences

Master of Philosophy

# MEAN TRANSPORT AND VARIABILITY IN THE SUBPOLAR NORTH ATLANTIC

by Elizabeth Anne Comer

The Atlantic Meridional Overturning Circulation (AMOC) plays an important role in the Earth's heat and carbon budgets and sets the properties of the global water masses. Deep water formed in high latitudes, travel southwards as part of the AMOC's lower limb and have properties that can be traced globally. As the AMOC's upper limb transports warm water northwards it releases heat to the atmosphere, contributing to the moderate climate of Western Europe and impacts all aspects of high latitudinal climate. In the northern North Atlantic there is a lack of long-term transoceanic measurements, enabling estimates of the AMOC's transport variability. For this reason, it is essential that quantification of the AMOC's mean transports in the subpolar region are as accurate as possible. Furthermore, the possibility of quantifying the AMOC's variability in this region could improve our understanding of the AMOC's driving mechanisms.

The Extended Ellett Line (EEL) is a repeat hydrographic section located between Iceland and Scotland and is the focus area for this study. This section captures 90% of the water flowing northwards into the Nordic Seas and half the returning dense water; two key parts of the AMOC. Data has been collected near-annually at the EEL since 1996, providing two decades of hydrographic and direct velocity measurements. The first objective of this study is to quantify the long-term averages of the currents that shape the AMOC across the EEL, using direct velocity measurements. Improved estimates of the long-term (1997-2015) mean absolute velocity field and volume, temperature and freshwater transports are presented. Analysis of the time-mean velocity field contributes to knowledge of the location and variability of the currents transporting water northwards. There is evidence that a branch of the North Atlantic Current is located at the Rockall-Hatton Plateau (RHP). The net transport at the EEL is 3.5 ± 0.9 Sv, of which there is 5.9 ± 1.4 Sv in the upper ocean and -3.3 ± 0.7 Sv in the overflow water. There is a temperature transport of 0.22 ± 0.04 PW, dominated by the transport strength, and a freshwater transport of 44.1 ± 8.8 mSv southwards. The slope current and RHP are identified as key routes for the transport of heat northwards.

The second objective of this study is to assess the spatial resolution of the EEL over the slope current North of Scotland. Comparisons of the EEL spatial resolution with altimetry and the OSNAP array, shows that the slope current is better resolved in the former. The altimeters do represent the large-scale circulation pattern at the EEL, but they do not capture the narrow slope current. The OSNAP array does not have a high enough spatial resolution to resolve the key heat pathway of the slope current. This study shows the necessity of a higher sampling spatial resolution in this location.

# Table of Contents

# List of Tables

# List of Figures

UNIVERSITY OF Southampton

# Research Thesis: Declaration of Authorship

| | |
|---|---|
| Print name: | |

| | |
|---|---|
| Title of thesis: | |

I declare that this thesis and the work presented in it is my own and has been generated by me as the result of my own original research.

I confirm that:

1. This work was done wholly or mainly while in candidature for a research degree at this University;
2. Where any part of this thesis has previously been submitted for a degree or any other qualification at this University or any other institution, this has been clearly stated;
3. Where I have consulted the published work of others, this is always clearly attributed;
4. Where I have quoted from the work of others, the source is always given. With the exception of such quotations, this thesis is entirely my own work;
5. I have acknowledged all main sources of help;
6. Where the thesis is based on work done by myself jointly with others, I have made clear exactly what was done by others and what I have contributed myself;
7. Either none of this work has been published before submission, or parts of this work have been published as: [please list references below]:

_____

_____

_____

| | | | |
|---|---|---|---|
| Signature: | | Date: | |

# Acknowledgements

I have completed this thesis under the supervision of Dr Penny Holliday, Prof Sheldon Bacon, Dr Ivan Haigh and Prof Stuart Cunningham (The Scottish Association for Marine Science). I would also like to acknowledge my panel chair Dr Eleanor Frajka-Williams. I am grateful for the opportunity to have been part of the 2016 Extended Ellett Line scientific team, onboard RRS Discovery. I thoroughly enjoyed this experience and feel the skills I gained will be invaluable in the future. I have appreciated the chance to attend conferences and summer schools, where I was able to build relationships and discuss my research. I found that demonstrating in undergraduate classes was something that benefitted me greatly. I loved seeing the pupils develop their knowledge. I would like to thank Dr Simon Boxall and Mr John Davis for giving me this opportunity. I have been based at The Scottish Association for Marine Science for the last year and I am grateful for all the support they have provided. I have enjoyed the Physics coffee mornings, which provided a relaxed environment to ask questions and chat about marine physics over a biscuit and coffee.

I would especially like to thank my friends and family for their continued support and help proofreading my work. They have always listened and been there for me throughout hardships and difficult decisions during my research.

# 1 Introduction

## 1.1 Background

The Atlantic Meridional Overturning Circulation (AMOC) transports heat and freshwater, playing an important role in the Earth's climate system and its variability (Buckley and Marshall, 2016). A key region for the AMOC is the subpolar North Atlantic (SPNA), because it is modified along its path by mixing and water mass transformation. In this region, the AMOC is characterised by northward heat advection in its upper limb, which is released to the atmosphere impacting the climate of western Europe. The heat transport northward is also connected to mass loss from the Greenland Ice Sheet (Straneo *et al.*, 2010) and the loss of Arctic Sea Ice cover (Serreze, Holland and Stroeve, 2007). Changes in the strength of the AMOC are believed to influence the SPNA heat content and sea surface temperature, which impacts: the rainfall over the African Sahel, Amazon, western Europe and parts of the United States; Atlantic hurricane activity; and the climate in Europe and North America (Sutton and Hodson, 2005; Knight, Folland and Scaife, 2006; Zhang and Delworth, 2006; Smith *et al.*, 2010; Dunstone, Smith and Eade, 2011; Duchez *et al.*, 2016).

The North Atlantic acts as a large sink for atmospheric $CO_2$ (Khatiwala *et al.*, 2013) and plays a pivotal role in the uptake of anthropogenic $CO_2$ (Sabine *et al.*, 2004; Halloran *et al.*, 2015; Li *et al.*, 2016). North of 50°N, because of the high rates of heat loss, the North Atlantic sink accounts for nearly 20% of annual mean global air–sea $CO_2$ flux. The AMOC not only plays a role in creating this sink for anthropogenic $CO_2$ (Pérez *et al.*, 2013) but transports it northwards from the subpolar gyre (Rosón, 2003). Furthermore, the AMOC can enhance primary productivity through the transport of nutrients (Palter and Lozier, 2008). Thus, the AMOC plays an important part in driving the carbon cycle as primary production is a key mechanism in removing atmospheric $CO_2$ (Körtzinger *et al.*, 2008).

The local overturning is of great interest, not only for its role in heat and carbon budgets but because it is considered to set the properties of the global water masses. Deep water formed in the high latitudes of the North Atlantic and Nordic Seas have signatures that can be traced globally, making these areas of high interest scientifically (Lazier, Pickart and Rhines, 2001). It is therefore important that estimates of the AMOC'S mean transport in these regions are as accurate as possible and that its variability can be established. This will lead to an improved mechanistic understanding of the processes that control the AMOC and its variability.

The full-depth time-mean absolute velocity field that spans two decades, and associated transports, has not yet been quantified in the Eastern SPNA (ESPNA). The Extended Ellett Line (EEL) is a hydrographic line, in the ESPNA, and its data will be used in this study. The section runs between Iceland and Scotland, across the northern boundaries of Rockall Trough, Rockall-Hatton Plateau and Iceland Basin. Along the EEL, there are two regions where transport of the warmest water into the Nordic Seas takes place, the Rockall-Hatton Plateau and the Scottish shelf edge. These are conceivably key regions for heat transport northwards, showing the necessity for accurate quantification. These knowledge gaps, and others, are explained fully in Chapter 2.

## 1.2 Thesis aims

The overall aim of this thesis is to investigate the subpolar North AMOC mean circulation, volume, heat and freshwater transport, at the EEL. A secondary aim is to assess the spatial resolution of the EEL over the slope current North of Scotland. This study uses a variety of observational data (hydrographic, direct velocity and Sea Surface Height (SSH)) from a period of 1997 to 2015. The specific objectives are:

(a) to evaluate the time-mean velocity field and its variability using direct velocity measurements;

(b) compute the time-mean geostrophic velocity field referenced with direct velocity data and compute the net volume transport;

(c) compute the time-mean net temperature and freshwater transport across the EEL.

(d) to determine whether the altimetry data can be used as a reference velocity at the EEL.

The structure of the thesis is as follows: Chapter 2 provides a review of the current literature and highlights the knowledge gaps; Chapter 3 and Chapter 0 details all the data types and methods that are used in this study; Chapter 5 shows the results of the above objectives; Chapter 6 discusses these results; and Chapter 7 concludes the findings of this study and shows how it could be developed.

# 2 Literature Review

A large reservoir of warm salty water in the upper ocean is transported northward in the ESPNA losing its heat to the atmosphere, which either enters the Nordic Seas or re-circulates and becomes North Atlantic Deep Water in the Labrador Sea. The energy that is lost to the atmosphere from the upper limb of the AMOC as it travels northwards has a large impact on the western European climate as well as all aspects of high latitude climate. In the Nordic Seas these upper waters go through intense cooling, producing a deep dense layer that becomes part of the AMOC lower limb traveling southward. Section 2.1 describes the currents that make up the AMOC in the SPNA and discusses the AMOC's long-term mean volume, heat and freshwater transport. The European Slope Current (ESC) and Rockall-Hatton Plateau (RHP) are highlighted as key regions along the EEL, which is explained in Section 2.2. Section 2.3 details the current research at the EEL, stressing the importance of the hydrographic section in the North Atlantic.

## 2.1 ESPNA circulation and transport

The subpolar gyre is strongly controlled by topography. The Reykjanes Ridge separates the eastern and western subpolar gyre, and in the eastern North Atlantic the topography further splits the region into several basins: Rockall Trough, RHP and Iceland Basin. Overflow waters formed in the Nordic Sea circulate cyclonically around the Irminger Basin into the Labrador Sea, where they are either transported southward from the subpolar gyre in the deep western boundary current, or re-circulated within the subpolar gyre (Bower *et al.*, 2002, 2009; Käse, 2003).

The North Atlantic Current (NAC) is shown by the red arrows heading north-eastwards across the Mid-Atlantic Ridge (MAR) in Figure 2.1. It is the dominant flow of water within the region and is thought to travel through Iceland Basin as a series of eddies and intense jets, as well as flowing through Rockall Trough (Holliday and Cunningham, 2013). The NAC and Irminger Current transport 40% of upper ocean water into the Nordic Sea, between Greenland and Scotland, with the rest recirculating in the SPG (Sarafanov *et al.*, 2012). A large proportion (~90%) of this Atlantic inflow takes place between Iceland and Scotland (Hansen *et al.*, 2003; Jónsson and Briem, 2003; Turrell *et al.*, 2003). Dense water formation in the Nordic Sea produces 6-7 Sv that flows southward as overflow water, with nearly half (~3 Sv) traveling over the Iceland-Scotland

Ridge - known as the Iceland Scotland Overflow Water (ISOW in Figure 2.1; Hansen and Østerhus, 2000; Sarafanov *et al.*, 2012). The other half flows between Denmark and Iceland as the Denmark Strait Overflow Water (DSOW in Figure 2.1).

The NAC flows north-eastward, on the southern side of the subpolar gyre, in three branches, from east to west: the Rockall Trough branch, which is warmest and most saline, the subpolar front (SPF) branch and the central Iceland Basin branch. The Irminger Current is also part of the north-eastern currents flowing from the Reykjanes Ridge (Fratantoni, 2001; Flatau, Talley and Niiler, 2003; Reverdin, 2003; Pollard, 2004). The central Iceland Basin branch carries water cyclonically around Iceland Basin, connecting to the Irminger Current (Brambilla and Talley, 2008). This circulation is depicted in Figure 2.1.

Between Iceland and Scotland, the location of the EEL, these currents transport several water masses. The Upper Ocean Water (UOW) is located above the thermocline (500-1000 dbar) and has warm (~10 °C), salty water (~35.3) characteristics (Pollard, 2004; Brambilla and Talley, 2008). This layer flows north-eastward towards the Nordic Seas, whilst the Labrador Sea Water (LSW) recirculates cyclonically at intermediate depths in both Iceland Basin and Rockall Trough, due to the shoaling topography (Holliday *et al.*, 2000; Lankhorst and Zenk, 2006). Dense water formation in the Nordic Sea supplies the overflow water, which flows at depth along the Reykjanes Ridge in Iceland Basin (Saunders, 1996; Read, 2001). Wyville-Thomson Ridge Overflow Water flows southward in the intermediate water masses with densities >27.70 kg $m^{-3}$ and has been detected in western Rockall Trough (Johnson *et al.*, 2010).

Over the last couple of decades, a variety of methods have been used to measure direct velocity in the North Atlantic. For example, Vessel-Mounted Acoustic Doppler Current Profiler (ADCP) data is one form of direct velocity measurement (Bacon 1997; Cokelet *et al.* 1996; Osinski *et al*. 2003; Rossby & Flagg 2012; Childers *et al.* 2014), along with ADCP's mounted on moorings (Hansen *et al*. 2003; Hughes *et al.* 2006), subsurface float data (Bower *et al.*, 2002; Lavender, Brechner Owens and Davis, 2005; Willis and Fu, 2008) and Lowered-Acoustic Doppler Current Profiler (LADCP, Hall *et al.* 2013). Some of these studies use direct velocity measurements, providing a level of known motion, to gain a more accurate estimate of ocean transport, as there can be no 'level of no motion' within the water column. Also, by referencing geostrophic velocity shear to the bottom or surface only, many features, such as top-to-bottom velocities and barotropic recirculation, would be missed (Donohue, Firing and Chen, 2001). The transport estimates of mean full-depth circulation and Atlantic inflow that do exist along sections north of the EEL, in the ESPNA, include measurements of modified Atlantic inflow and are sampled over

a time of less than one decade (Hansen *et al.*, 2003; Hughes *et al.*, 2006; Rossby and Flagg, 2012; Childers, Flagg and Rossby, 2014). The only exception being Holliday et al. 2015 that quantifies the net transport across the EEL to be 1.4 ± 5.8 Sv using a level of no motion.

A source of velocity used to reference the geostrophic velocity field at the surface is derived from altimeter sea surface height measurements. Altimetry provides a global coverage and collects measurements frequently, enabling high spatial and temporal sampling. In the ESPNA, the mean AMOC at 59.5°N has been estimated when combining altimetric derived velocities and hydrographic measurements (Sarafanov *et al.*, 2012). Both Chafik, Rossby and Schrum, (2014) and Rossby *et al.*, (2017) find that the altimetric sea surface height agrees well overall with the geostrophically determined sea-level difference from the SADCP data in the ESPNA. However, the fine structure around irregular topography is not necessarily resolved.

A recent study by Lozier *et al.*, (2019) highlights the importance of the ESPNA region within the overturning circulation. It shows water transformations that take place in this region are largely responsible for the overturning circulation and its variability. The previous view was that variations in the overturning circulation were dominated by the changes in deep water formation in the Labrador Sea. The recent transoceanic observing system used in this study crosses the SPNA, the OSNAP array, provides mean MOC estimates between 2014-2016. At OSNAP East (Greenland to Scotland) the mean MOC was 8.2 ± 0.6 Sv in depth space (15.6 ± 0.8 Sv in density space; Lozier *et al.*, (2019)). The array uses gliders, ARGO and RAFOS floats, and moored instruments to measure temperature, salinity and velocity. These measurements have a low spatial resolution, with moorings located at the basin boundaries and at key locations for dynamic height measurements (Lozier *et al.*, 2017).

Hansen and Østerhus (2000b) combine previous work to show that there is a long-term mean of 0.25 PW temperature transport between Iceland and the Shetlands (their Figure 7). In the same location, but for a later time period, there has been a consistent estimate of ~0.25 PW (Hansen *et al.*, 2003; Turrell *et al.*, 2003; Rossby *et al.*, 2018). Similarly, a study by (Østerhus *et al.*, 2005) estimates a temperature transport from mooring data of 0.29 PW (their Table 1). As previously stated, all these estimates include modified Atlantic water and are located north of the EEL. The heat flux between Greenland and Shetland has an estimated 0.26 PW (Rossby *et al.*, 2018), indicating that heat transport across the EEL and into the Nordic Seas could account for roughly 90% of this value. At the OSNAP array and OVIDE line between Greenland and Scotland greater temperature transports were estimated, 0.38 ± 0.02 and 0.51 ± 0.06 PW respectively (Mercier *et al.*, 2015; Lozier *et al.*, 2019).

## 2.2 European Slope Current and Rockall-Hatton Plateau

Along with the NAC, the relatively warm ESC transports Atlantic waters poleward. The ESC is in eastern Rockall Trough and flows along the Scottish shelf edge, as shown in Figure 2.2. This current is largely comprised of waters from the ESPNA and is influenced by waters from more southern latitudes that advect with the slope current (Marsh *et al.*, 2017). This southern influence means that the ESC carries the warmest and most saline waters across the EEL, providing the main source of saline and warm Atlantic waters to the Arctic.

The ESC is driven by the along-shelf poleward decline of dynamic height. The poleward decline in dynamic height is produced by the oceanic density gradient and wind stress (Huthnance and Huthnance, 1984). These forcing mechanisms are depicted in Figure 2.3, which show the density gradients, wind forcing, Ekman transports, and sea surface slopes related to a weak or strong slope current transport. The forcings change with a strong or weak SPG and a positive or negative NAO phase. A positive NAO phase and strong SPG leads to a strong transport, and the opposite takes place with a weak transport. During strong slope current transport, colder water in the North deep ocean means there is a stronger northward density gradient and the sea surface slope steepens; there is strengthened along-shore winds and increased Ekman transport towards the shore, that combined with the density gradient leads to eastward geostrophic flow; steepening of the North cross-slope gradient in SSH is more pronounced when compared to inflow given to the barotropic slope current (Marsh *et al.*, 2017).

The ESC transports 3.0 ± 2.1 Sv, as reported by Holliday *et al.* (2000), although previous measurements estimated 0.5-1.5 Sv. A study by Holliday *et al.* (2015) shows that it has a strong mean geostrophic velocity of 0.08 - 0.10 m $s^{-1}$. Throughout the literature, Rockall Trough is estimated to have a volume transport between 2.7 - 3.7 Sv, with a high level of interannual variability. The transport through Rockall Trough is thought to be masked by mesoscale eddies and seamount recirculation (Ellett, Edwards and Bowers, 1986; Holliday *et al.*, 2000). *Xu et al.* (2015) finds a long-term decreasing trend of ~1% over a 20-year period, with a peak poleward flow in 1995-1997. Reductions in the gradient in the 1990's, hence the ESC strength, are primarily due to warming in this region. The warming, with an increase in density, is coincident with weakening of the gyre (Marsh *et al.*, 2017). The study mentioned also finds evidence of reversal in more recent years with a strengthened Atlantic inflow.

Measurements from the OSNAP array between 2014-2016 show no significant transport at the ESC (Lozier *et al.*, 2019). Moorings in the Rockall trough are located at the basin boundaries and one at depth at the ISOW (Lozier *et al.*, 2017). This lower spatial resolution, in relation to the EEL, may affect how well the currents are resolved. The ESC is likely to be an important heat pathway, which needs to be resolved. A single mooring at the ESC location in the OSNAP array may not be able to do this.

The RHP is characterised by shallow and irregular topography, with Hatton Bank on the west side and Rockall Bank on the east. Two of the North Atlantic Current (NAC) branches are located here (Subpolar Front and Rockall Jet), which are bathymetrically steered, and their transport accounts for 43% of the total NAC transport (Houpert *et al.*, 2018). This basin is a key region for property extremes because it is the location where the SPF shifts (Holliday *et al.*, 2015). Thus, it is important for these NAC branches to be correctly resolved when estimating transport to accurately quantify the region's Atlantic inflow variability.

## 2.3 Extended Ellett Line

The Ellett Line hydrographic timeseries was established by David Ellett in 1975 and ran across the Rockall Trough over the Anton Dohrn Seamount. Repeated measurements have been made across this section since 1975, which has provided scientists with a high quality physical timeseries and is one of a small number in the North Atlantic. In 1996 the line was extended to Iceland, crossing the Iceland Basin, and has been occupied since that time by the Scottish Association for Marine Science and the National Oceanography Centre (Holliday and Cunningham, 2013). This is the EEL (Figure 2.4) and it completes the measurement of warm salty water flowing north-eastward into the Nordic Sea, from the North Atlantic extension in the subpolar gyre (Pollard, 2004; Brambilla and Talley, 2008). Cold water from the Nordic Sea flows over the sills between Iceland and Greenland, as well as Iceland and Scotland, forming deep overflow water returning to the Atlantic. The EEL measures half of this overflow water located between Iceland and Scotland. This timeseries has become one of the rare multi-decadal timeseries which is still on-going (Holliday and Cunningham, 2013).

The annual cruises along the Ellett Line and the EEL have allowed for many new discoveries. In 1978, Ellett found several signature water masses in the Rockall Trough, one of which being a deep-water mass (900-1400 m) that originated in the Gulf of Gibraltar and is now called

Mediterranean Outflow Water (Ellett, 1978). Another is the LSW that was detected at 1800m. LSW, also, flows through the Iceland Basin northward along with the main inflow of the two fronts from the North Atlantic Current (Pollard, 2004). Early hydrographic data was analysed by Ellett and Martin, (1973), and the erosion of bottom sediments on Feni Ridge from vigorous bottom-current activity by Howe, Stoker and Woolfe (2001), resulted in the suggestion of southward overflow water from the Nordic Seas to be present in Rockall Trough. It has been established that a southward overflow from the Wyville-Thompson Ridge can be detected in West Rockall Trough in certain years, and that this overflow can also be present on RHP (Johnson *et al.*, 2010). Although, this has been observed, there is currently no accurate transport quantification of the overflow across Wyville-Thompson Ridge and RHP.

## 2.4 Summary

Atlantic inflow into the Nordic Sea has been estimated at the Greenland-Scotland Ridge. However, these sections include modified Atlantic waters and are sampled over a time period of less than one decade. Mean transport estimates at the EEL either do not include a level of known motion within its calculation or are averaged over a much shorter time span. Consequently, there is no quantification of the full-depth time-mean absolute velocity field, and associated transports, that spans two decades in this region. The ESC and RHP, at the EEL, are likely to be key regions for heat transport into the Nordic Sea and need to be accurately quantified. Particularly the ESC may not be well resolved in the recent transport estimates. Therefore, the overall aim of this study is to investigate the subpolar North AMOC mean circulation, volume, heat and freshwater transport, at the EEL. A secondary aim is to assess the spatial resolution of the EEL over the slope current North of Scotland.

## 2.5 Figures

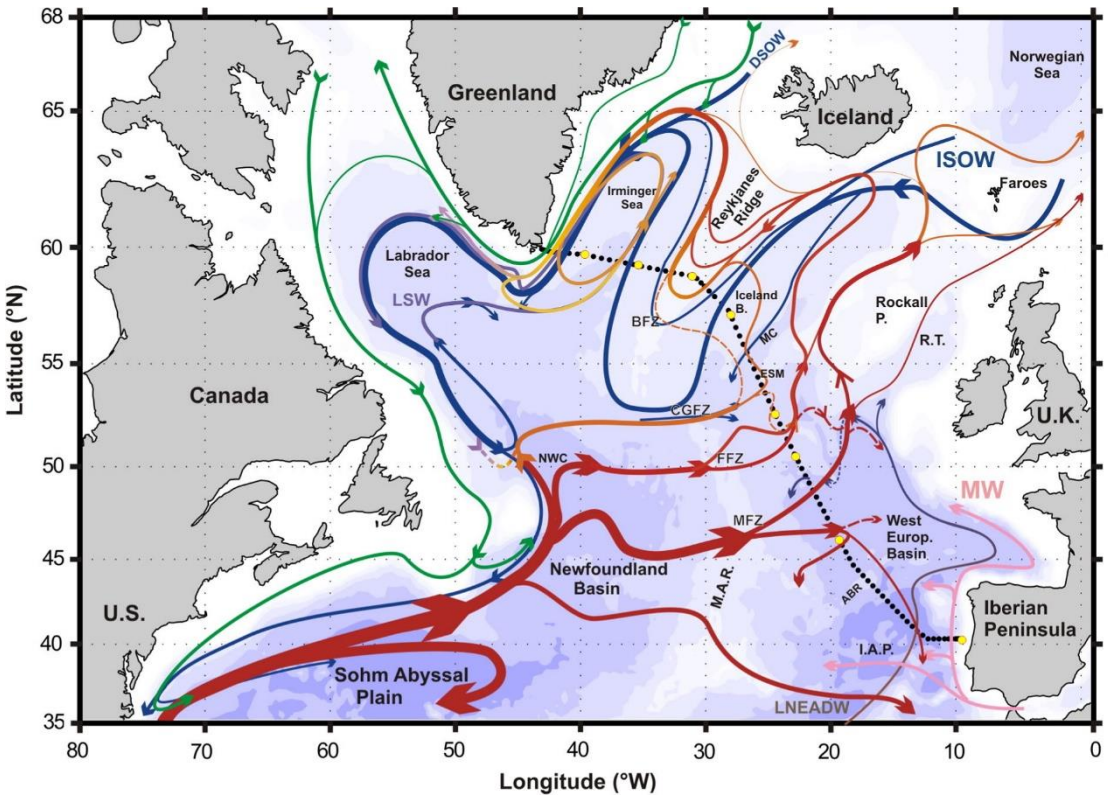


**Figure 2.1:** North Atlantic large-scale circulation schematic including the NAC branches and overflows. The labels are the main topographical features (black text) and water masses (coloured text) where: ABR: Azores-Biscay Rise, Bight Fracture Zone (BFZ), Charlie–Gibbs Fracture Zone (CGFZ), Faraday Fracture Zone (FFZ), Maxwell Fracture Zone (MFZ), Mid-Atlantic Ridge (M.A.R.), Iberian Abyssal Plain (I.A.P.), Northwest Corner (NWC), Rockall Trough (RT), Rockall Plateau (Rockall P.) and Maury Channel (MC), Denmark Strait Overflow Water (DSOW), Iceland–Scotland Overflow Water (ISOW), Labrador Sea Water (LSW), Mediterranean Water (MW), and Lower North East Atlantic Deep Water (LNEADW). The bathymetry is indicated by colour and the colour changes represent 100 m, 1000 m and every 1000 m below 1000 m (Daniault *et al.*, 2016).

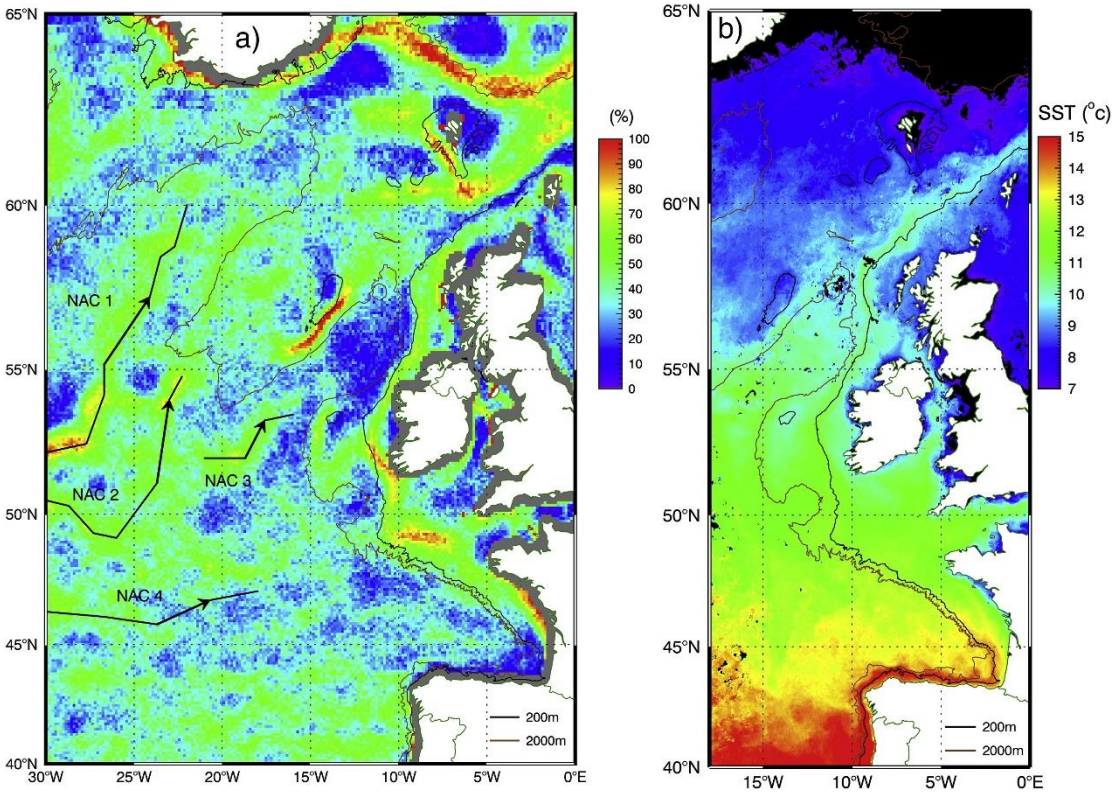


**Figure 2.2** ESC shown using temperature from Xu *et al.*, (2015). Diagram a) is the winter front frequency in percentage of time using merged microwave and infrared SST, from 1996 to 2012. Four NAC branches are identified. b) The SST in January 1996 around the UK and Europe, which indicates the warm waters of the winter Slope Current.

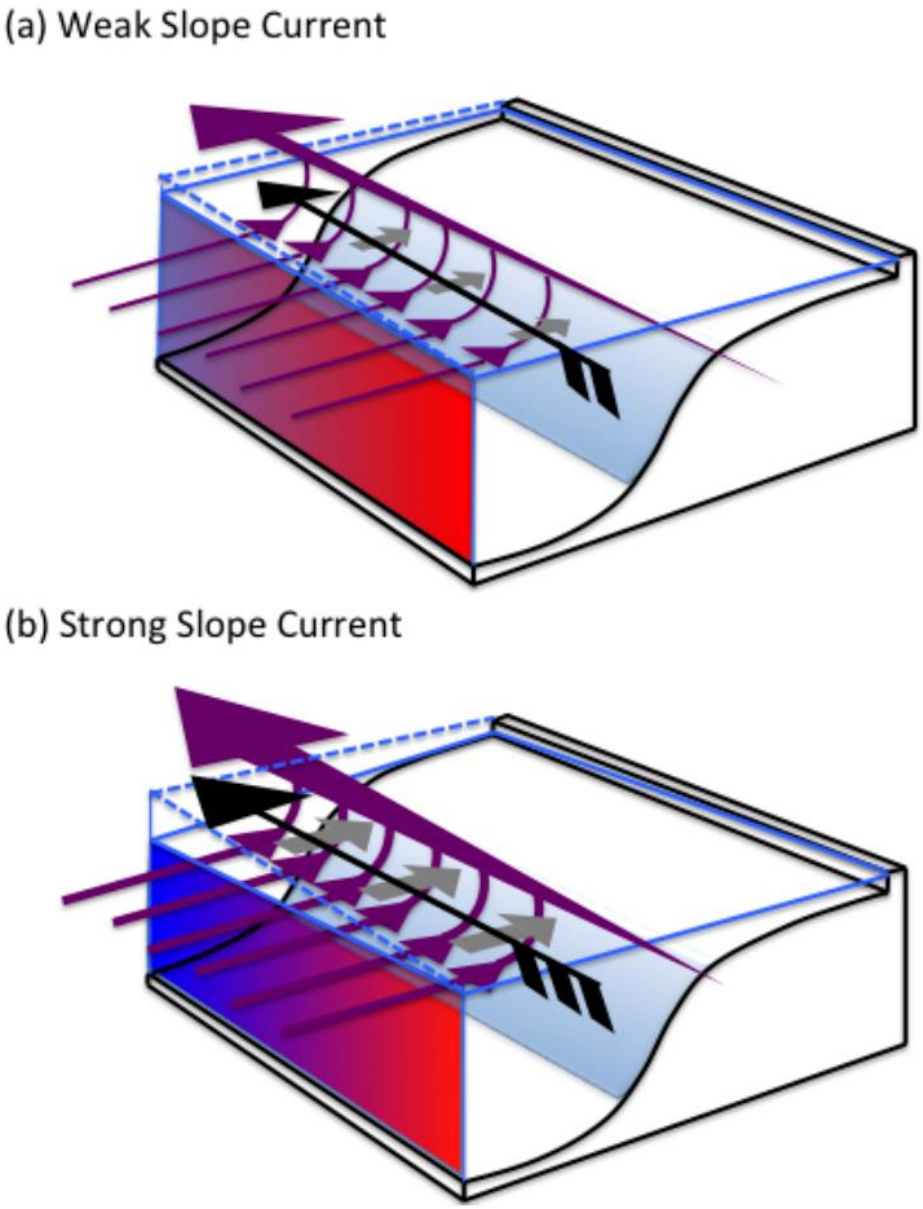


**Figure 2.3** Schematic from Marsh *et al.*, (2017) of an idealised a) weak and b) strong slope current transport. The density gradients are shown as red to dark blue, the wind forcing as a black arrow, Ekman transport as the grey on-shore arrows, sea surface slope in blue lines and the eastward geostrophic inflow as purple arrows. The size of the arrows demonstrates the strength of these forcings.

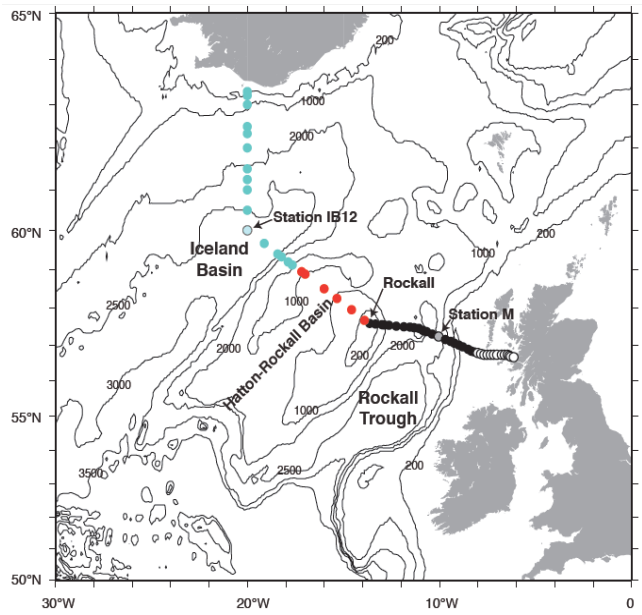


**Figure 2.4:** A map with the location of the Extended Ellett Line. The dots are the positions of the standard stations, where the open dots represent stations on the continental shelf, the filled black dots are stations in the Rockall Trough, red dots are stations in the Hatton-Rockall Basin and the blue are in the Iceland Basin (Holliday and Cunningham, 2013).

# 3 Data

Four sources of data have been used in this study, namely: (1) Conductivity, Temperature and Pressure (CTD) data; (2) LADCP datasets; (3) Shipboard-Acoustic Doppler Current Profiler (SADCP) data; (4) and Altimeter records. These sources of data are described in the sections below.

## 3.1 CTD operation and data

The first source of data is CTD data, which has been collected along the EEL almost annually in spring or summer since 1996 (a full list of the EEL cruises can be found at http://prj.noc.ac.uk/ExtendedEllettLine/project-information/individual-sections). Each occupation is given an identification code and the year is included as the last two digits of the code (as in Table 5-1). The EEL contains 63 standard full depth CTD stations, with spacing between stations typically 20 km in Rockall Trough, 30 km in Iceland Basin and 30-50 km in RHP. In some cases, extra stations were occupied, especially if there is a feature of interest such as strong mesoscale eddies. Throughout most occupations, station spacing is at its finest resolution at the boundary currents, especially over the ESC (not shown). At each station the CTD provided measurements of potential temperature, salinity and potential density, at a 2 dbar vertical resolution. The CTD data were calibrated to give a potential temperature accuracy of 0.002°C and salinity to 0.001, which meet international repeat hydrography standards (www.go-ship.org). Depth measurements are established from the CTD's pressure data by applying the United Nations Educational, Scientific and Cultural Organization (UNESCO) equation (Fofonoff and Millard, 1983).

## 3.2 LADCP operation, processing and data

The second source of data is LADCP data, collected alongside the CTD measurements, which was measured using a 150 kHz (before 2005) or 300 kHz (2005 to present) broadband Acoustic Doppler Current Profiler (ADCP). The configuration of the CTD frame mounted ADCPs changes, with either two ADCPs mounted in an upward-looking and downward-looking fashion or one

downward looking. The LADCP was configured to record single pings in depth cells of 8 or 16 m. The water-track measurements were processed using software produced by either the University of Hawaii (1996-2001) or Lamont-Doherty Earth Observatory software version 7/10 (2005-2013; (Visbeck, 2002)). The LADCP water track measurements taken in 1999 were processed by software developed by Brian King, Southampton Oceanographic Centre.

Absolute velocity profiles are derived from the raw LADCP measurements using the 'shear method' (Firing and Gordon, R., 1990; Fischer and Visbeck, 1993) up to 2005. The processing then switched to the 'inverse method' (Visbeck, 2002), which includes a combination of velocity referencing constraints such as the bottom tracking and navigation. Thurnherr [2010] finds a root mean square (RMS) velocity error of <0.03 m $s^{-1}$ within the processing despite the method used. After the LADCP measurements have been processed, the up and down casts of *u*, *v* and mean velocities are compared to check for data consistency. Any data inconsistencies are then recorded and, in this case, any large data inconsistencies that were notable have been removed, for example, generally when stations are very shallow, <200 m. There are occupations where no LADCP measurements were taken (2002, 2003, 2004, 2008 and 2012) and the occupation in 2000 is also excluded as it was carried out in winter.

## 3.3 Shipboard-ADCP operation and data

The third source of data is SADCP data, similarly, collected during each occupation since 1996. In terms of data coverage, in addition to the occupations excluded above (Section 3.2), there are no SADCP measurements in 2005 and 2007. Two instruments were used throughout the surveys – RDI 150 kHz and 75 kHz narrowband systems. Either both systems or just one system were used depending on technical faults or weather condition. The SADCP continuously transmits acoustical pulses from beneath the ship, in four oblique directions relative to its axis and to one another. After each pulse the instrument then "listens" for the backscattered signal to measure the Doppler shift. A vertical profile of velocity relative to ship along each of the beams is obtained. The velocities are mapped onto horizontal and vertical components relative to the ship if the currents at all depths are horizontal and non-divergent. The ships heading, movement, which are determined from GPS navigation, and compass are removed, to yield the absolute velocity (Chafik, Rossby and Schrum, 2014; Rossby *et al.*, 2017). The instrument records 2-minute averaged data in 64 x 8 m bins.

## 3.4 Altimetry and MDT

The fourth data source is altimetry. For this daily delayed global absolute (ADT) and mean sea-surface dynamic topography (MDT) is used. This is produced by the SSALTO/DUCAS system (Pujol *et al.*, 2016), and is distributed by The Copernicus Marine and Environment Monitoring Service (CMEMS). ADT is the sum of the sea-level anomaly (SLA) and the MDT, both referenced over a 20-year (1993-2012) period. Altimetric data is combined with other datasets, such as in-situ, gravimetric and satellites to determine the geoid at a horizontal resolution of 125 km. A final gridded dataset at a resolution of 0.25° is constructed using multivariate objective analysis, which improves the large-scale solution.

A second altimetry data set is used which is referred to as the Combined MDT (CMDT). This dataset is determined by utilising the latest version of GOCE gravity data, establishing a new mean sea surface (MSS) and incorporating a lower spatial filtering (Raj *et al.*, 2018). Thus, a higher spatial resolution of 25 km is established. Combined ADT (CADT) is a combination of the CMDT plus the SLA (obtained from SSALTO/DUCAS system).

# 4 Methods

## 4.1 Computing the time-mean velocity field and variability

The first objective is to evaluate the time-mean velocity field and its variability using direct velocity data. Within the ADCP data, barotropic tides, internal waves and near-inertial oscillations are assumed to be the main elements of ageostrophic motion (Donohue, Firing and Chen, 2001). The barotropic tides have been removed from the LADCP measurements using estimates from Oregon State University's Ocean Topography Experiment (TOPEX)/Poseidon Global Inverse Solution 1/4° dataset, version 7.2 (Egbert, Bennett and Foreman, 1994; Egbert and Erofeeva, 2002). The cross-track barotropic tidal predictions for an example survey (DY03115 not shown) are <0.1 m $s^{-1}$. The tidal predictions are much larger in the shallow regions, such as Rockall Bank and the Scottish shelf. These are not included within the velocity field. The tidal predictions in Rockall Trough are greater than in Iceland Basin, which is generated by the greater tidal amplitude near the Scottish shelf. LADCP velocities are then rotated from geographical coordinates to along-track and cross-track coordinates.

The SADCP data have also been de-tided using the method described above and then separated into on-station and off-station data. The off-station data are selected from the full cruise SADCP dataset using each CTD station start and end time. The SADCP data are then rotated onto cross-track coordinates.

Before the time-mean velocity field can be established, the EEL cruise data distribution needs to be examined, in order to assess whether there is sufficient spatial distribution to resolve the major circulation features that are expected in the cruise sections. This is carried out in Appendix A and shows that there is no clear preferred direct velocity type in terms of data coverage for each section. However, a comparison between Table 5-1 and Appendix Table A.1 it is shown that there are more individual sections that have LADCP measurements, than SADCP. For this reason, the LADCP velocity is chosen to establish the time-mean velocity field at the EEL.

The de-tided LADCP velocity profile is interpolated onto a standard vertical profile, from 20 m depth in intervals of 40 m to a maximum depth of 3000 m, using a linear fit method. The cross-track velocity profiles are merged and interpolated onto a horizontal grid with 10 km spacing. The LADCP velocity field for 13 occupations are averaged to produce the time-mean velocity and

the standard error of the mean (SEM) velocity fields. The SEM is defined as the standard deviation divided by the square root of the sample size, which gives an idea of the accuracy of the mean.

## 4.2 Using LADCP to reference the geostrophic velocity and transport calculation

The second sub-objective is to compute the time-mean geostrophic velocity field referenced with direct velocity data and compute the net volume transport. In order to do this, an assessment of SADCP, on-station and off-station, and LADCP data as a reference velocity is carried out in Appendix A. It is concluded that there is no preferred data type and so the time-mean velocity field computed form the LADCP velocity will be used as a reference velocity. As mentioned above, the LADCP velocity has a greater data coverage over the ~20 years and it provides a full-depth coverage, unlike the SADCP velocity.

Next, the time-mean velocity field is used to provide a reference velocity for geostrophic velocity computed from the time-mean density field. The reference velocity ($v_{ref}$) for each station pair along the section is computed:

$$v_{ref}(x) = \overline{v_{LADCP}(x,z) - v_g(x,z)} \quad (1)$$

where $v_{LADCP}$ is the time-mean cross-track component of the station-pair LADCP velocity profile, $v_g$ is the geostrophic velocity, x is the along-track direction and z is depth. The overbar represents the depth average over all depths below 300 m (to eliminate fast upper-ocean variability). The reference velocity is added to the geostrophic shear (computed with initial level of no motion at the surface) to derive the absolute geostrophic velocity field ($v_{abs}$), as shown in the following equation:

$$v_{abs}(x,z) = v_{ref}(x) + v_g(x,z) \quad (2)$$

With the referenced (absolute) velocity field, the volume transport across the section is then computed. Volume transport is defined as the velocity multiplied by area (units Sv). The area between the deepest common level and the maximum depth of each station pair must be considered, known as the bottom triangle. For each station pair the bottom triangle is assumed to be a constant velocity and is equal to the deepest common level (Holliday *et al.*, 2015). Volume transport ($T_{obs}$,Sv) normal to the section is computed from the absolute velocity ($v_{abs}$) and the cross-sectional area (A).

$$T_{obs} = \sum_{x_w}^{x_e} \sum_{z_{max}}^{z_{min}} v_{abs}(x,z) \cdot A(x,z) \tag{3}$$

The time-mean Ekman transport, produced by the wind-driven surface circulation, is calculated from ERA Interim once daily wind speed data recorded during the month of each cruise and rotated onto the EEL. This results in a net Ekman transport across the EEL of -1.0 Sv, which takes place in the upper 30 m (Lherminier *et al.*, 2010). This is added to the volume transport computed from the absolute geostrophic velocity.

The total volume transport is decomposed into each of the water masses captured by the EEL. The isopycnal boundaries, which are used to define these, can be seen in Figure 5.1a and Figure 5.1b. The upper layer (UOW, < 27.50 kg $m^{-3}$) is located above the thermocline (500-1000 dbar) and has warm (~10 °C; Figure 5.1b), and salty (~35.3; Figure 5.1b) characteristics (Pollard, 2004; Brambilla and Talley, 2008). This layer flows northeastward towards the Nordic Seas, whilst the Labrador Sea Water (LSW, 27.70-27.80 kg $m^{-3}$), recirculates cyclonically at intermediate depths in both Iceland Basin and Rockall Trough due to the shoaling topography (Holliday *et al.*, 2000; Lankhorst and Zenk, 2006). Dense water formation in the Nordic Sea supplies the overflow water (>27.80 kg $m^{-3}$), which flows at depth along the Reykjanes Ridge in Iceland Basin (Saunders, 1996; Read, 2001). Wyville Thomson Ridge Overflow Water flows southward in the intermediate water masses with densities >27.70 kg $m^{-3}$ and has been detected in western Rockall Trough (Johnson *et al.*, 2010), but this is not a boundary used in this study.

The measurement error is provided by Thurnherr (2010) who shows that the rms error in the LADCP velocity is ±0.03 m $s^{-1}$. The SEM across the section is the sampling error. These two errors can be combined at each grid cell using the root sum square, which assumes that the errors are independent of each other. The mean error across the section equates to 0.039 m $s^{-1}$ and seeing

as the maximum range within the currents is 0 to 0.2 m $s^{-1}$, then the uncertainty has a maximum value of 20%. This 20% uncertainty is applied to the transport estimates in this chapter, whereas velocity uncertainties are given by the SEM.

Due to the regional bathymetry at the EEL, no water below 800 m can continue into the Nordic Seas, resulting in the recirculation of LSW in Iceland Basin and Rockall Trough (Ellett, Edwards and Bowers, 1986; Holliday *et al.*, 2000). Thus, it is expected that the net LSW transport will be 0 Sv. In *Holliday et al.*, (2015) which uses a time-mean density field and a level of no motion in the mid-depth ocean, the LSW layer is defined as $\sigma_0$ = 27.7 – 27.85 kg $m^{-3}$ and has a transport estimate of -4.0 ± 2.4 Sv. The net southward transport suggests that the LSW transport estimate likely includes a less dense form of ISOW. In the literature different boundary definitions are used, which will be discussed in the rest of this section.

In *Sarafanov et al.*, (2012), ISOW had a net transport across the EEL of -2.2 ± 0.4 Sv, which included some recirculation of the overflow northwards, and is directly comparable to the estimated -2.1 ± 0.9 Sv computed using the same density boundary definition ($\sigma_0$ = 27.85 kg $m^{-3}$, *Holliday et al.*, (2015)). This value is located downstream of the 3.1 Sv overflow estimated to flow from the Norwegian Sea into the Iceland Basin (Hansen and Østerhus, 2007; Olsen *et al.*, 2008) and upstream of the -3.7 ± 0.8 Sv ($\sigma_0$ = 27.80 kg $m^{-3}$) estimated by combining altimetry and hydrographic data (ISOW measured between the Reykjanes Ridge and Scotland) (Sarafanov *et al.*, 2012). It would be expected that the estimate given at the location of the EEL is greater than 3.1 Sv due to entrainment. This is not the case for the previous estimates at the EEL, which may be due to a too dense boundary definition being used. Kanzow and Zenk, (2014) provide a summary of previous ISOW transport estimates, ranging from 1.2-5.4 Sv ($\sigma_0$ = 27.80 kg $m^{-3}$). Saunders, (1996) indicates that the $\sigma_0$ = 27.80 kg $m^{-3}$ upper boundary for ISOW is the most ideal definition by analysing the ISOW properties using CTD sections.

## 4.3 Calculating temperature and freshwater transport

The third sub-objective is to compute the time-mean net temperature and freshwater transport across the EEL. The heat transport cannot be estimated due to the non-zero net mass transport across the EEL (Bryden and Imawaki, 2001). The temperature transport is calculated relative to 0°C and should only be compared to other estimates derived in the same way, as a change in

units from °C to K results in a change in the transport magnitude (Berx *et al.*, 2013). The temperature transport (PW) is calculated using:

$$Temperature\ transport = \iint \rho(x,z)C_p(x,z)\theta(x,z)v(x,z)\partial x\partial z \quad (4)$$

where $\rho$ is the density (kg m$^{-3}$), $C_p$=Specific heat of water at constant pressure (J kg$^{-1}$ °C$^{-1}$), $\theta$ is potential temperature (°C), $x$ is along-track distance (m), $z$ is depth (m) and $v$ is cross-track velocity (m s$^{-1}$).

For freshwater transport a reference salinity is needed. This value needs to be chosen carefully, especially when mass is not conserved as the freshwater transport is dependent on it (Talley, 2008). The freshwater transport (mSv) is calculated using:

$$Freshwater\ transport = \frac{\int (S - S_{ref})v\ \partial A}{S_{ref}} \quad (5)$$

$$S_{ref} = \frac{\int S\partial A}{A} \quad (6)$$

where $S$ is the absolute salinity (g/kg) and $S_{ref}$ is 35.20, defined as the area-weighted mean salinity (g/kg; Bacon et al. 2015).

## 4.4 Altimetric derived velocity

The third sub-objective is to determine whether the altimetry data can be used as a reference velocity at the EEL. Surface geostrophic velocities from satellite data are derived via the geostrophic relations. Geostrophic approximation at the surface leads to the relation: surface

geostrophic currents are proportional to surface slope. Absolute geostrophic velocity at the surface ($u_s^2 + v_s^2$) is calculated using the following equations:

$$v_s = \frac{g}{f}\frac{\partial \xi}{\partial x} \qquad u_s = -\frac{g}{f}\frac{\partial \xi}{\partial y} \tag{6}$$

Where g is gravitational acceleration (m $s^{-2}$), f is the Coriolis parameter (rad $s^{-1}$) and d$\xi$ is the change in sea-surface height between two points in the horizontal, dx, or vertical, dy (m).

# 5 Results

## 5.1 LADCP average velocity field and variability

The first sub-objective is to evaluate the time-mean velocity field and its variability using LADCP data. The time-mean velocity field along the EEL section is shown in Figure 5.1c. Similarly, the 13 sections were averaged to compute time-mean fields of temperature, salinity and potential density (Figure 5.1). Cruise information in Table 5-1 and sample number shown in Figure 5.1d are used to compute the 18-year average, in Figure 5.1c. Negative velocities (blue) are defined "outwards" (approximately southwestward), positive (red) "inwards" (approximately northeastward). Figure 5.1e compliments Figure 5.1c by presenting the standard error of the mean. The temperature and salinity field along the EEL has been included in Figure 5.1a and Figure 5.1b for completeness. The flows have a large barotropic component, with velocities extending from the surface to the seafloor and alternating in bands of unidirectional flow throughout the full section (Figure 5.1c). The velocities demonstrate enhanced vertical shear in the upper ocean, primarily in Rockall Trough and boundary currents, and in the densest water (ISOW) close to the seabed. However, no LONM can be observed within the water column in west Iceland Basin.

The average velocity and its temporal variance in the upper 500m across the EEL are shown in Figure 5.2. The two branches of the dominant NAC flowing northward are in central and eastern Iceland Basin, with a velocity of 0.20 and 0.25 m $s^{-1}$ respectively. The latter branch is the SPF, which is constrained by bathymetry to follow Hatton Bank, as seen in Figure 5.2 by the strong flows in southeast Iceland Basin. The NAC has a low temporal variance as indicated by the small ellipse size, highlighting its stability in strength throughout the occupations. A stable northward flow can also be seen within the RHP, with a value of 0.1 ± 0.02 m $s^{-1}$ (Figure 5.2, Figure 5.1c and Figure 5.1e).

Another prevailing feature throughout Figure 5.2 and Figure 5.1c, is the boundary currents, that are found adjacent to steep topography. The ESC, located in east Rockall Trough, is a stable flow within the section that is indicated by the low temporal variance in Figure 5.2, and travels at an average speed of 0.20 ± 0.03 m $s^{-1}$ (Figure 5.2, Figure 5.1c and Figure 5.1e). There is a high station spatial resolution (10-20 km station spacing) across the ESC (~50 km in width) throughout the occupations; thus, it can be interpreted as the mean flow of the ESC transporting warm light

water that does not differ much in its location. Figure 5.1a and Figure 5.1b show similarly to *Holliday et al.*, (2015) that the highest temperature and salinity across the section is located here and so we might expect there to be large temperature and salinity transport in this current.

The ISOW is represented in Figure 5.1c by the increased velocity at depth in Iceland Basin, with an average velocity core of -0.40 ± 0.06 m $s^{-1}$. The velocity is highly variable leading to the higher uncertainty (Figure 5.1e).

The flows in the upper ocean interior of Rockall Trough and Iceland Basin have a high SEM, ~0.07 m $s^{-1}$, and large variance ellipses, which is consistent with the fast upper-ocean variability and eddying (Figure 5.2 and Figure 5.1e). Figure 5.1e highlights an increased SEM (~0.05 m $s^{-1}$) down to ~1000 m in both basins and, in Rockall Trough close to the seabed. The higher variability throughout the sections could be an indication of decreased temporal sampling, which is not the case at these locations (Figure 5.1d). The waters above and around Anton Dohrn Seamount display high variability (0.04 - 0.07 m $s^{-1}$ SEM) that is representative of the well-documented anti-cyclonic recirculation (Booth, 1988; Burrows, Thorpe and Meldrum, 1999; Holliday *et al.*, 2000).

## 5.2 Adjusted mean geostrophic velocity and its transport

The second sub-objective is to compute the time-mean geostrophic velocity field referenced with the LADCP data and compute the net volume transport. Figure 5.3a show the LADCP referenced mean geostrophic velocity over the 18 years, giving a very similar structure to the flows in the mean LADCP velocity section in Figure 5.1a, but with less vertical variability (note the different colour scales). The cumulative volume transport across the EEL (from 0-1135 km, excluding the Scottish continental shelf), in Figure 5.3b, shows a net northward transport of 4.5 ± 0.9 Sv (also in Table 5-2). With Ekman transport included in this estimate it becomes 3.5 ± 0.9 Sv. There is a net northward volume transport in Iceland Basin of ~2 Sv, which increases to ~3 Sv across RHP. In Rockall Trough most of the net northward transport is within the ESC (far right positive transport in Figure 5.3b).

In Figure 5.3c the cumulative volume transport is separated into water masses using density layers. The net volume transport for each layer is also summarized in Table 5-2. The UOW, $\sigma_0$ =

27.15 – 27.50 kg $m^{-3}$, has a transport of 6.9 ± 1.4 Sv (5.9 ± 1.4 Sv with Ekman), with 3 Sv taking place above the RHP. Similarly to Sarafanov et al., (2012) the UOW of the SPF and the north NAC branch carry the largest volumes of water northward. The thermocline produces -0.4 ± 0.1 Sv (Figure 5.3c, $\sigma_0$ = 27.5 – 27.7 kg $m^{-3}$), whilst the LSW transports 0.5 ± 0.1 Sv (Figure 5.3c, $\sigma_0$ = 27.70 – 27.80 kg $m^{-3}$) and the ISOW gives –3.3 ± 0.7 Sv (Figure 5.3c, $\sigma_0$ > 27.80 kg $m^{-3}$). The ESC (1065 – 1135 km, Table 5-2) has a net transport of 2.3 ± 0.5 Sv.

## 5.3 Temperature and Freshwater transport

The third sub-objective is to compute the time-mean net temperature and freshwater transport across the EEL. The cumulative temperature transport across the EEL, shown in Figure 5.3d, follows a similar structure to the cumulative volume transport. The northward temperature transport largely takes place in Iceland Basin, as seen from the ~0.5 PW increase in the eastern side of the basin. Similarly, to the volume transport this shows that most of the northward heat transport takes place in the north NAC branch and the SPF. The remainder, a notable amount of ~0.2 PW, is split between RHP and the ESC. The temperature transport thus closely follows the strength of volume transport and is less dependent on the magnitude of temperature across the section. If the latter were the case, we would see a larger temperature transport within the eastern side of the section, especially across the ESC and shallower region of the RHP.

The net temperature transport derived from the mean LADCP referenced geostrophic velocity is 0.22 PW ± 0.04 PW (Figure 5.3d and Table 5-2). The net freshwater transport across the EEL is 44.1 ± 8.8 mSv (southward), using a reference salinity of 35.20 (Figure 5.3d and Table 5-2).

## 5.4 Assessment of altimeter data as a reference velocity

The fourth sub-objective is to determine whether the altimetry data can be used as a reference velocity at the EEL. First, in order to qualitatively determine the representativeness of the remotely-sensed data a comparison is made between the altimeter surface velocities and the ADCP data. The satellite data are not directly comparable to the ADCP data in space or time because satellites measure the sea surface slope over a large swath, and the AVISO products are

averaged over time and space. The surface geostrophic velocities are computed using the sea surface slope and a mean dynamic topography field (MDT; Equation 6), so they are also sensitive to the MDT.

In order to make a valid comparison between altimeter velocities and cruise data we need to consider the time-averages of both data sets (Chafik, Rossby and Schrum, 2014). The time-averaged altimetric derived surface geostrophic velocities (calculated from the average SSALTO/DUCAS ADT) are compared to the time-averaged surface SADCP off-station data (0-100 m average), (Figure 5.4a). The correlation between the two datasets is significant (R=0.44 and p=0.0006). The altimetric derived geostrophic velocity is consistent with the surface SADCP off-station data in terms of the general circulation pattern. In Iceland Basin the difference between the two datasets does not exceed 0.05 m $s^{-1}$, but the difference is greater in west Iceland Basin where the southward flow is located. East (>600 km) over RHP the difference exceeds 0.05 m $s^{-1}$ and greater still in Rockall Trough, with 0.10 m $s^{-1}$. At 1100 km the ESC's northward flow is shown in the SADCP off-station velocity as 0.15 m $s^{-1}$ but it is barely noticeable in the altimeter-derived velocity. The average velocity across EEL is 0.004 m $s^{-1}$ for the SADCP off-station surface velocity and 0.015 m $s^{-1}$ for the altimeter derived surface velocity. A rough transport estimate is calculated using these values over the whole section (product of mid depth of 1000 m, distance of 1100 km and average velocity), resulting in ~4 Sv and ~17 Sv respectively.

Next, it is considered whether a different MDT provides a closer match between the altimetry data and the cruise data. The averaged new CADT is compared to the mean surface SADCP (0-100m) off-station velocity in Figure 5.4b. They are significantly correlated (R=0.45 and p=0.0005), but there are larger differences between the SADCP off-station velocity and the new altimeter velocities than between the SADCP data and the SSALTO/DUCAS altimeter derived velocity. The difference in the northward flows in east Iceland Basin and central Rockall Trough exceeds 0.1 m $s^{-1}$. The two datasets follow more closely in the southward flows in west Iceland Basin and Rockall Hatton Plateau, than with the SSALTO/DUCAS altimeter derived velocity. In Rockall Trough the new CADT derived velocity is not consistent with the SADCP off-station velocity, although the ESC flow is present. Using the average SADCP off-station surface velocity across the EEL and 0.02 m $s^{-1}$ for the average altimeter derived surface velocity, the transports can be calculated across the whole section (product of mid depth of 1000 m, distance of 1100 km and average velocity), ~4 Sv and ~22 Sv respectively. The transport estimated for the new CADT altimetry dataset is 5 Sv greater than that for the SSALTO/DUCAS altimeter dataset.

Finally, the agreement between the altimeter data and the cruise data is examined after the cruise data are projected on to a similar spatial resolution. The altimeter has a coarser horizontal resolution than the SADCP and LADCP measurements, and so the agreement between these may be improved if the ADCP velocity has a comparative horizontal scale. Pujol et al., [2016] shows that the along track velocity needs to be smoothed onto a resolution of >65 km to be compared to the altimetry. This is because at the 60 to 300 km wavelengths, roughly 60 % of the energy measured in the along-track is missing. Figure 5.5a show the mean surface SADCP off-station velocity, with and without smoothing applied, plotted with the altimeter derived surface velocity averaged over all cruises. The ADCP velocity is smoothed using a running mean with a length scale of 65 km, which is the lowest resolution needed to be compared to the altimetry. In Figure 5.5a, the SADCP smoothed velocity is not very dissimilar to the unsmoothed velocity in Iceland Basin and RHP, but it does improve the agreement with the altimetry velocity. In Rockall Trough, the unsmoothed SADCP velocity has more detail and greater extremes than the smoothed velocity. The velocity extreme on the east side of Anton Dohrn Seamount decreases by 0.05 m $s^{-1}$.

Figure 5.5b shows the altimeter derived surface velocity alongside the mean surface LADCP velocity, with and without smoothing applied. The smoothing is applied in the same way and over the same scale as in the previous paragraph. In Iceland Basin and Rockall- Hatton Plateau the smoothing improves the agreement with the altimeter derived velocity, by reducing the property extremes by <0.05 m $s^{-1}$. In Rockall Trough, the smoothing decreases the velocity peaks and troughs by >0.05 m $s^{-1}$.

# Tables

**Table 5-1** Extended Ellett Line occupation identification code, year and dates. These are the 13 occupations used in this study, covering 18 years (1997-2015).

| Cruise ID | Year | Start | Finish |
|---|---|---|---|
| **DY031** | 2015 | May 28 | June 18 |
| **JR302** | 2014 | June 6 | July 22 |
| **JC086** | 2013 | May 6 | May 26 |
| **D365** | 2011 | May 11 | Jun 2 |
| **D351** | 2010 | May 10 | May 28 |
| **D340a** | 2009 | Jun 10 | Jun25 |
| **D321** | 2007 | Jul 24 | Sep 9 |
| **D312** | 2006 | Oct 11 | Oct 31 |
| **CD176** | 2005 | Oct 6 | Oct 28 |
| **D253** | 2001 | May 4 | Jun 20 |
| **D245** | 2000 | Jan 27 | Feb 20 |
| **D242** | 1999 | Sep 7 | Oct 6 |
| **D233** | 1998 | Apr 2 | Jun 1 |
| **D230** | 1997 | Aug 7 | Sep 17 |

**Table 5-2** Net long-term volume, temperature and freshwater transports across the EEL (18-year period).

| | Density layer (Kg $m^{-3}$) | Net EEL (Sv) | Temperature (PW) | Freshwater (mSv) |
|---|---|---|---|---|
| **Total** | <27.90 | 4.5 ± 0.9 | 0.22 ± 0.04 | 44.1 ± 8.8 (southward) |
| **Upper Ocean Water** | 27.15 - 27.50 | 6.9 ± 1.4 | - | - |
| **Permanent Thermocline** | 27.50 – 27.70 | -0.4 ± 0.1 | - | - |
| **Labrador Sea Water** | 27.70 – 27.80 | 0.5 ± 0.1 | - | - |
| **Iceland Scotland Overflow Water** | >27.80 | -3.3 ± 0.7 | - | - |
| **European Slope Current** | - | 2.3 ± 0.5 | - | - |

## Figures

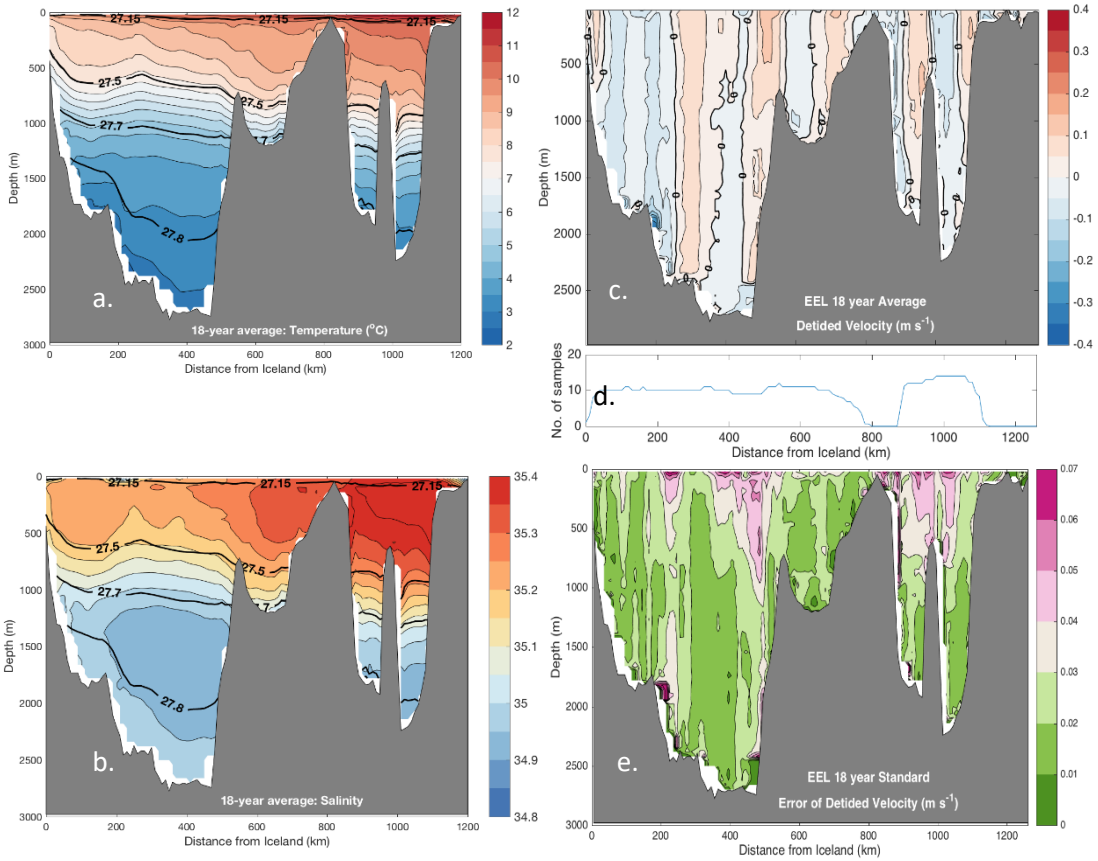


**Figure 5.1 a.** 18-year average Extended Ellett Line temperature (°C) and **b.** salinity field of the 14 occupations. The bold black lines indicate the isopycnals bounding the regional water masses. **c.** 18-year average LADCP velocity (m $s^{-1}$) **e.** along with corresponding standard error of the mean (m $s^{-1}$). **d.** The middle image is the number of occupations included in the average and standard error of the mean.

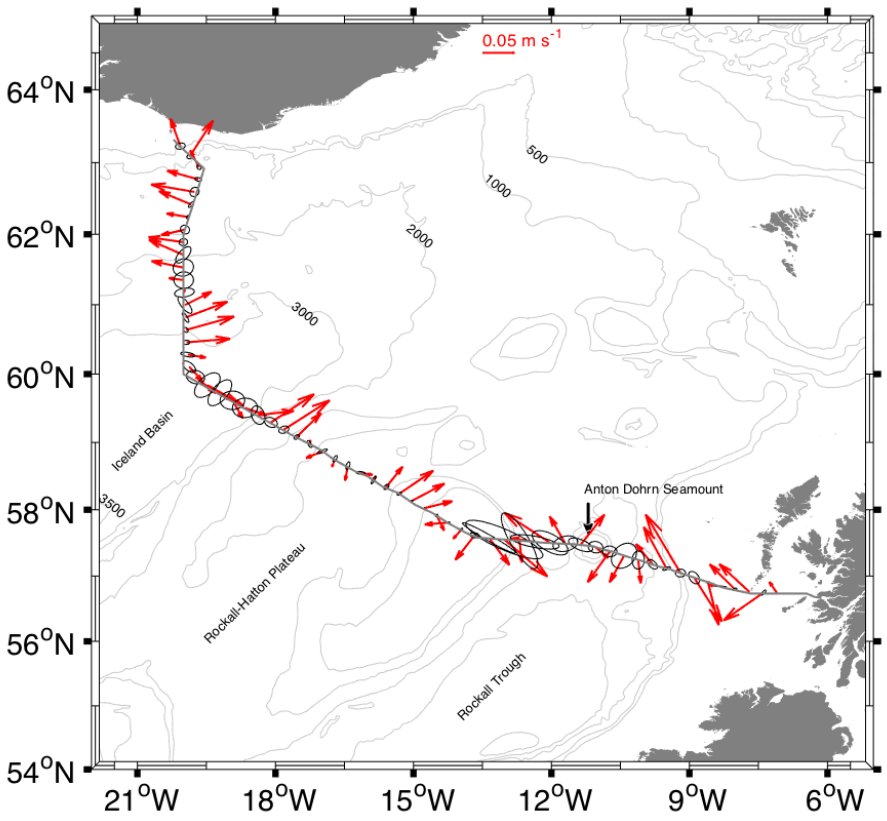


**Figure 5.2** Map showing location of Extended Ellett Line with the 18-year mean velocity over the upper 500 m (m $s^{-1}$, red vectors) and their corresponding temporal variance ($m^2$ $s^{-1}$, black ellipses).

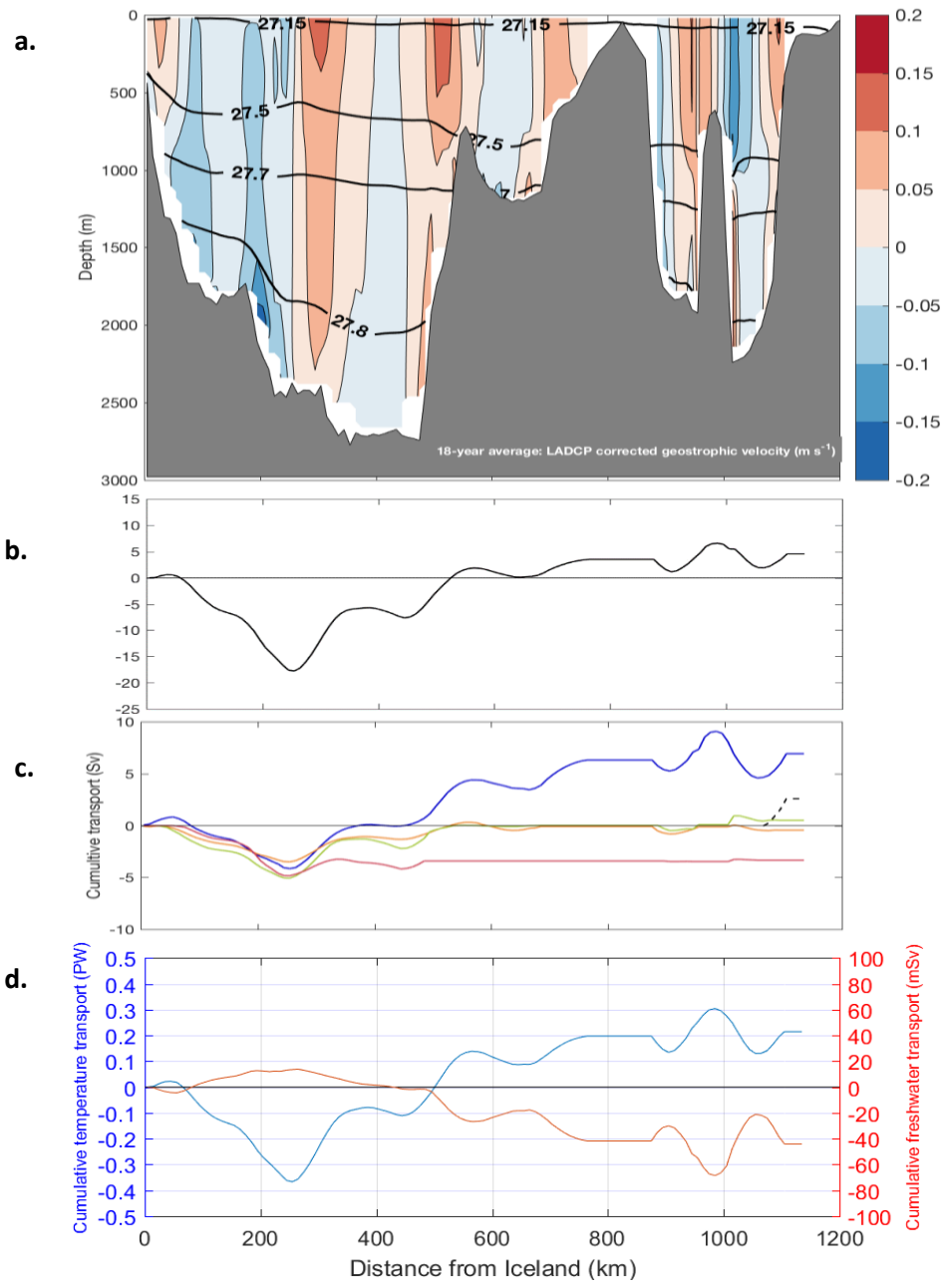


**Figure 5.3 a.** LADCP referenced mean geostrophic velocity, calculated from the 13 occupations (over 18-years). The bold black lines represent the isopycnals delimiting regional water masses. **b.** Is the corresponding cumulative transport (bold black line). **c.** The cumulative transports of each density layer (blue represents Upper Ocean Water, orange is the Permanent Thermocline, green is the Labrador Sea Water, red the Iceland-Scotland Overflow Water and the dashed black line is the European Slope Current). **d.** The cumulative temperature (PW) and freshwater (mSv) transport across the EEL.

a.

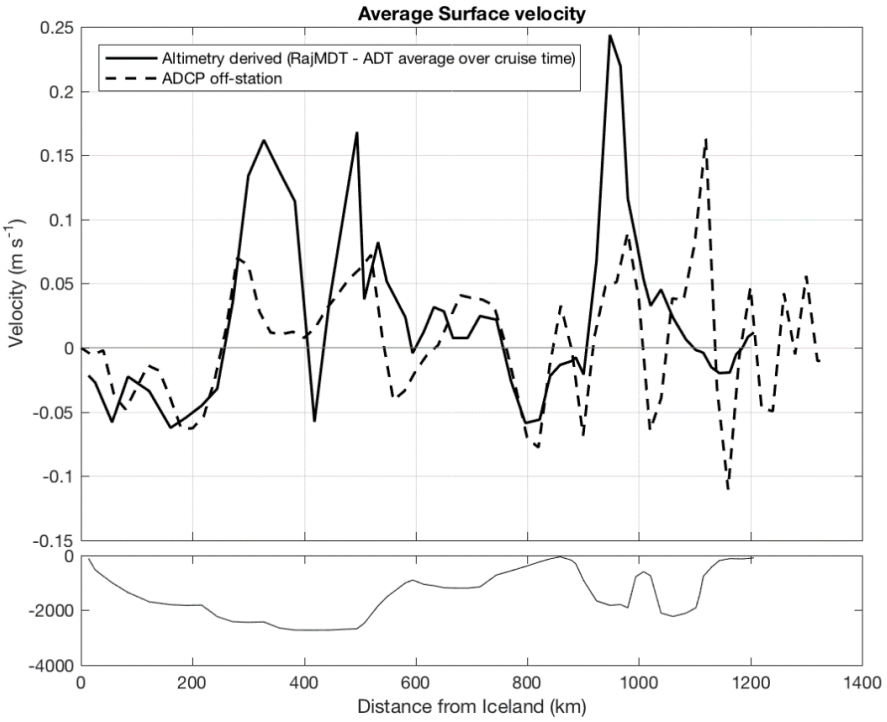


b.

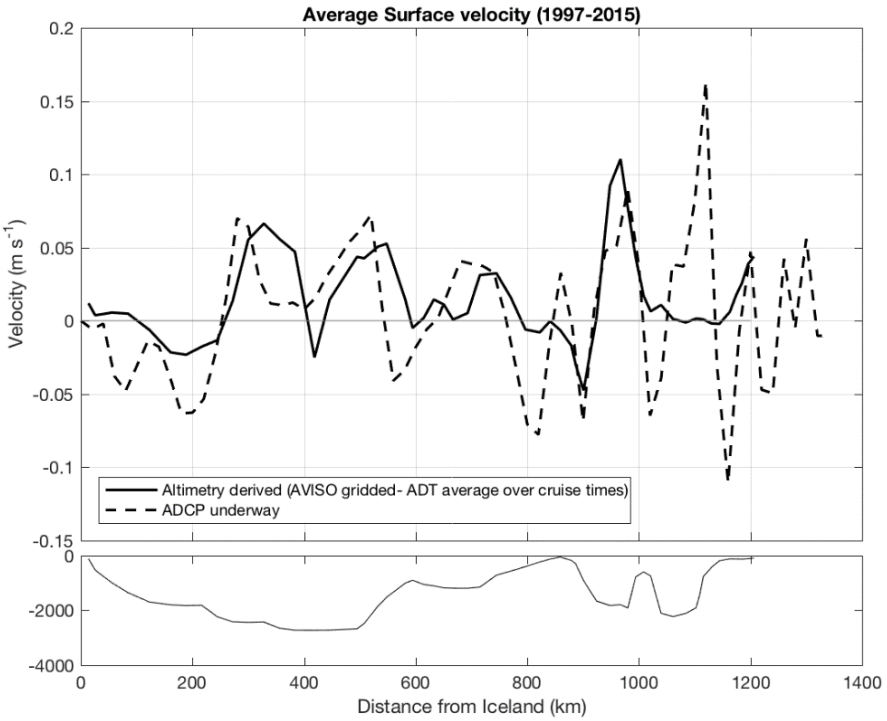


**Figure 5.4** Surface velocity from SADCP underway (off-station; dashed line) compared to surface geostrophic velocity derived from **a.** SSALTO/DUCAS ADT altimetric data (bold line) and **b.** CADT altimetric data (bold line). Both altimetric ADT datasets have been averaged over the occupations to match the ADCP data.

a.

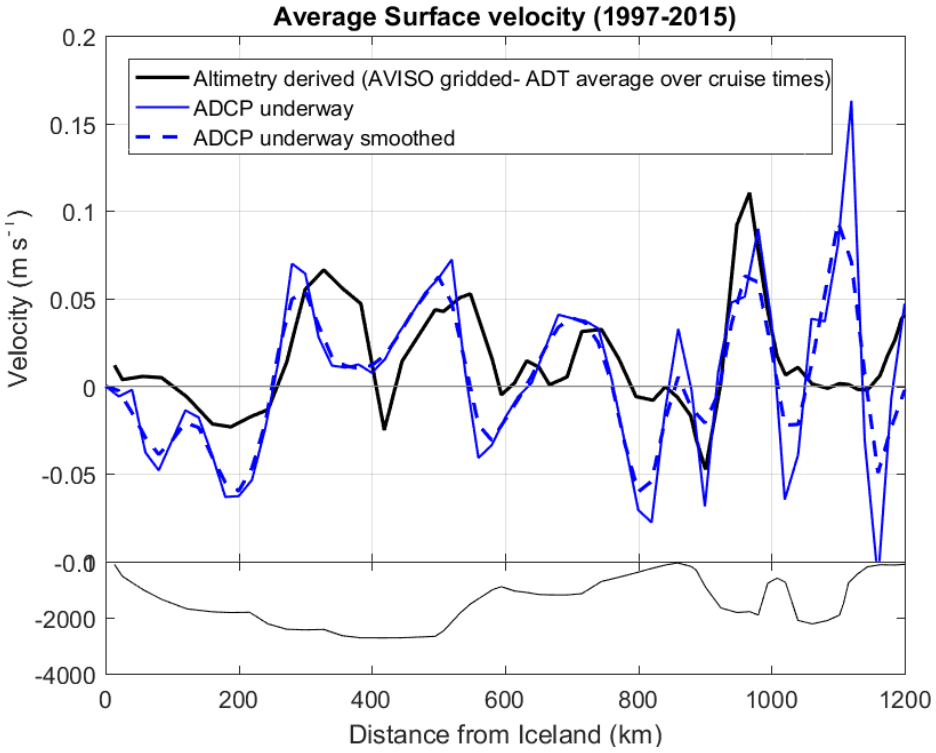


b.

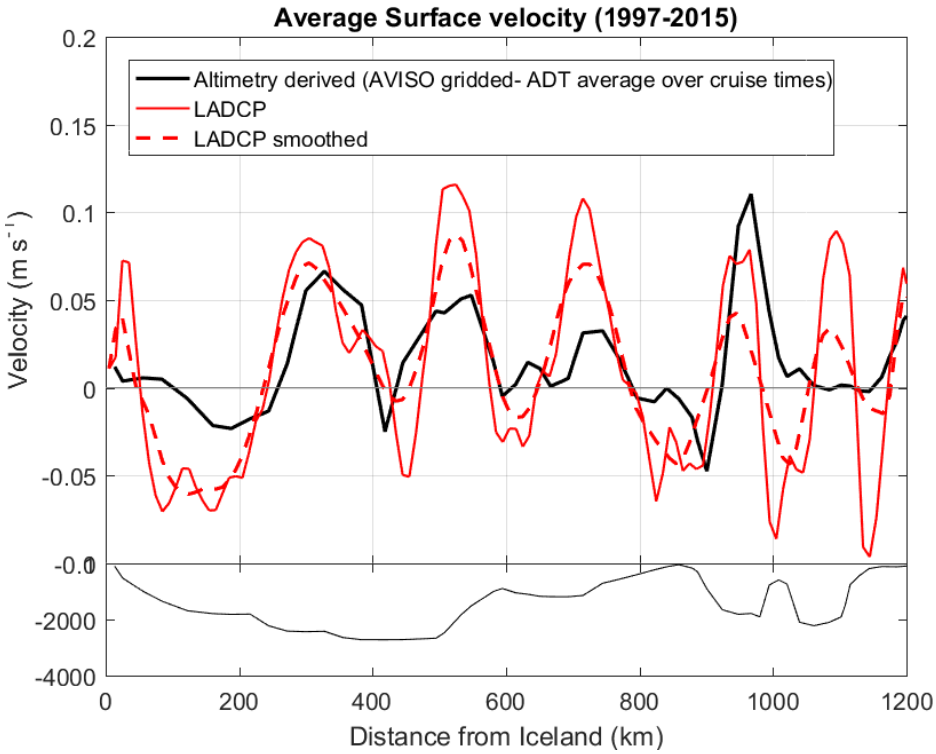


**Figure 5.5** Altimetric, SSALTO/DUCAS, derived surface plotted with **a.** surface SADCP underway (off-station) with no smoothing and smoothing to a scale of 65 km and **b.** surface LADCP with no smoothing and smoothing to a scale of 65 km. The SADCP and LADCP velocities have been averaged over the upper 0-100 m.

# 6 Discussion

In this chapter, the average long-term full-depth velocity field and transports over nearly two decades have been estimated, using direct velocity measurements and hydrographic data. This is the first time that full-depth in situ velocity data has been examined, at the EEL, to obtain a long-term average velocity field and transports of the MOC. By using the direct velocity measurements, a net volume transport of 3.5 ± 0.9 Sv across the EEL has been estimated, larger than the previous estimate of 1.4 ± 5.8 Sv computed with mid-depth level of no motion (Holliday *et al.*, 2015).

For the first time, the long-term temperature and freshwater transport at this section have been estimated, 0.22 ± 0.04 PW northward, and 44.1 ± 8.8 mSv southward (reference salinity of 35.20), respectively. *Hansen and Østerhus*, (2000) show that there is a long-term mean of 0.25 PW temperature transport between Iceland and the Shetlands (their Figure 7). In the same location, but for a later time period, there has been a consistent estimate of 0.25 PW (Hansen *et al.* 2003 - their Table 4; Turrell *et al.* 2003 - their Table 1). Similarly, the more recent study by (Østerhus *et al.*, 2005) estimates a temperature transport of 0.29 PW using mooring data (their Table 1). These are all in close agreement with our temperature transport estimate. The hypothesis that the RHP and ESC are important routes for northward temperature transport is supported by our results, although the NAC and SPF in Iceland Basin are the largest contributors. This novel finding furthers our understanding of the transport pathways through this region and shows that it is important that the RHP is included in future transport estimates.

The similar structure in volume and temperature transport highlights that there is a greater dependency on the transport strength rather than the magnitude of temperature. *Mercier et al.*, (2015) supports this finding showing that the heat flux along OVIDE is linearly related to the MOC intensity. However, unraveling the processes underpinning the temperature transport variability within the subpolar region has been an ongoing study, with investigations using models and/or observations (Eden and Willebrand, 2001; Balmaseda *et al.*, 2007; Desbruyères, Mercier and Thierry, 2014; Williams *et al.*, 2014, 2015; Mercier *et al.*, 2015; Holliday *et al.*, 2018).

Due to the regional bathymetry, no water below 800 m can continue in to the Nordic Seas, therefore, causing the LSW to recirculate in Iceland Basin and Rockall Trough (Ellett, Edwards and Bowers, 1986; Holliday *et al.*, 2000). It is thus expected that the net LSW transport is 0 Sv, and our estimate is 0.5 ± 0.1 Sv which is closer to the expected value than an earlier estimate -4.0 ± 2.4 Sv (Holliday *et al.*, 2015), and suggests the section volume transport estimated given here may also be an improvement over the earlier study. The 0.5 Sv may be transferred diapycnally from ISOW to the intermediate layer.

The absolute velocity field shows the central Iceland Basin and SPF branches of the NAC running through Iceland Basin are rather barotropic and have low temporal variance. The northward flow across RHP, with an average velocity of 0.1 ± 0.02 m $s^{-1}$, is likely to be an outcrop of the NAC, consistent with *Daniault et al.*, (2016) who finds that the southern NAC branch splits, with this being its northern extension. The properties in the RHP are not indicative of the flow being part of the SPF (wide gentle isopycnals; Holliday *et al.* (2015) their Figure 2 and 3). The fast upper-ocean variability and eddying in Rockall Trough and Iceland Basin interior is consistent with previous studies within the region (Fratantoni, 2001; Rossby and Flagg, 2012), along with Holliday *et al.*, (2015).

The UOW transport of 5.9 ± 1.4 Sv, agrees well with previous geostrophic calculations of 6.7 ± 3.7 Sv ($\sigma_0$ = 27.15 – 27.5 kg $m^{-3}$) across the same section (Holliday *et al.*, 2015) and 7.6 ± 0.9 Sv (surface to 27.55 kg $m^{-3}$) between the Reykjanes Ridge and Scotland (Sarafanov *et al.*, 2012). Multiple vessel-mounted ADCP sections derived upper-ocean transport and estimated 6.1 ± 0.3 Sv between Iceland and Shetland. This in good agreement with the results of this study, within the degrees of uncertainty (Childers, Flagg and Rossby, 2014).

This study provides the first estimates of mean ESC and RHP transports from repeat hydrography. The ESC has an absolute transport of 2.3 ± 0.5 Sv with low inter-cruise variability. This is most likely due to a stable core location and consistent strength. This transport value lies within the range of previous estimates, 0.5-3 Sv (Booth and Ellett, 1983; Ellett, Edwards and Bowers, 1986; Holliday *et al.*, 2000). Above RHP we observe a mean of 3 Sv of UOW. Houpert *et al.*, (2018) finds that from 2014 to 2016 there is a mean flow of 1.5 ± 0.7 Sv above RHP and along with the SPF branch, this accounts for 43% of the total NAC upper ocean transport northwards.

The ISOW has an estimates net transport across the EEL of -3.3 ± 0.7 Sv. This is higher than an earlier estimate from Holliday at al., 2015, although we had anticipated a slightly higher net transport of these dense waters given the transport of 3 Sv of the overflow water at the sill.

The transports estimated in this study strengthen the recent results by Lozier *et al.*, (2019) at the OSNAP East section. A comparison between the cumulative transport estimates, in their figure 2a and our results, shows a similar pattern and magnitude across the ESPNA. However, it is not expected that the magnitude at each NAC branch and ESC would be the same because of a much shorter (21-month) and different averaging period in the OSNAP data. In the study presented here, the ESC displays a significant transport, which is a contrast to the estimate given in Lozier *et al.*, (2019). This could be caused by the different averaging periods or the coarser sampling resolution along the OSNAP section. Averaging the EEL data across 2 cruise sections (2014 and 2015), which are more comparable to the OSNAP data, results in a ESC transport of ~1 ± 0.2 Sv (not shown). Although this value is smaller than the estimate given by the long-term average, it is still significant.

It may be possible that the altimeter data can provide the high-resolution information missing from the OSNAP array, especially over the important heat pathway of the ESC. The satellite altimetry derived geostrophic velocities do represent the large-scale circulation pattern across the EEL. However, they are unable to resolve the small mesoscale features, especially over the irregular and shallow topography around Rockall-Hatton Bank and Rockall Trough. This is in agreement with other studies from the subpolar North Atlantic (Chafik, Rossby and Schrum, 2014; Rossby *et al.*, 2017; Houpert *et al.*, 2018). The altimeter has an inability to resolve these features because of the lower spatial resolution and the inaccuracy of the geoid over irregular topography (Pujol *et al.*, 2016). By using the new CADT averaged over all cruises, the agreement with the SADCP off-station velocity does not improve. Smoothing the SADCP off-station surface velocity onto the lowest resolution (65 km) needed when comparing with the altimetry, goes some way to reducing the velocity differences and improves the agreement.

It is promising that most of the currents along the EEL are present in the altimeter data. Although, the narrow nature of the eastern boundary current (ESC) means that the altimeter is

unable to capture the flow. This result proves that the altimeter data can provide a reference velocity, except for at the ESC, for the long-term average geostrophic velocity field.

The results provided in this chapter are representative of the long-term mean transports, between 1997 and 2015. Averaging over time is beneficial to filter out noise, such as mesoscale eddies, but we must also make sure that there were no major changes that occurred to the system within the time period. This can be assessed by using the annual winter NAO index as Sarafanov *et al.*, (2012) describes. The winter mean NAO index remains in a neutral phase throughout this study period which may suggest that the circulation state was relatively stable during these observations. However, we have no evidence to support this speculation, and this study is not able to account for any climate-relevant low frequency changes.

# 7 Conclusions and Future Work

## 7.1 Conclusions

This study investigates the eastern subpolar North Atlantic mean circulation and transport and assesses the potential to determine interannual transport variability at the EEL. The EEL dataset provides high quality full-depth hydrographic data near-annually since 1996, spanning two decades (Holliday *et al.*, 2015). Direct velocity measurements, collected regularly at the EEL, provide a previously unknown reference velocity. These hydrographic and direct velocity measurements are used to investigate the mean circulation at the EEL, and along with altimeter data, the potential to determine the interannual variability is assessed.

The first aim of this study was to quantify the long-term mean transport of the currents that shape the AMOC across the EEL. This was achieved using de-tided LADCP data to obtain the time-mean velocity field and its variability. The main currents transporting warm water northwards (NAC branches and ESC) show little change in velocity over time. It is evident that the RHP currents are likely an extension of the southern NAC branch, and not part of the SPF.

The time-mean LADCP dataset was then used to reference the time-mean geostrophic velocity field in order to compute the net volume, temperature and freshwater transport. The long-term mean transport at the EEL was 3.5 ± 0.9 Sv. After confirming that the ideal LSW/ISOW boundary definition for this study was $\sigma_0 = 27.80$ kg m$^{-3}$, the net volume transport was separated into water masses. There was 5.9 ± 1.4 Sv in the upper ocean and –3.3 ± 0.7 Sv in the ISOW. Approximately 0.5 Sv of ISOW appears to have been diapycnally mixed into LSW density class by the time the overflow water reaches the EEL. It was shown that roughly half of upper ocean transport takes place at the RHP. The ESC had a long term mean transport of 2.3 ± 0.5 Sv and with the RHP form key routes for the northward transport of heat. The net temperature transport had a greater dependence on the transport strength than temperature and had a mean of 0.22 ± 0.04 PW. The long-term freshwater transport at the EEL was 44.1 ± 8.8 mSv southwards, with a reference salinity of 35.20.

The second aim of this study was to assess the spatial resolution of the EEL over the slope current North of Scotland. The agreement between the altimeter data and cruise data was compared, which improved when the cruise data was projected on to a similar spatial resolution. It was found that the satellite altimetry derived geostrophic velocities do represent the large-scale

circulation pattern across the EEL. The narrow nature of the ESC means that it is not captured by altimetry. Therefore, it has been determined that altimetry data can be used as a reference velocity at the EEL, except for the slope current. Furthermore, the OSNAP array does not find a significant transport at the ESC, which is most likely because of the coarser spatial resolution. It can be concluded that both the altimeters and the OSNAP array do not resolve the ESC well. This highlights the importance of the higher spatial resolution in the EEL across this important heat pathway.

This study provides improved estimates of the AMOC's mean circulation and transport between Iceland and Scotland, using a level of known motion and excluding modified Atlantic waters. At the ESC and RHP, it is the first time that long-term mean volume transports have been estimated. They are also newly identified as key routes for the transport of heat northwards into the Nordic Sea. It is established that the slope current, an important heat pathway, can only be properly resolved with a high enough sampling spatial resolution, such as at the EEL.

## 7.2 Future work

This study could be developed further by establishing the AMOC at the EEL in density coordinates, because of the widespread presence of diapycnal mixing and the sloping nature of isopycnals in this region (Mercier *et al.*, 2015; Xu, Rhines and Chassignet, 2016; Li *et al.*, 2017; Holliday *et al.*, 2018). It would be beneficial to combine the time-mean transport estimates with the results in Daniault *et al.*, (2016), and to quantify the nearly interannual velocity field and transports at the EEL, using the EEL cruise and altimeter data. The rest of this section describes possible ideas for future work.

It has been suggested, in models, that the AMOC has weakened since the mid-1990's because of a recent decline in the deep-sea densities (e.g. 1000-2500m) in the Labrador Sea (Robson *et al.*, 2014). These deep-sea density anomalies in the Labrador Sea are an indicator of dense water formation. However, the relationship between the AMOC variability and deep-water formation can be impacted by wind-driven changes across the SPNA. The density structure each side of the basin sets the overall shear of the geostrophic circulations (Hirschi *et al.*, 2007). Therefore, the link between AMOC variability and the gradient of the east west density field across the SPNA needs to be investigated, using observational measurements. At the EEL, east SPG, there is over

2 decades of hydrographic data (almost annually from 1996-present), with a similar timeseries, AR7W, in west SPG (almost annually; 1990-present). These datasets can be used to determine the East-West density gradient across the SPG and then compared to the AMOC variability.

# Appendices

## Appendix A: Supplementary material to Chapter 4

# Appendix A: Supplementary material to Chapter 4

**Cruise data distribution**

In this section the EEL cruise data distribution is examined, in order to assess whether there is sufficient spatial distribution to resolve the major circulation features that are expected in the cruise sections. The coverage of data is summarised in **Error! Reference source not found.**.

One test of the suitability of CTD station distribution is to consider the size of the Rossby Radius of Deformation (RRD) at the location of the section. The RRD is 24 km (2 x 12 km) at the EEL, calculated using the internal wave speed divided by the Coriolis parameter (Gill, 1982). This is in agreement with estimates within the literature from the ESPNA (Chelton *et al.*, 1998 (~10 km); Lavender, Brechner Owens and Davis, 2005 (10-20 km)).

The EEL has a planned standard station spacing of 30-50 km, but this is not always achieved because of weather or technical problems. The data distribution for each cruise is shown in Figure A.1. There is a good coverage of CTD data, shown by the CTD stations (black crosses), for the cruises from 2000 onwards. However a large gap in station spacing is found in D31206, ~300 km over the SPF in East Iceland Basin (Figure A.1g) and another one in D24299, ~200 km in West Iceland Basin (Figure A.1i). There is also a gap in D23097 in central Iceland Basin that is roughly ~100km (Figure A.1k). All these gaps are larger than twice the RRD and so mean some part of the circulation was under-resolved. Most cruises have an average station spacing that is better than twice the natural horizontal scale (RRD) of the region, with the exception being the D23398 cruise, with an average station spacing of 42 km (Figure A.1j).

As described in Chapter **Error! Reference source not found.**, the approach to computing total geostrophic transport is to use ADCP data to provide a reference velocity for geostrophic shear, derived from thermal wind. Next, the distribution of ADCP data at each cruise is considered In this text we refer to "on-station" data, which are the data collected while the ship is stationery as a CTD cast is in operation, and "off-station" which are the data collected while the ship is steaming between stations. Between 1997 and 2015, SADCP direct velocity are measured on-station and off-station, which enables a complete dataset across an occupation (red velocity vectors in Figure A.1). Figure A.1 shows that the JC08613 (Figure A.1c), D36511 (Figure A.1d), D35110 (Figure A.1e), D34009 (Figure A.1f) and D24299 (Figure A.1i) cruises have complete

SADCP datasets. The large gap in the SADCP coverage in D31206 (Figure A.1g) corresponds to the CTD station gap. There is a large gap with missing SADCP data in DY03115 (Figure A.1a), covering west Iceland Basin, and in D25301 (Figure A.1h), with data missing across the whole of Rockall Trough. The D23097 (Figure A.1k) and D23398 (Figure A.1j) cruises have a poor level of SADCP completeness with data missing from stations across the section. The distribution of SADCP data does not change much deeper in the water column (Figure A.2), however some data is missing in locations where the water depth is <200 m, e.g. around Rockall Bank. In the sections at 200 m, overall the velocity vectors are smaller. The velocity around shallow topography can be very variable, and possibly includes suspect data, as shown by the individual long velocity vectors in the D36511 (Figure A.2d), D35110 (Figure A.2e), D34009 (Figure A.2f), D23398 (Figure A.2j) and D23097 (Figure A.2k) cruises. This is most likely because of reflections from the seabed. Data at 50 m have high variability in velocity.

**Assessment of S-ADCP and LADCP as reference velocity**

The potential to use LADCP and SADCP as a reference velocity for the geostrophic field at each cruise is assessed in this section. First, the shape of ADCP shear profiles are examined to see how closely they match the shape of the geostrophic shear profiles. For each station pair we have computed the geostrophic shear from thermal wind equations, and LADCP shear which is an average of the two LADCP station profiles, and a SADCP shear which is an average of the off-station SADCP data between the two stations. Plots comparing these profiles are shown in Figure A.3 to Figure A.13.

Figure A.3 to Figure A.13 shows that the agreement between geostrophic and direct velocity shear are good, particularly, where the vertical shear is strong such as in the boundary currents. There is less vertical shear in the interior velocity profiles, but the agreement still holds. There are several profiles where there is no agreement (e.g. at 0.90 m $s^{-1}$ in Figure A.3), likely because the two stations are located within different circulation features. The agreement between LADCP (red line) and SADCP underway (off-station, blue line), is varied. This indicates that the LADCP station-pair average is not always representative of the velocity shear between stations.

The agreement between the geostrophic shear (referenced with best match ADCP data) and the LADCP station pair velocity shear are quantified, using the mean and standard deviation

differences at each depth and for every cruise in Figure A.14 (LADCP station pair profile minus geostrophic profile). In most cruises the mean difference (blue dots) is smallest, close to 0 m $s^{-1}$, between 200m and 2000m. This indicates an agreement in the water column shear between the profiles. There is a larger difference at depth (>1000 m). The standard deviation is order ±0.10 m $s^{-1}$ and, in some cruises (e.g. Figure A.14g), it increases with depth. At the deepest profiles the standard deviation typically decreases because of the reduced sample size.

To evaluate the agreement between the referenced geostrophic velocity shear and the off-station SADCP shear profiles the mean and standard deviation differences at each depth and for every cruise are shown in Figure A.15 (SADCP off-station profile minus geostrophic profile). Like Figure A.14, the mean difference in the profiles lie close to 0 m $s^{-1}$ (<0.05 m $s^{-1}$) below 200 m, showing the agreement in the profiles' water column shear. Below 100 m the standard deviation is typically ±0.10 m $s^{-1}$ (like the LADCP) and is relatively consistent over depth. To summarise, there is no obvious "best choice" between LADCP and off-station SADCP when deciding on a reference velocity. Both have a low mean difference and the same standard deviation, when compared with the geostrophic shear profiles.

Next, the agreement between two SADCP data types, on-station and off-station, and LADCP is quantified. The differences and their standard deviations between the three data types for each occupation and over all depths is in Figure A.16 and Figure A.17. There is an overall mean difference in the velocity shears of < ± 0.05 $ms^{-1}$ between the LADCP and both types of SADCP data (on-station and off-station). The standard deviation is largely consistent with depth at around ± 0.15-0.20 $ms^{-1}$. The average difference and standard deviation between off-station and LADCP velocity shear is slightly lower than difference and standard deviation between on-station and LADCP velocity shear. The standard deviation of 0.15-0.20 $ms^{-1}$ is around 10% of the measured velocity (± 0-2.50 $ms^{-1}$).

**Table A.1** Table to summarise the LADCP and SADCP off-station velocity coverage for each cruise. Details of the data's shortcomings are included.

| Cruise ID | Year | Sufficient coverage for full velocity field (Y/N) | | Shortcoming |
|---|---|---|---|---|
| | | SADCP off-station | LADCP | |
| **DY031** | 2015 | N | Y | Gap in SADCP in west Iceland Basin |
| **JR302** | 2014 | N | Y | Gap in SADCP over Rockall-Hatton Plateau and east Iceland Basin |
| **JC086** | 2013 | Y | Y | |
| **D365** | 2011 | Y | Y | |
| **D351** | 2010 | Y | Y | |
| **D340a** | 2009 | Y | Y | |
| **D312** | 2006 | N | N | ~300 km gap in station spacing in east Iceland Basin |
| **D253** | 2001 | N | Y | Gap in SADCP over the whole of Rockall Trough |
| **D242** | 1999 | N | N | ~200 km gap in station spacing in west Iceland Basin |
| **D233** | 1998 | N | N | ~40 km average station spacing |
| **D230** | 1997 | N | N | ~100km gap in station spacing in central Iceland Basin |

a.

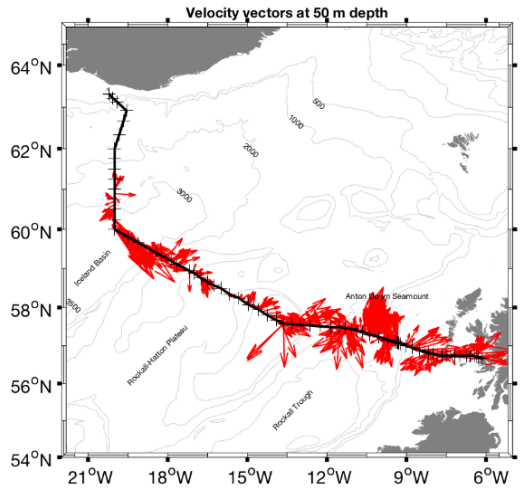
Velocity vectors at 50 m depth
64°N
62°N
60°N
58°N
56°N
54°N
21°W
18°W
15°W
12°W
9°W
6°W
500
1000
2000
3000
Iceland Basin
Rockall-Hatton Plateau
Rockall Trough
Anton Dohrn Seamount

b.

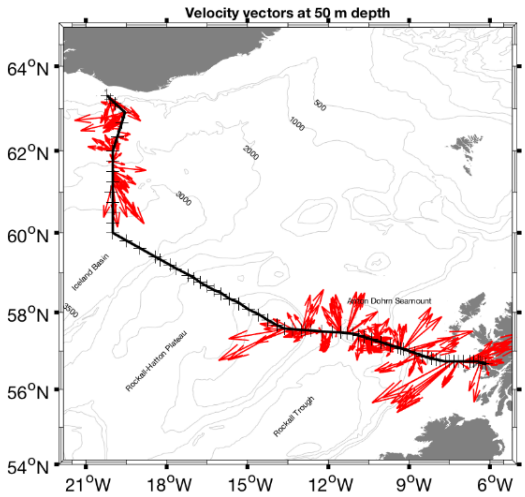
Velocity vectors at 50 m depth
64°N
62°N
60°N
58°N
56°N
54°N
21°W
18°W
15°W
12°W
9°W
6°W
500
1000
2000
3000
Iceland Basin
Rockall-Hatton Plateau
Rockall Trough
Anton Dohrn Seamount

c.

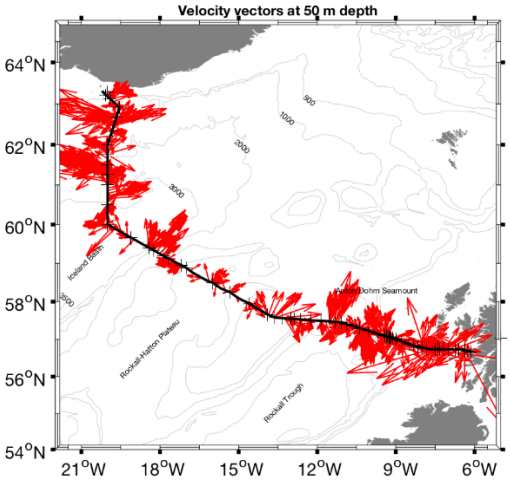
Velocity vectors at 50 m depth
64°N
62°N
60°N
58°N
56°N
54°N
21°W
18°W
15°W
12°W
9°W
6°W
500
1000
2000
3000
Iceland Basin
Rockall-Hatton Plateau
Rockall Trough
Anton Dohrn Seamount

d.

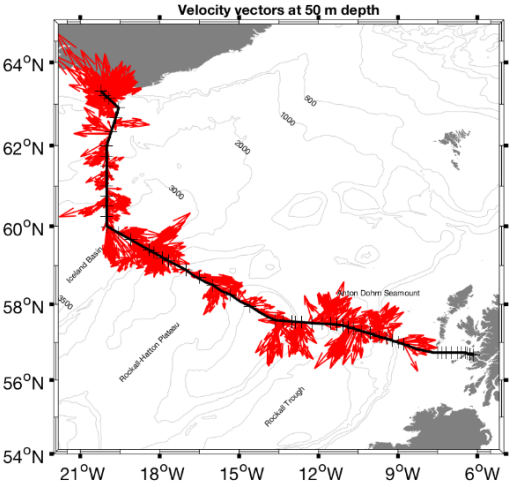
Velocity vectors at 50 m depth
64°N
62°N
60°N
58°N
56°N
54°N
21°W
18°W
15°W
12°W
9°W
6°W
500
1000
2000
3000
Iceland Basin
Rockall-Hatton Plateau
Rockall Trough
Anton Dohrn Seamount

e.

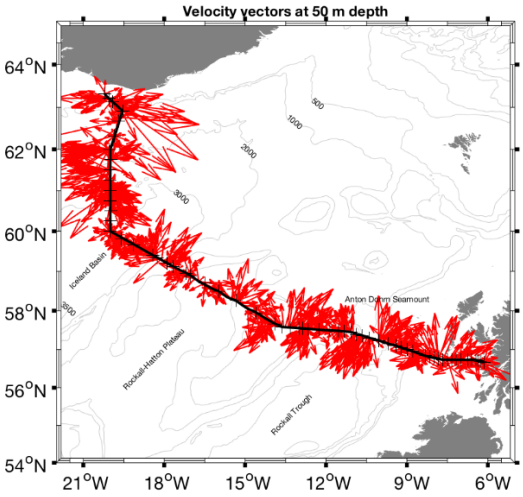
Velocity vectors at 50 m depth
64°N
62°N
60°N
58°N
56°N
54°N
21°W
18°W
15°W
12°W
9°W
6°W
500
1000
2000
3000
Iceland Basin
Rockall-Hatton Plateau
Rockall Trough
Anton Dohrn Seamount

f.

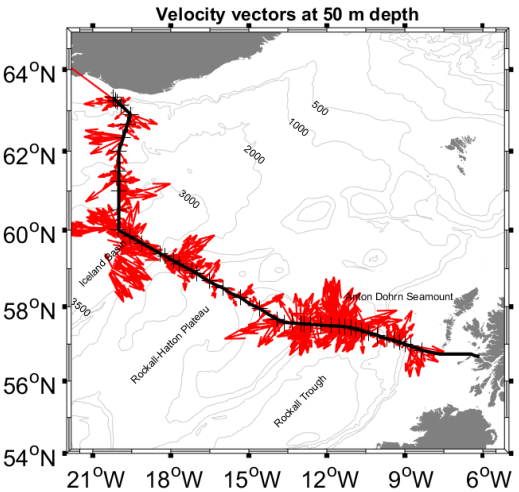
Velocity vectors at 50 m depth
64°N
62°N
60°N
58°N
56°N
54°N
21°W
18°W
15°W
12°W
9°W
6°W
500
1000
2000
3000
Iceland Basin
Rockall-Hatton Plateau
Rockall Trough
Anton Dohrn Seamount

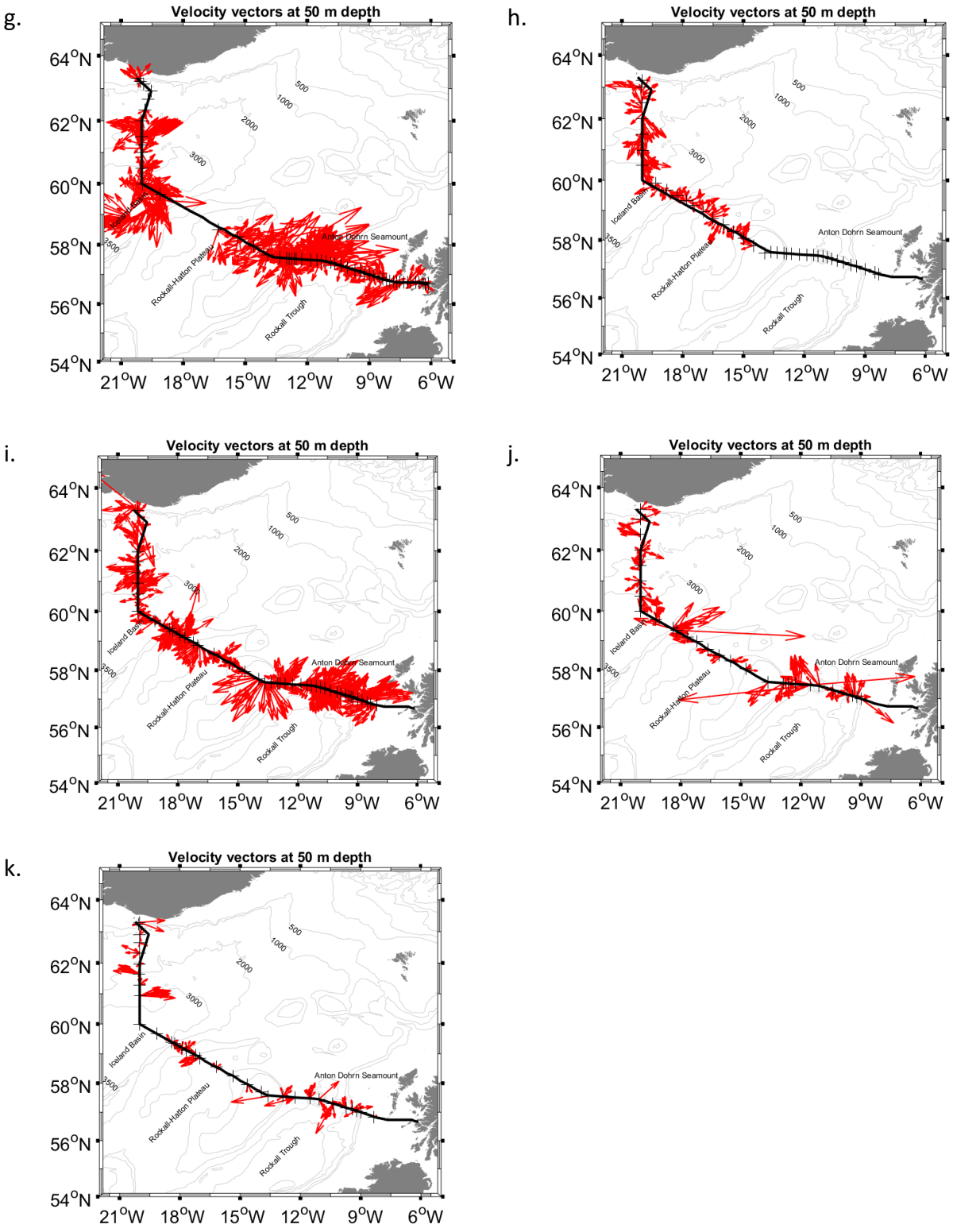


**Figure A.1** Along track SADCP (as red velocity vectors) at 50 m for each cruise: **a.** dy03115, **b.** jr30214**, c.** jc08613, **d.** d36511**, e.** d35110**, f.** d34009, **g.** d31206, **h**. d25301**, i.** d24299**, j**. d23398 and **k**. d23097. The black crosses represent CTD station spacing and the bold line shows the Extended Ellett Line track.

a

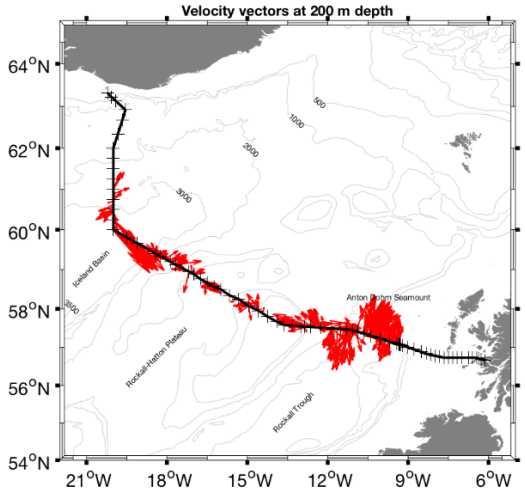
Velocity vectors at 200 m depth
64°N
62°N
60°N
58°N
56°N
54°N
21°W
18°W
15°W
12°W
9°W
6°W
500
1000
2000
3000
3500
Iceland Basin
Rockall-Hatton Plateau
Rockall Trough
Anton Dohrn Seamount

b

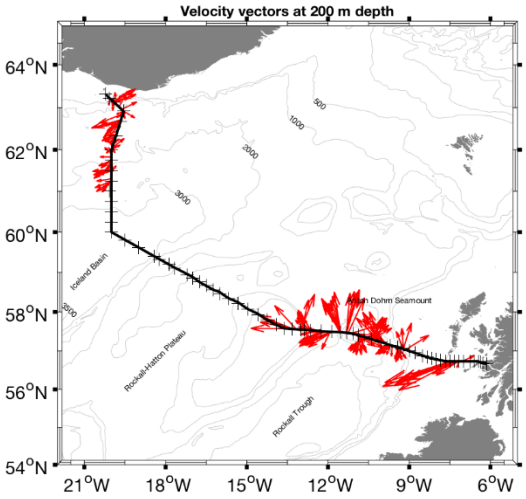
Velocity vectors at 200 m depth
64°N
62°N
60°N
58°N
56°N
54°N
21°W
18°W
15°W
12°W
9°W
6°W
500
1000
2000
3000
3500
Iceland Basin
Rockall-Hatton Plateau
Rockall Trough
Anton Dohrn Seamount

c

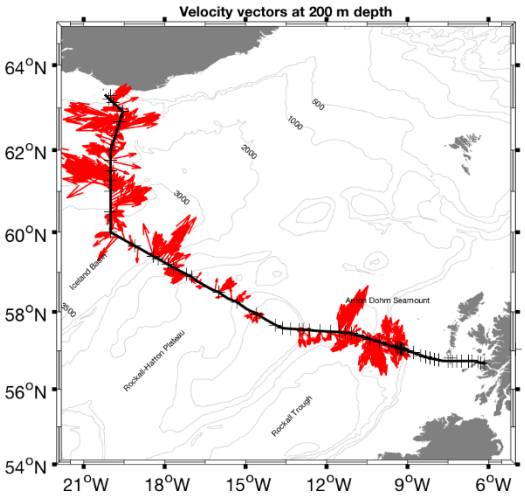
Velocity vectors at 200 m depth
64°N
62°N
60°N
58°N
56°N
54°N
21°W
18°W
15°W
12°W
9°W
6°W
500
1000
2000
3000
3500
Iceland Basin
Rockall-Hatton Plateau
Rockall Trough
Anton Dohrn Seamount

d

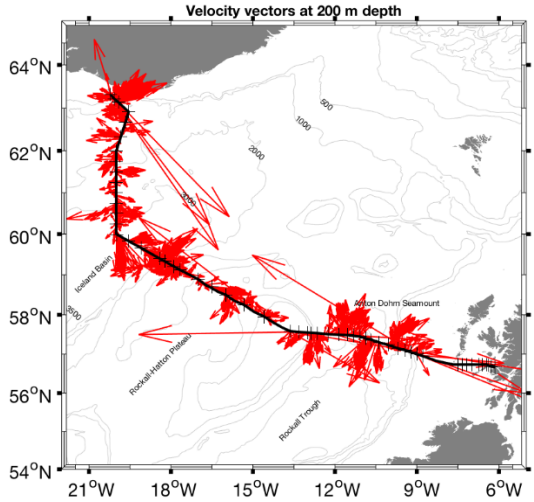
Velocity vectors at 200 m depth
64°N
62°N
60°N
58°N
56°N
54°N
21°W
18°W
15°W
12°W
9°W
6°W
500
1000
2000
3000
3500
Iceland Basin
Rockall-Hatton Plateau
Rockall Trough
Anton Dohrn Seamount

e

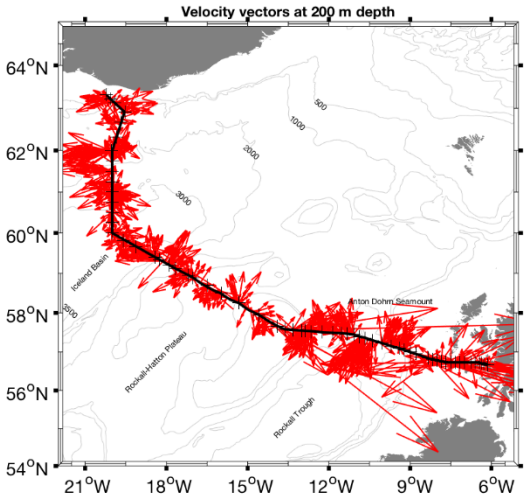
Velocity vectors at 200 m depth
64°N
62°N
60°N
58°N
56°N
54°N
21°W
18°W
15°W
12°W
9°W
6°W
500
1000
2000
3000
3500
Iceland Basin
Rockall-Hatton Plateau
Rockall Trough
Anton Dohrn Seamount

f

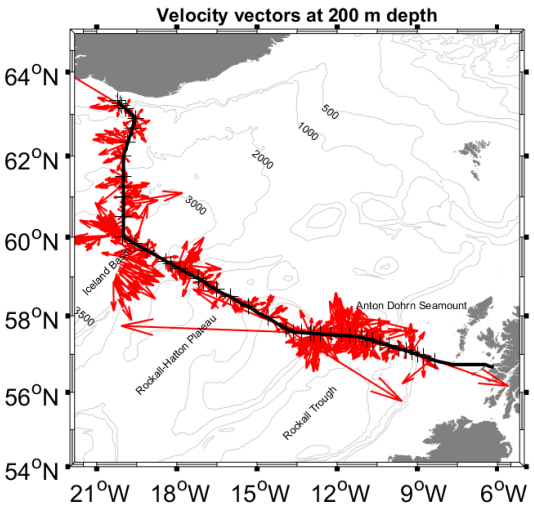
Velocity vectors at 200 m depth
64°N
62°N
60°N
58°N
56°N
54°N
21°W
18°W
15°W
12°W
9°W
6°W
500
1000
2000
3000
3500
Iceland Basin
Rockall-Hatton Plateau
Rockall Trough
Anton Dohrn Seamount

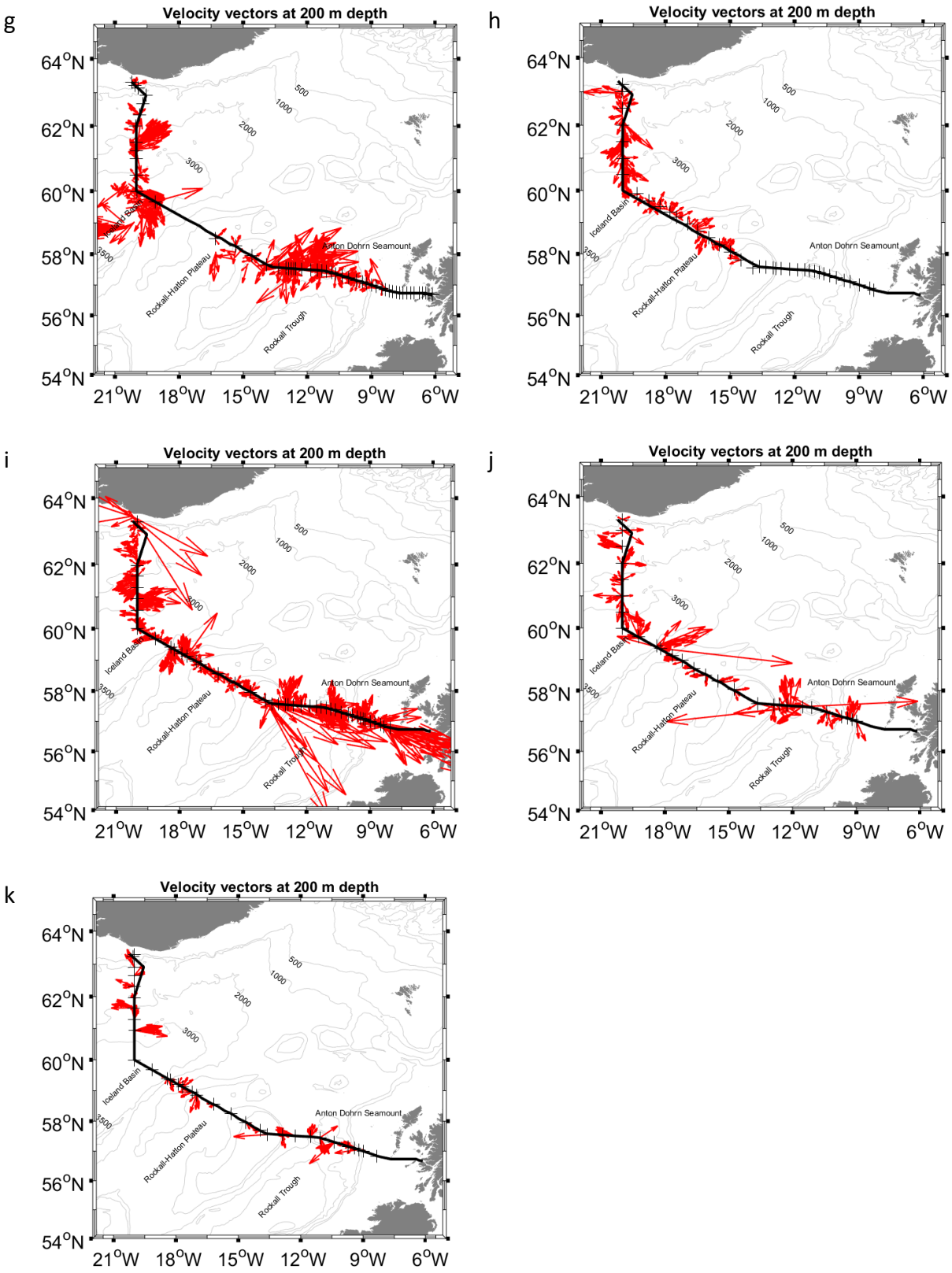


**Figure A.2** Along track SADCP (as red velocity vectors) at 200 m for each cruise: **a.** dy03115, **b**. jr30214, **c**. jc08613, **d**. d36511, **e**. d35110, **f**. d34009, **g**. d31206, **h.** d25301, **i.** d24299, **j**. d23398 and **k.** d23097. The black crosses represent CTD station spacing and the bold line shows the Extended Ellett Line track.

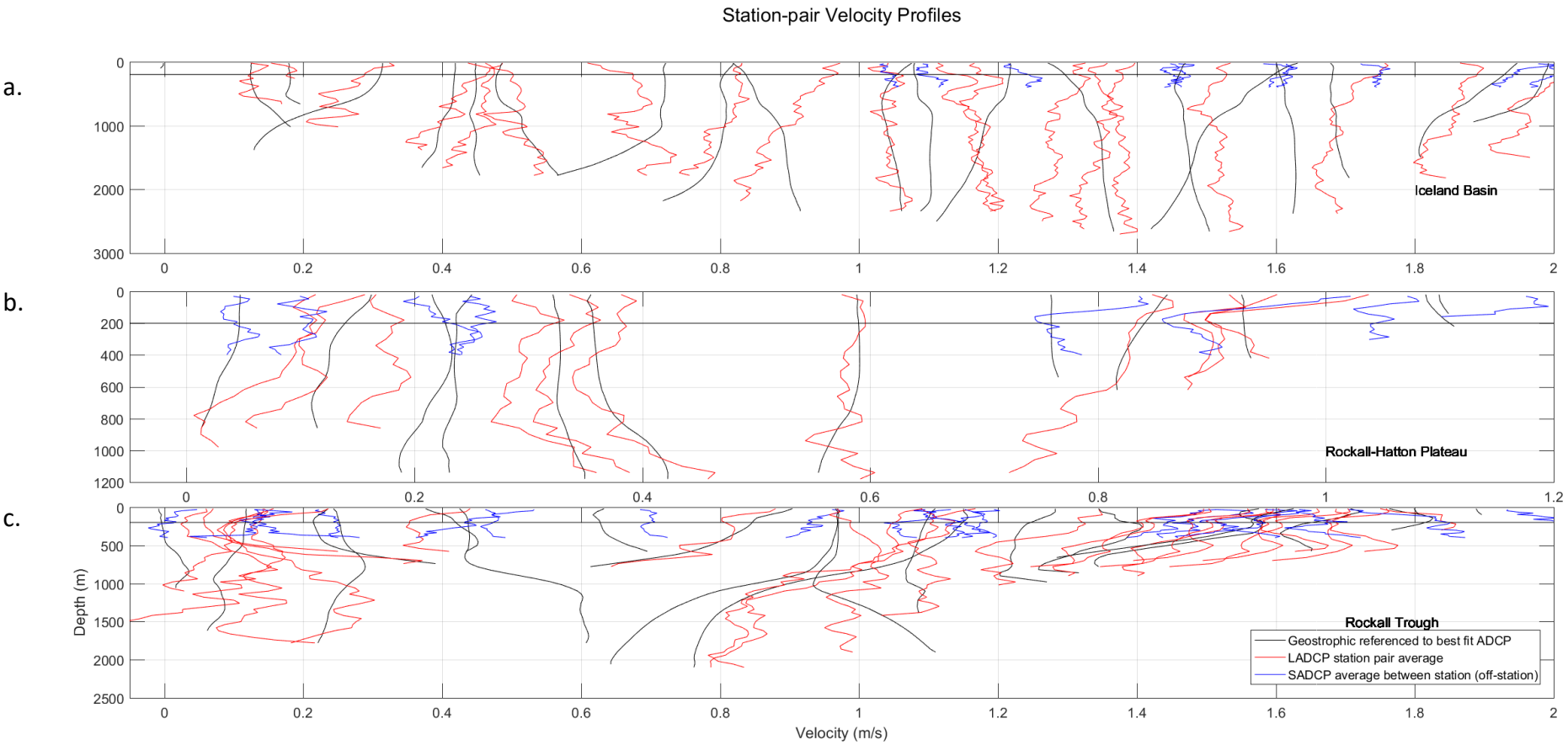


**Figure A.3** Station-pair velocity profiles for cruise dy03115, where each station-pair profile has been offset by 0.1 m $s^{-1}$. The full EEL is split into **a.** Iceland Basin, **b.** Rockall- Hatton Plateau and **c.** Rockall Trough.

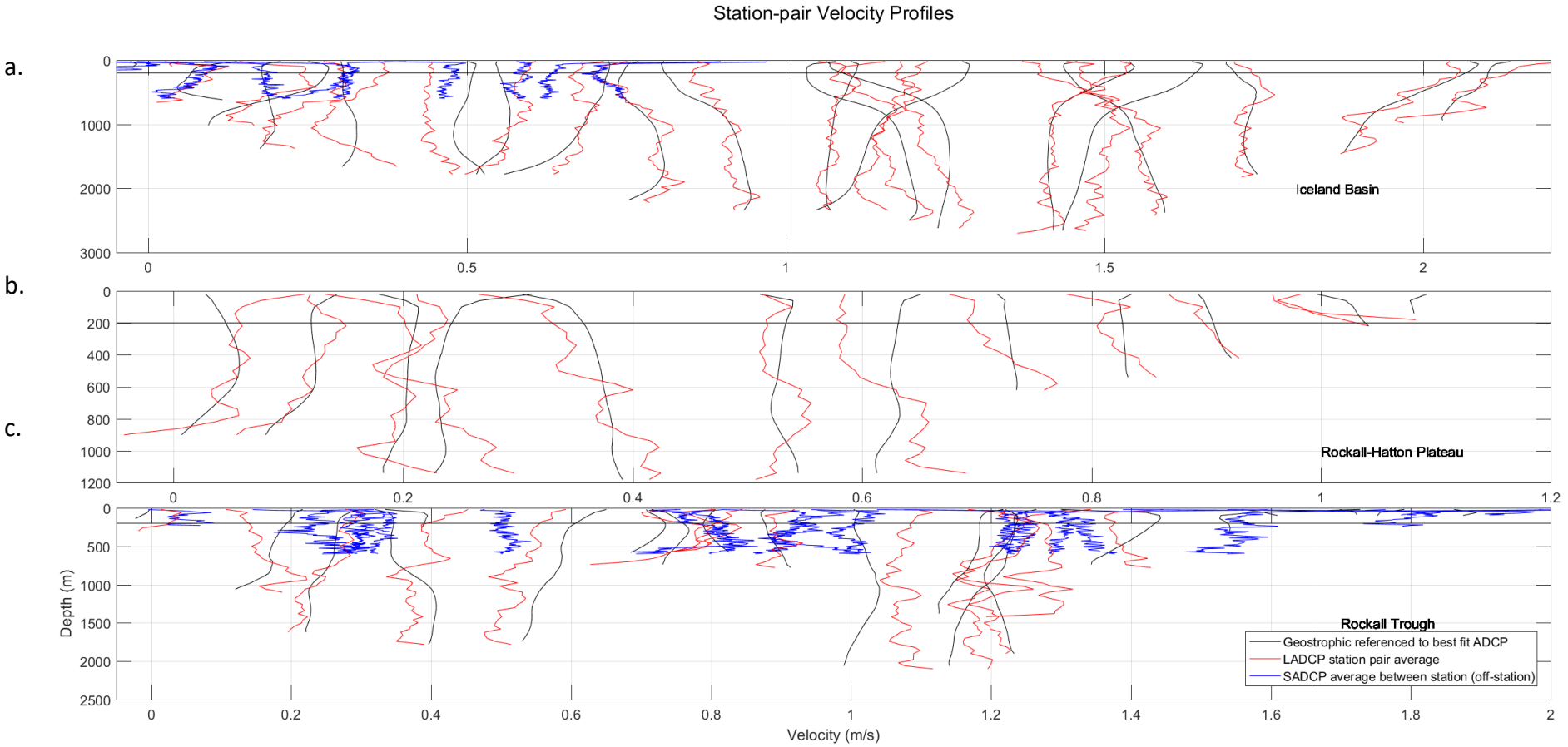


**Figure A.4** Station-pair velocity profiles for cruise jr30214, where each station-pair profile has been offset by 0.1 m $s^{-1}$. The full EEL is split into **a.** Iceland Basin**, b.** Rockall- Hatton Plateau and **c.** Rockall Trough.

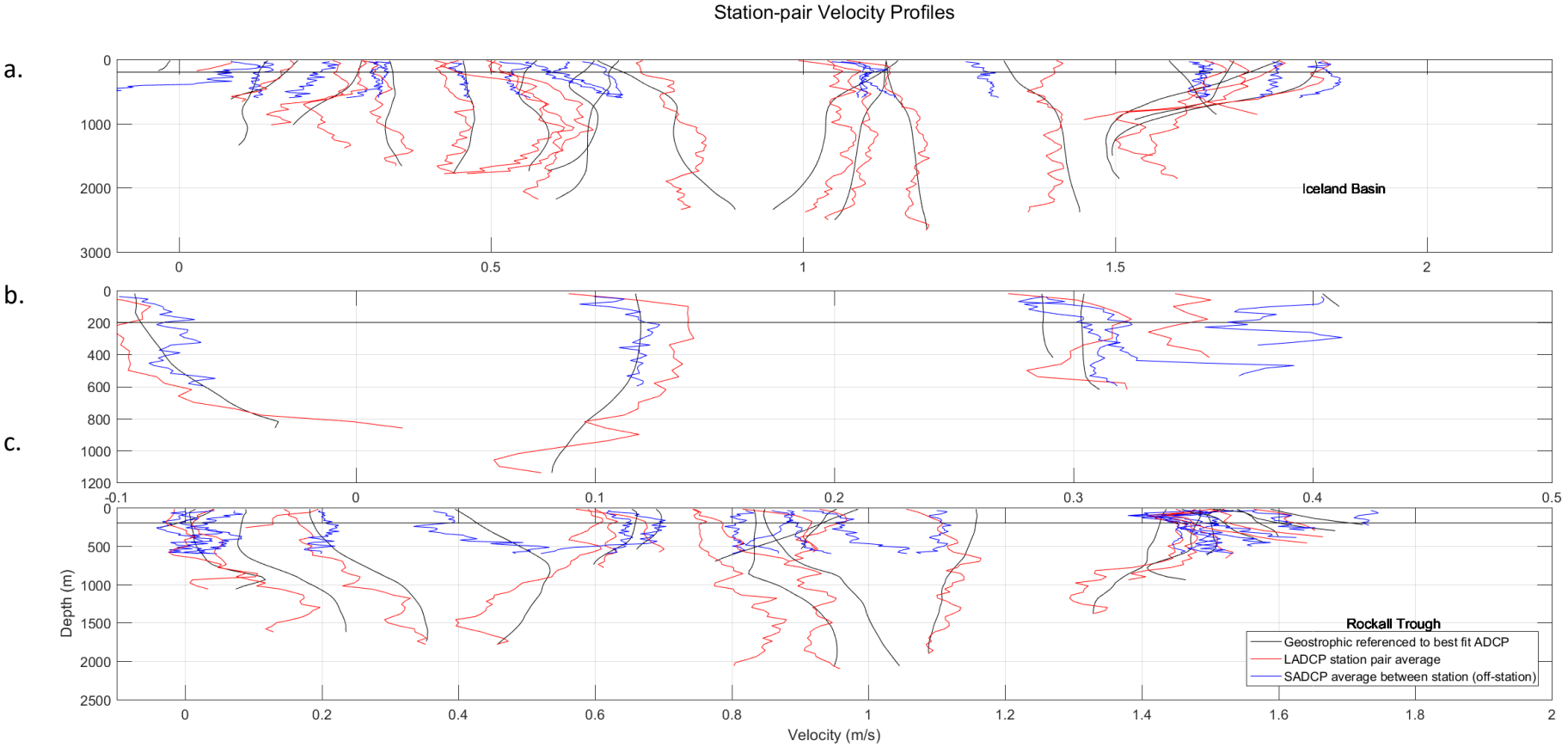


**Figure A.5** Station-pair velocity profiles for cruise jc08613, where each station-pair profile has been offset by 0.1 m $s^{-1}$. The full EEL is split into **a.** Iceland Basin, **b**. Rockall- Hatton Plateau and **c**. Rockall Trough.

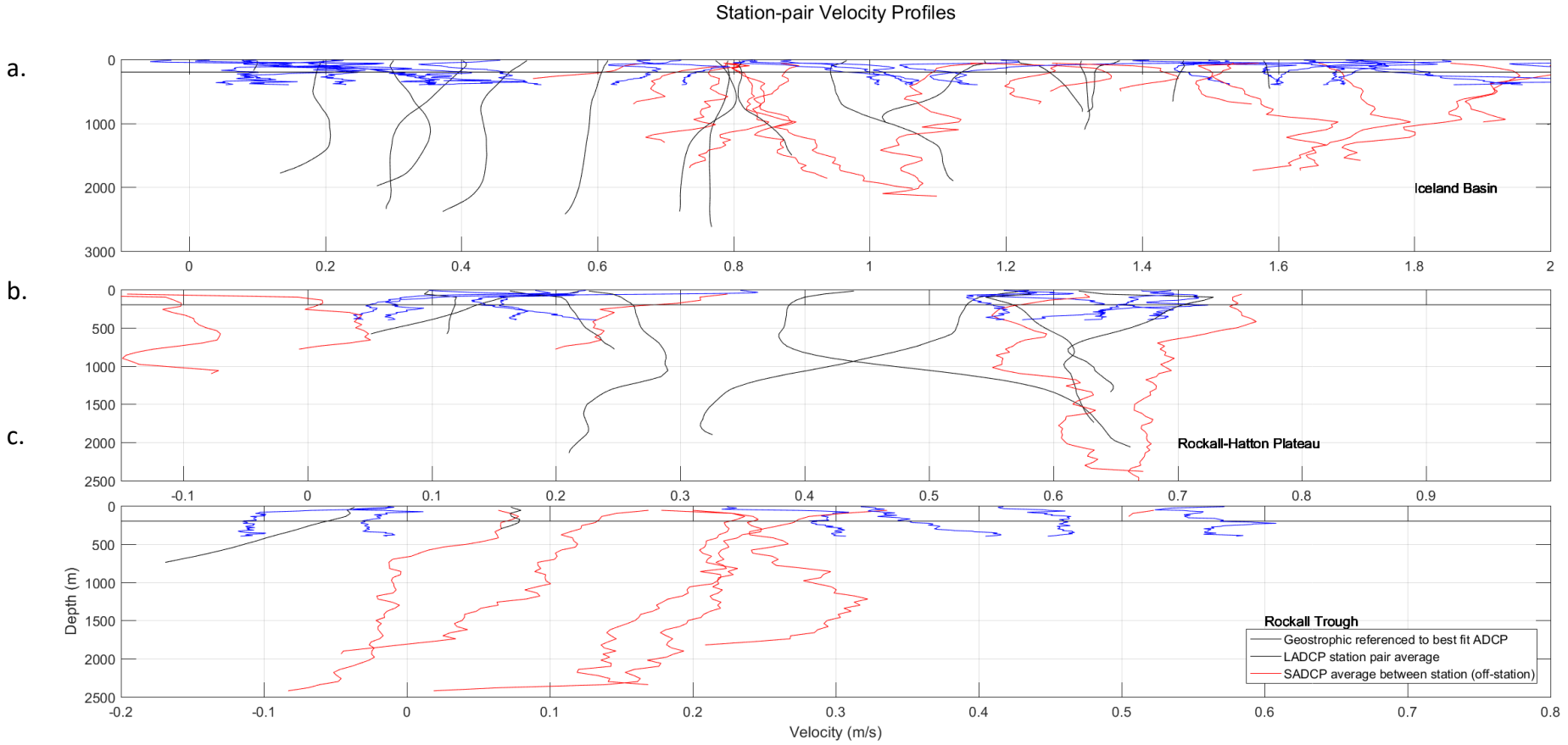


**Figure A.6** Station-pair velocity profiles for cruise d36511, where each station-pair profile has been offset by 0.1 m $s^{-1}$. The full EEL is split into **a.** Iceland Basin, **b**. Rockall- Hatton Plateau and **c.** Rockall Trough.

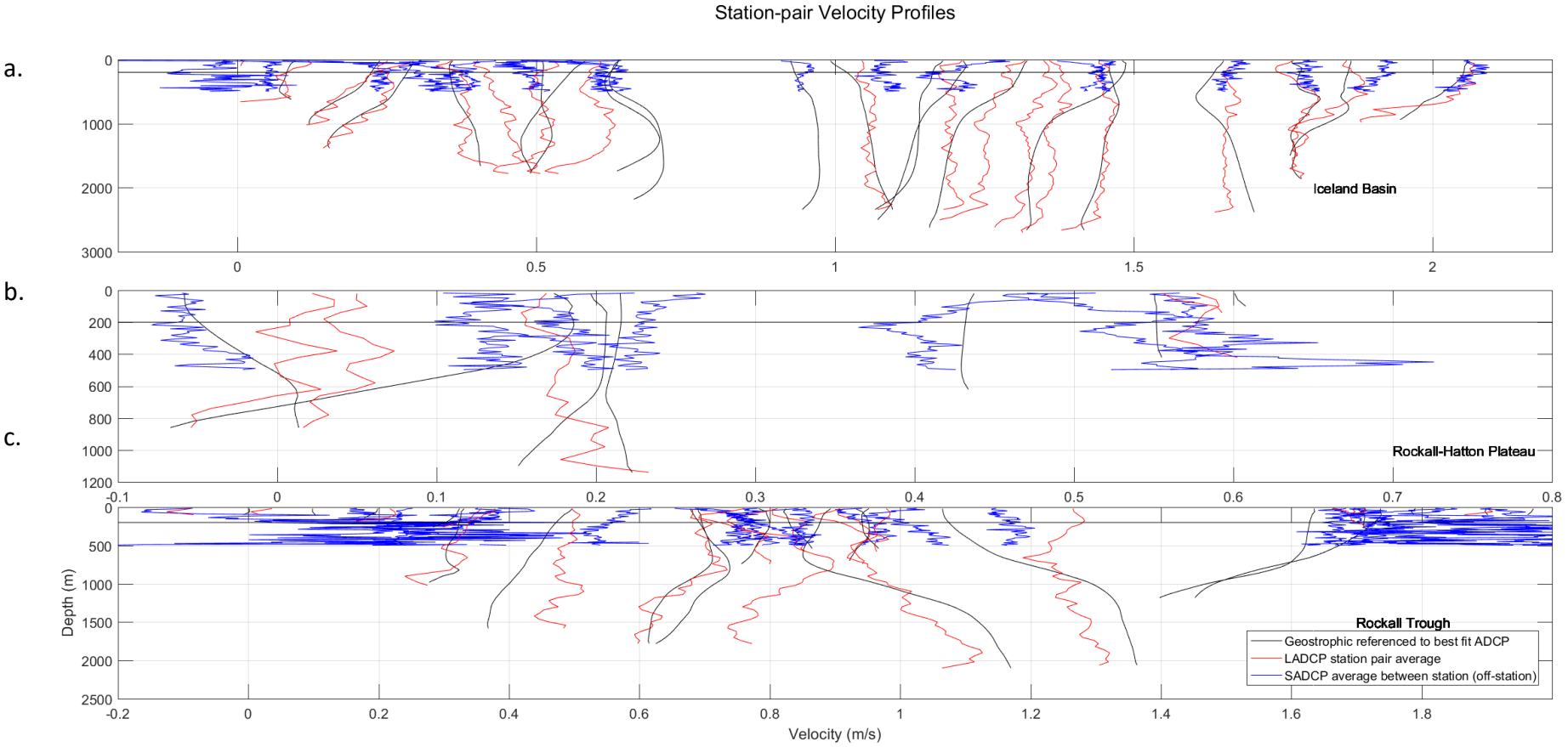


**Figure A.7** Station-pair velocity profiles for cruise d35110, where each station-pair profile has been offset by 0.1 m $s^{-1}$. The full EEL is split into **a**. Iceland Basin, **b.** Rockall- Hatton Plateau and **c**. Rockall Trough.

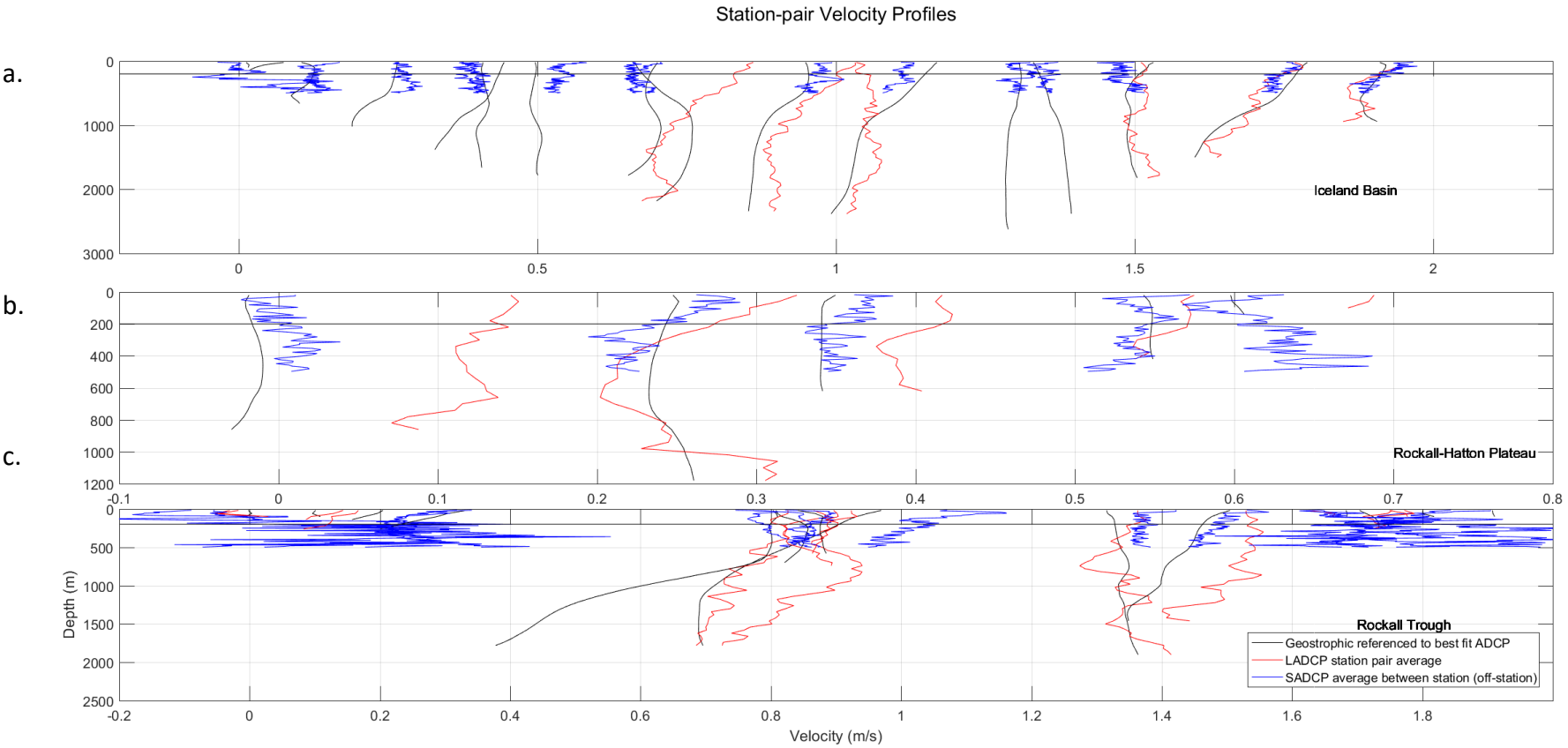


**Figure A.8** Station-pair velocity profiles for cruise d34009, where each station-pair profile has been offset by 0.1 m $s^{-1}$. The full EEL is split into **a.** Iceland Basin, **b**. Rockall-Hatton Plateau and **c.** Rockall Trough.

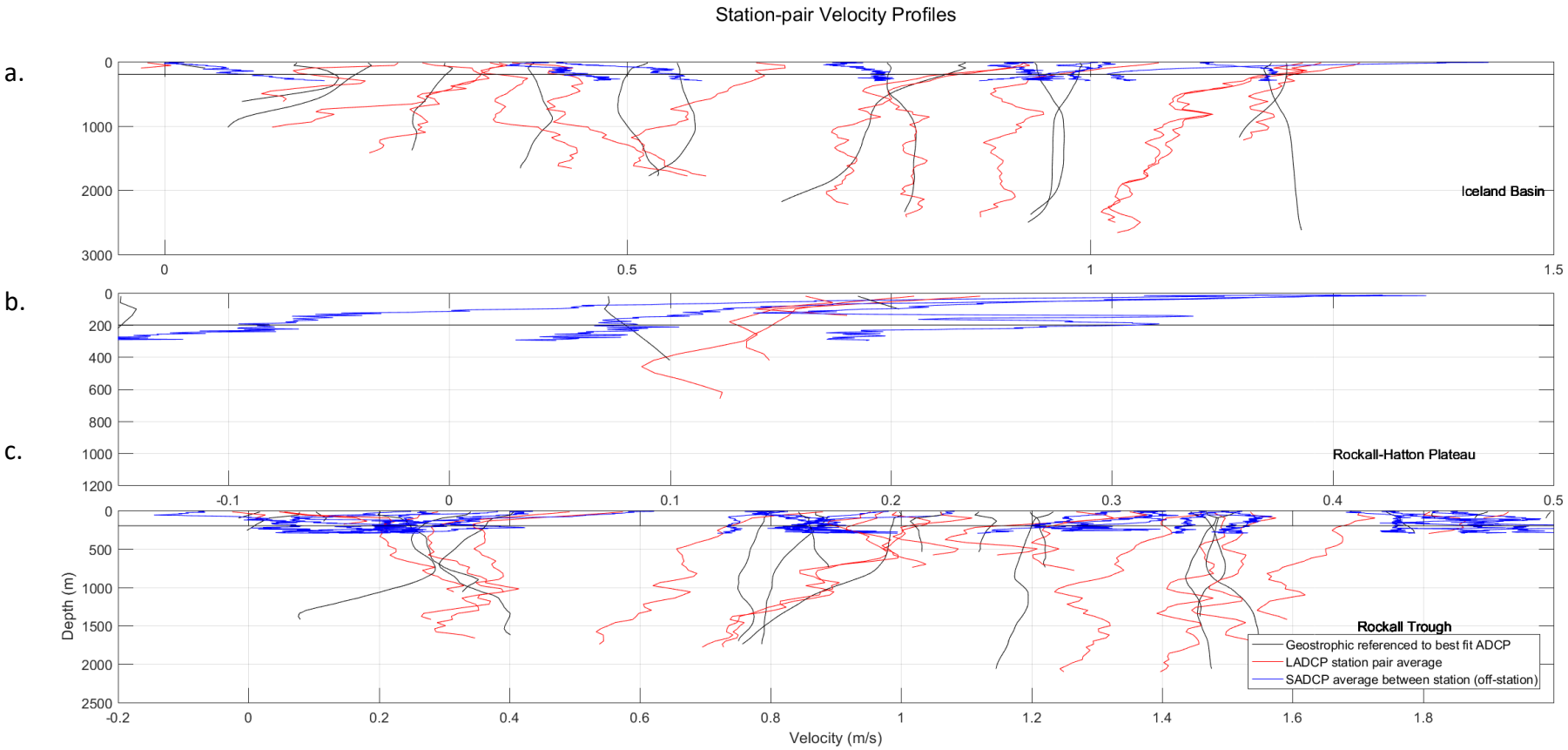


**Figure A.9** Station-pair velocity profiles for cruise d31206, where each station-pair profile has been offset by 0.1 m $s^{-1}$. The full EEL is split into **a.** Iceland Basin, **b**. Rockall- Hatton Plateau and **c.** Rockall Trough.

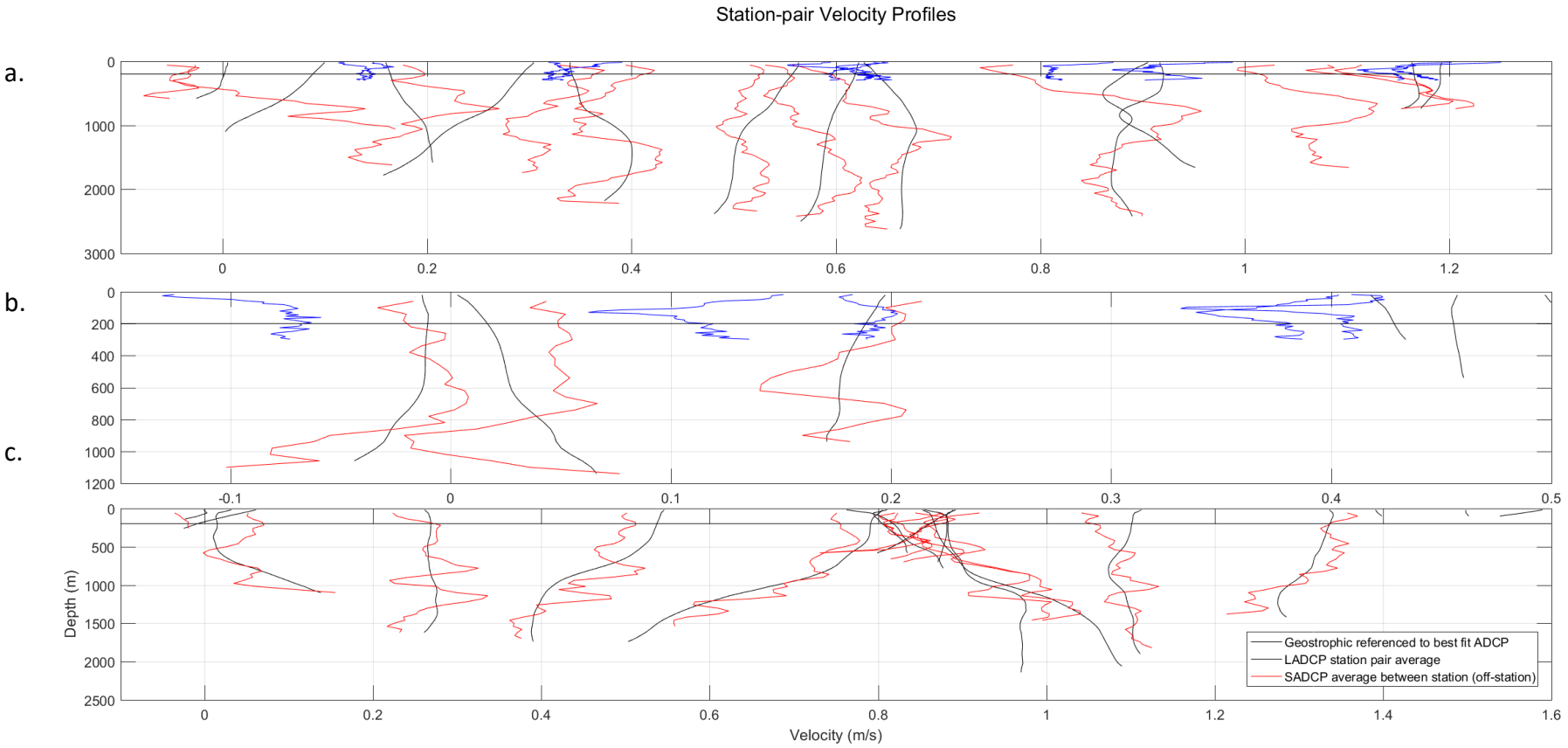


**Figure A.10** Station-pair velocity profiles for cruise d25301, where each station-pair profile has been offset by 0.1 m $s^{-1}$. The full EEL is split into **a.** Iceland Basin, **b.** Rockall-Hatton Plateau and **c**. Rockall Trough.

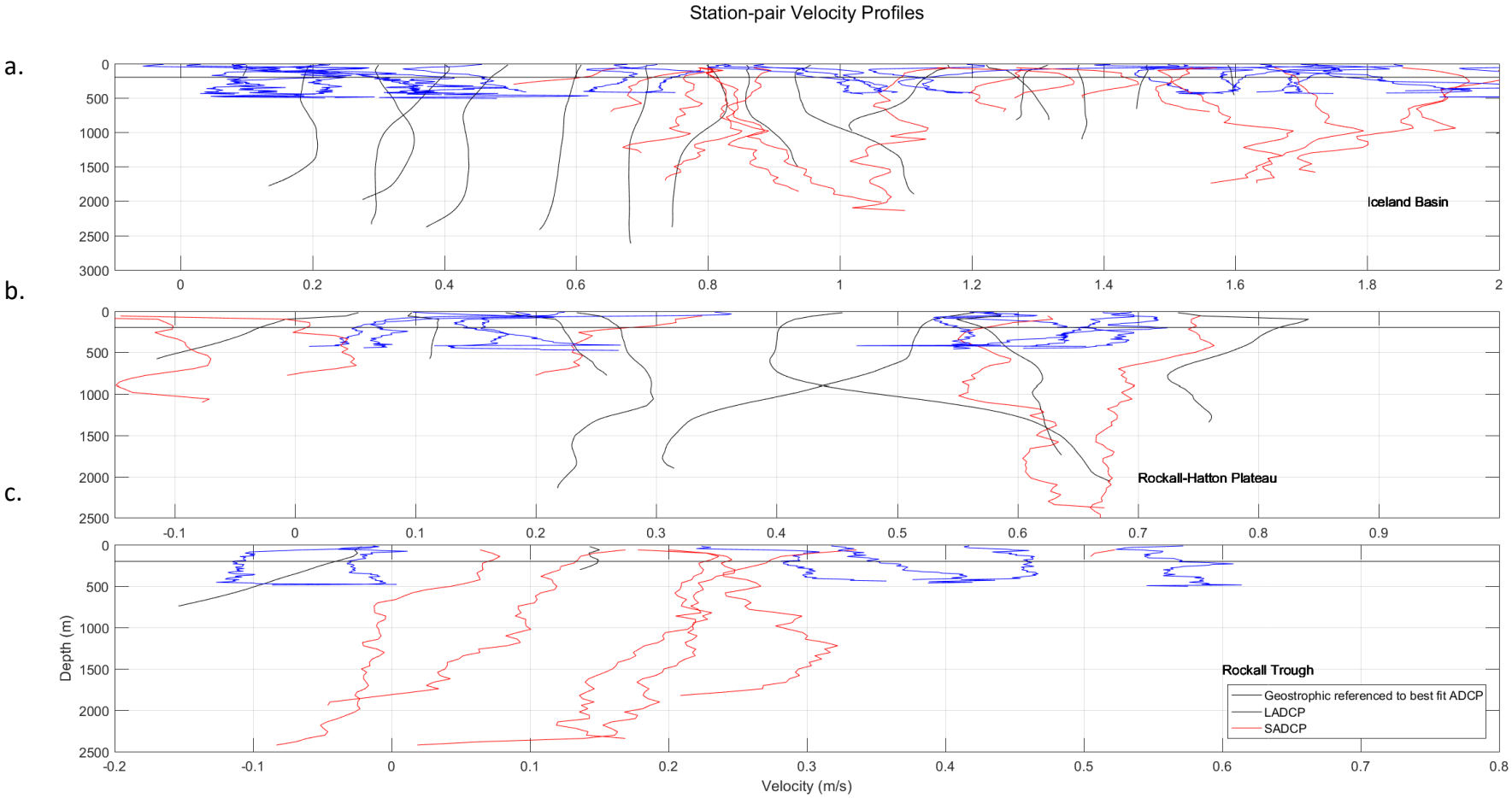


**Figure A.11** Station-pair velocity profiles for cruise d24299, where each station-pair profile has been offset by 0.1 m $s^{-1}$. The full EEL is split into **a.** Iceland Basin, **b.** Rockall-Hatton Plateau and **c.** Rockall Trough.

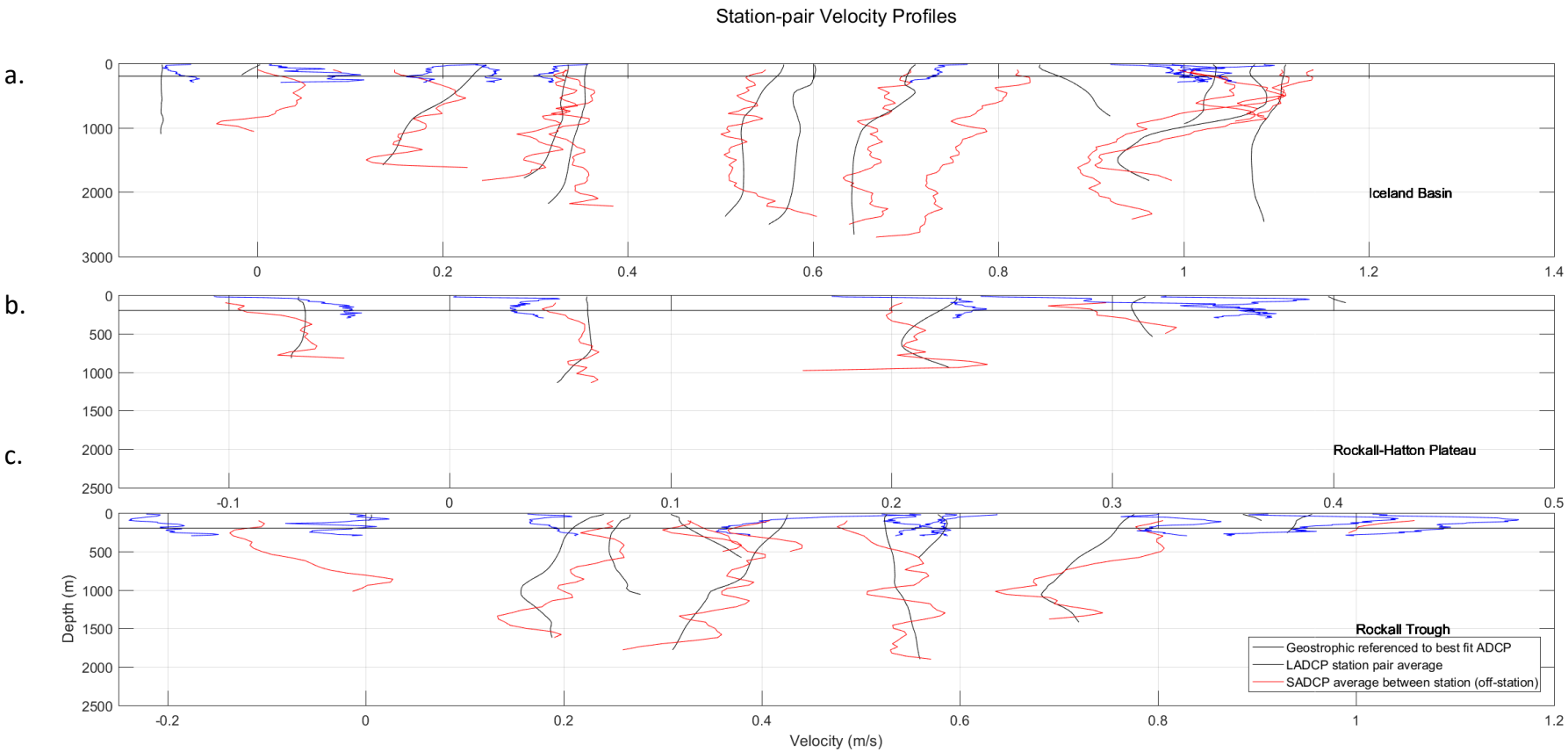


**Figure A.12** Station-pair velocity profiles for cruise d23398, where each station-pair profile has been offset by 0.1 m $s^{-1}$. The full EEL is split into **a.** Iceland Basin, **b.** Rockall-Hatton Plateau and **c**. Rockall Trough.

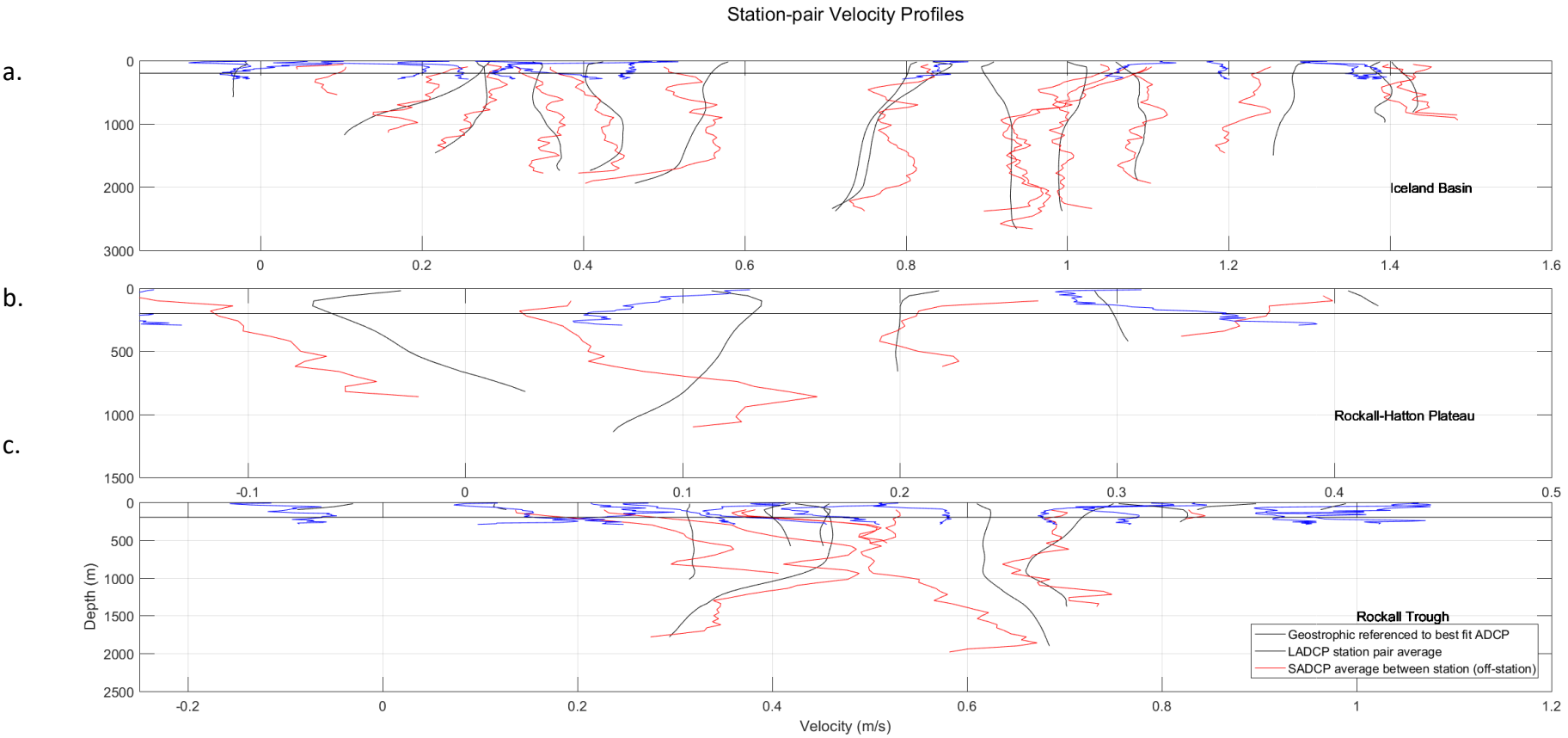


**Figure A.13** Station-pair velocity profiles for cruise d23097, where each station-pair profile has been offset by 0.1 m $s^{-1}$. The full EEL is split into **a.** Iceland Basin, **b**. Rockall-Hatton Plateau and **c.** Rockall Trough.

a.

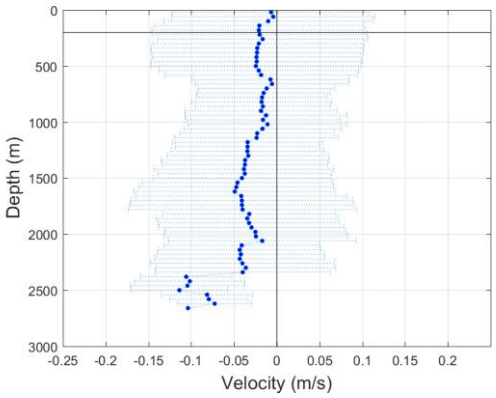
Depth (m)
0
500
1000
1500
2000
2500
3000
-0.25 -0.2 -0.15 -0.1 -0.05 0 0.05 0.1 0.15 0.2
Velocity (m/s)

b.

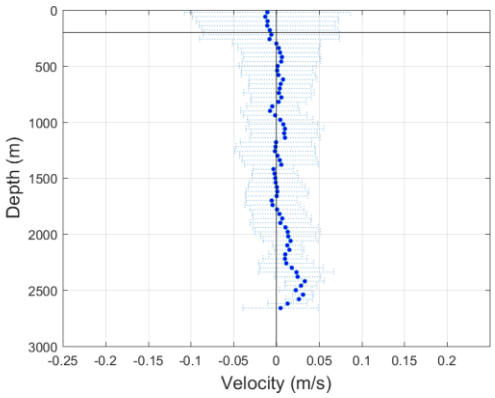
Depth (m)
0
500
1000
1500
2000
2500
3000
-0.25 -0.2 -0.15 -0.1 -0.05 0 0.05 0.1 0.15 0.2
Velocity (m/s)

c.

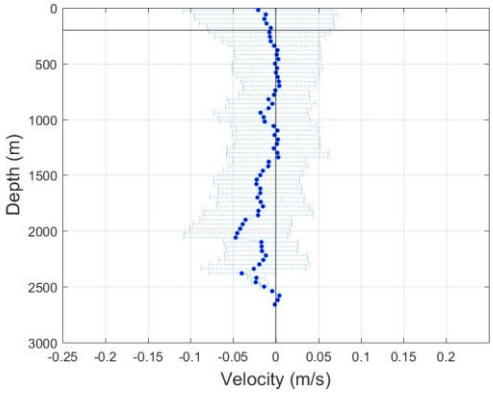
Depth (m)
0
500
1000
1500
2000
2500
3000
-0.25 -0.2 -0.15 -0.1 -0.05 0 0.05 0.1 0.15 0.2
Velocity (m/s)

d.

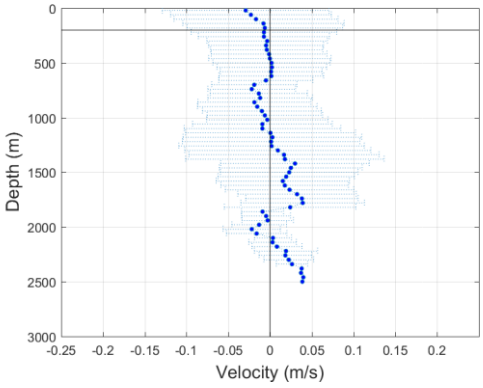
Depth (m)
0
500
1000
1500
2000
2500
3000
-0.25 -0.2 -0.15 -0.1 -0.05 0 0.05 0.1 0.15 0.2
Velocity (m/s)

e.

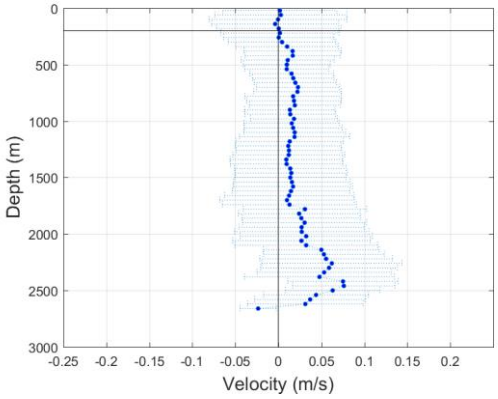
Depth (m)
0
500
1000
1500
2000
2500
3000
-0.25 -0.2 -0.15 -0.1 -0.05 0 0.05 0.1 0.15 0.2
Velocity (m/s)

f.

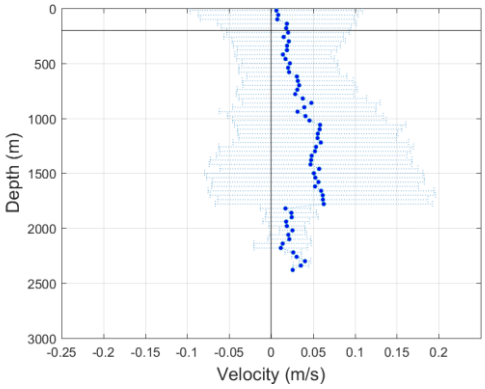
Depth (m)
0
500
1000
1500
2000
2500
3000
-0.25 -0.2 -0.15 -0.1 -0.05 0 0.05 0.1 0.15 0.2
Velocity (m/s)

g.

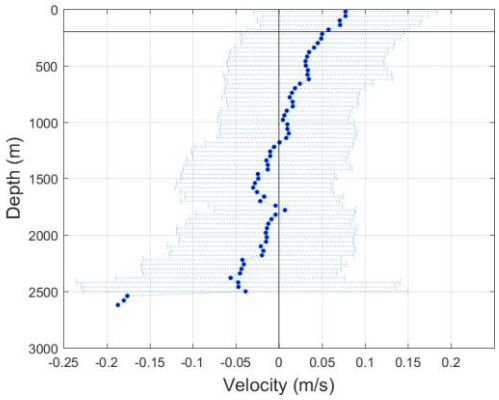


h.

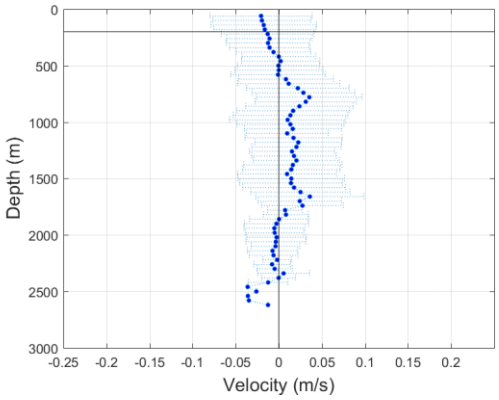


i.

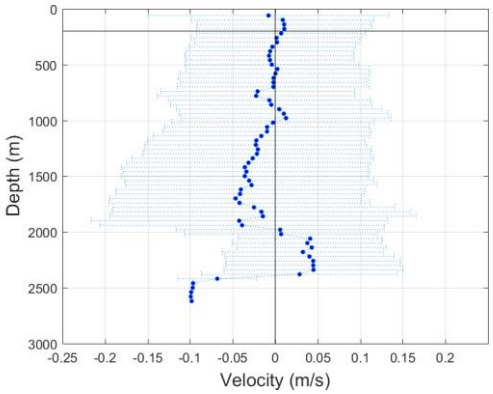


j.

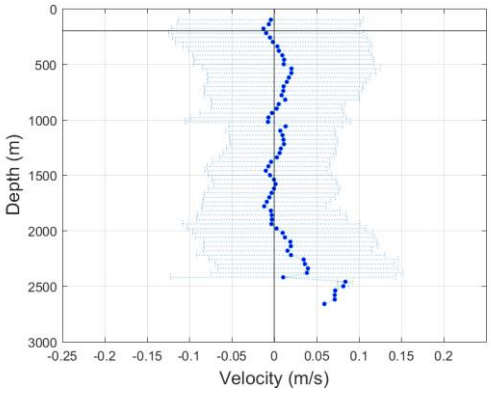


k.

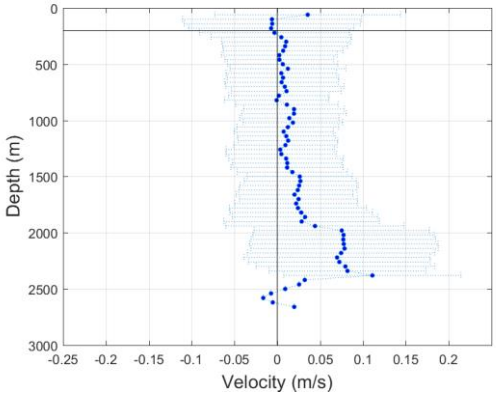


**Figure A.14** Average difference (dots) and standard deviation (bars) between the geostrophic and the LADCP station-pair velocity, across each cruise. **a.-k**. matches the cruise order in **Figure A.1**.

a.

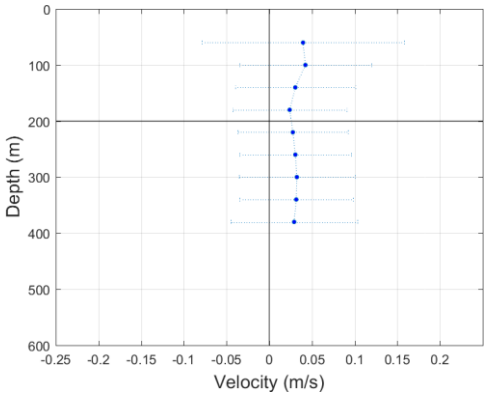
Depth (m)
0
100
200
300
400
500
600
-0.25 -0.2 -0.15 -0.1 -0.05 0 0.05 0.1 0.15 0.2
Velocity (m/s)

b.

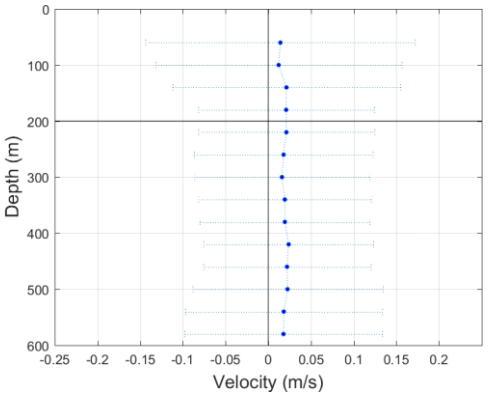
Depth (m)
0
100
200
300
400
500
600
-0.25 -0.2 -0.15 -0.1 -0.05 0 0.05 0.1 0.15 0.2
Velocity (m/s)

c.

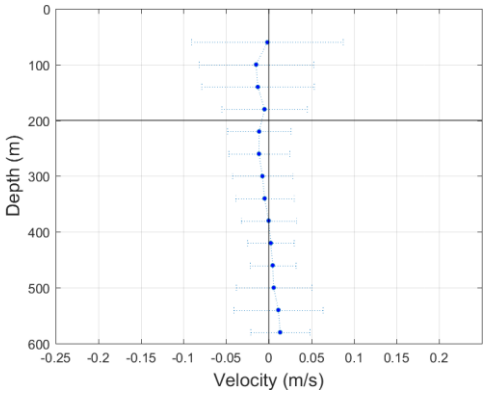
Depth (m)
0
100
200
300
400
500
600
-0.25 -0.2 -0.15 -0.1 -0.05 0 0.05 0.1 0.15 0.2
Velocity (m/s)

d.

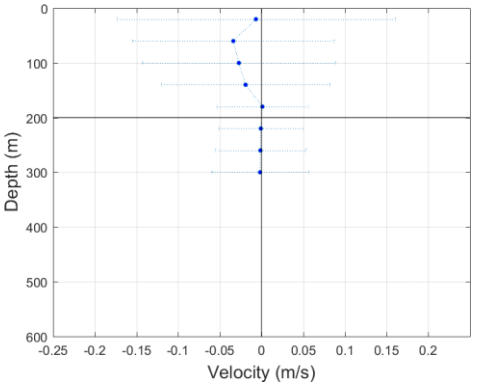
Depth (m)
0
100
200
300
400
500
600
-0.25 -0.2 -0.15 -0.1 -0.05 0 0.05 0.1 0.15 0.2
Velocity (m/s)

e.

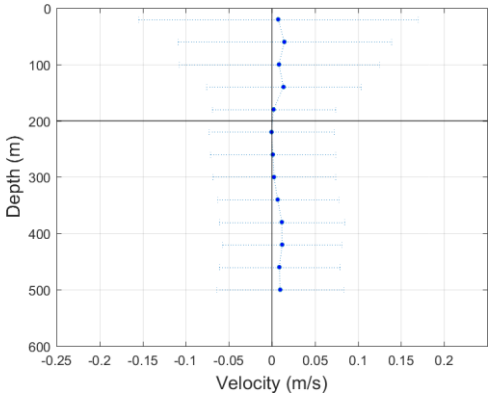
Depth (m)
0
100
200
300
400
500
600
-0.25 -0.2 -0.15 -0.1 -0.05 0 0.05 0.1 0.15 0.2
Velocity (m/s)

f.

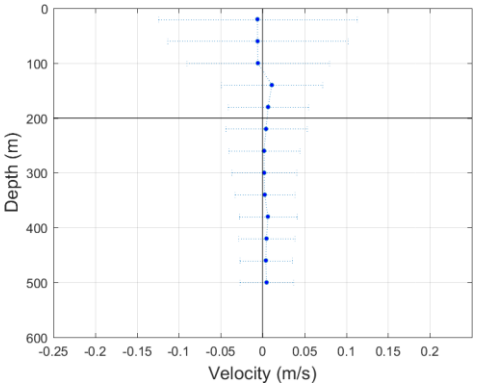
Depth (m)
0
100
200
300
400
500
600
-0.25 -0.2 -0.15 -0.1 -0.05 0 0.05 0.1 0.15 0.2
Velocity (m/s)

g.

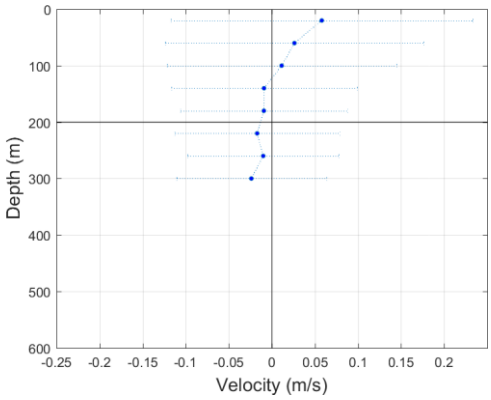


h.

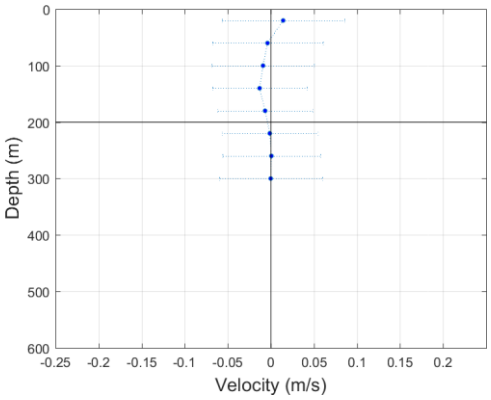


i.

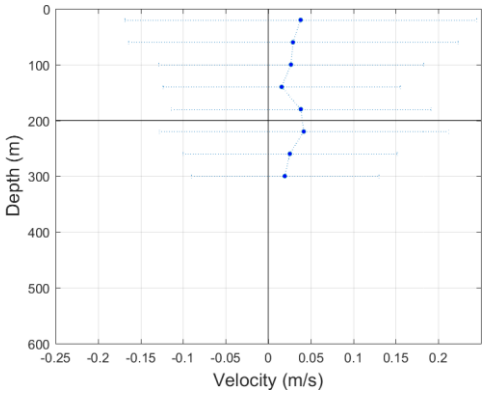


j.

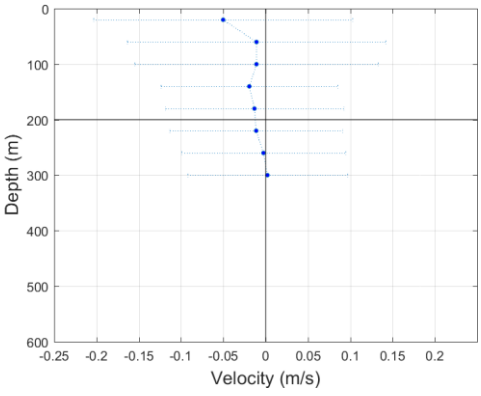


k.

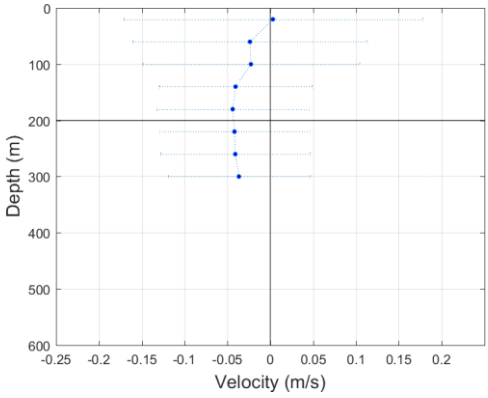


**Figure A.15** Average difference (dots) and standard deviation (bars) between the geostrophic and the SADCP along-track station-pair velocity, across each cruise**. a.-k.** matches the cruise order in **Figure A.1.**

a.

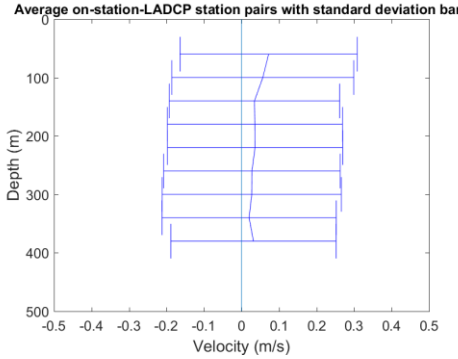
Average on-station-LADCP station pairs with standard deviation bars
Depth (m)
Velocity (m/s)

b.

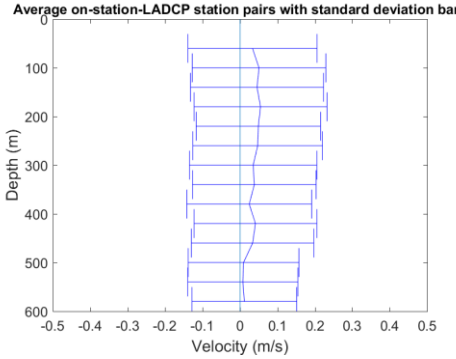
Average on-station-LADCP station pairs with standard deviation bars
Depth (m)
Velocity (m/s)

c.

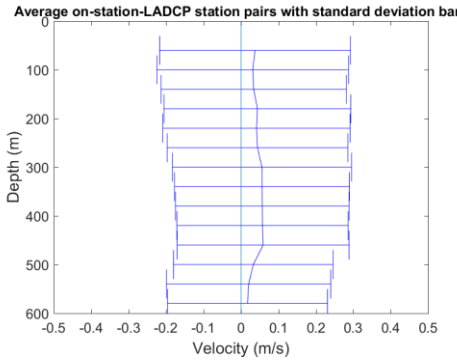
Average on-station-LADCP station pairs with standard deviation bars
Depth (m)
Velocity (m/s)

d.

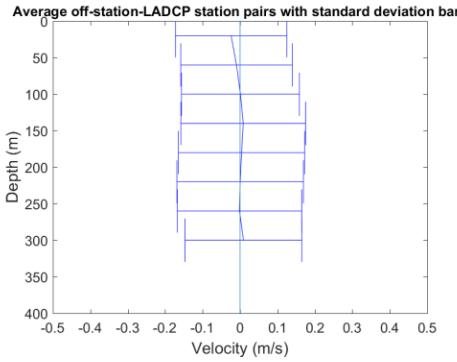
Average off-station-LADCP station pairs with standard deviation bars
Depth (m)
Velocity (m/s)

e.

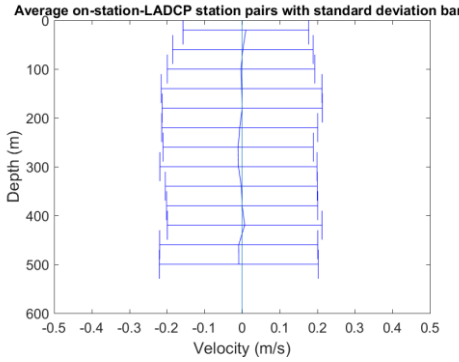
Average on-station-LADCP station pairs with standard deviation bars
Depth (m)
Velocity (m/s)

f.

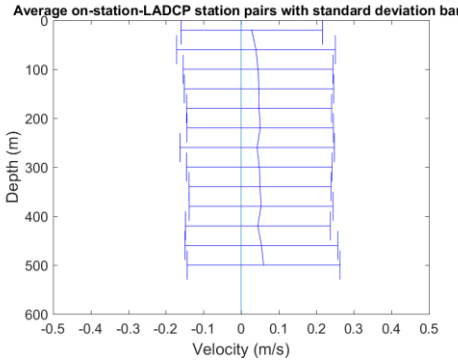
Average on-station-LADCP station pairs with standard deviation bars
Depth (m)
Velocity (m/s)

g.

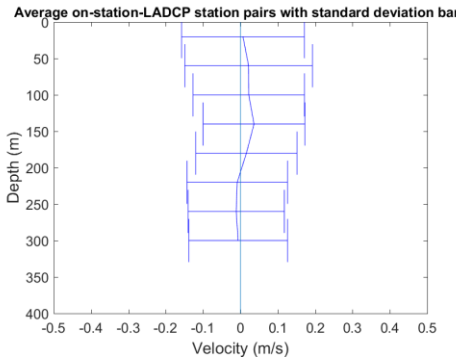
Average on-station-LADCP station pairs with standard deviation bars
Depth (m)
Velocity (m/s)

h.

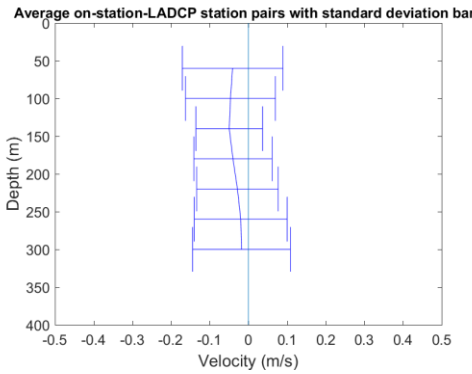
Average on-station-LADCP station pairs with standard deviation bars
Depth (m)
Velocity (m/s)

i.

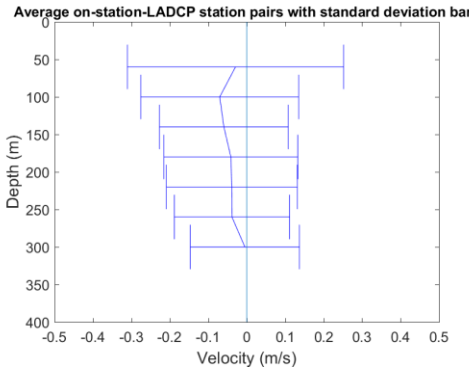


j.

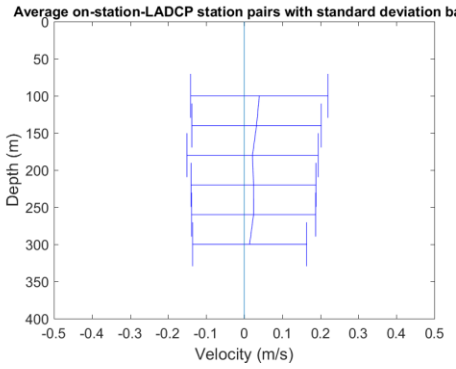


k.

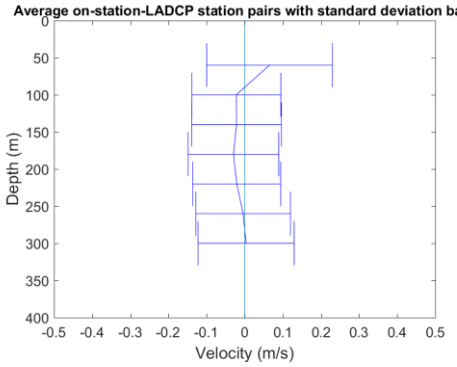


**Figure A.16** Average difference and standard deviation between the SADCP on-station and the LADCP station-pair velocity, across each cruise**. a.-k**. matches the cruise order in **Figure A.1.**

a.

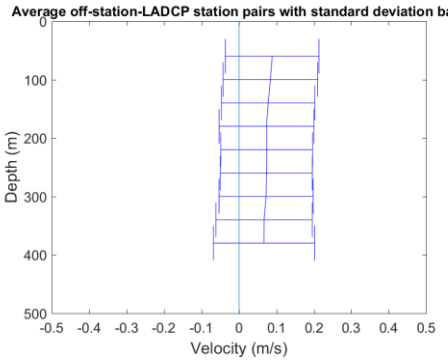
Average off-station-LADCP station pairs with standard deviation bars
Depth (m)
Velocity (m/s)

b.

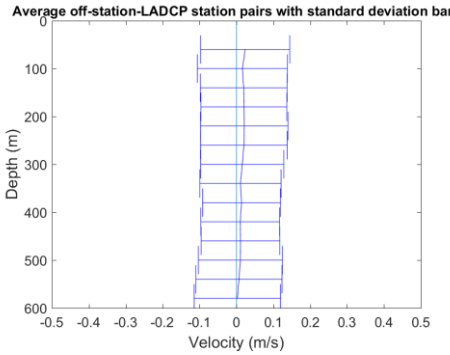
Average off-station-LADCP station pairs with standard deviation bars
Depth (m)
Velocity (m/s)

c.

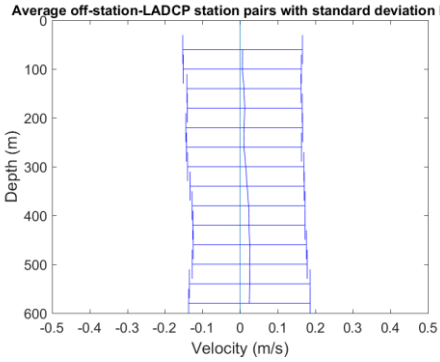
Average off-station-LADCP station pairs with standard deviation bars
Depth (m)
Velocity (m/s)

d.

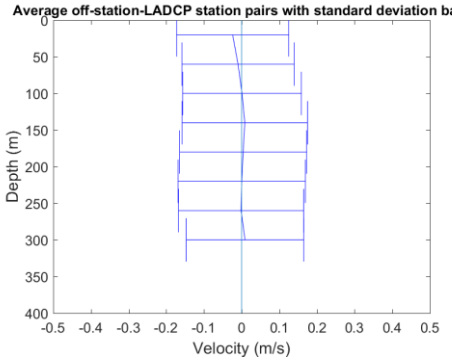
Average off-station-LADCP station pairs with standard deviation bars
Depth (m)
Velocity (m/s)

e.

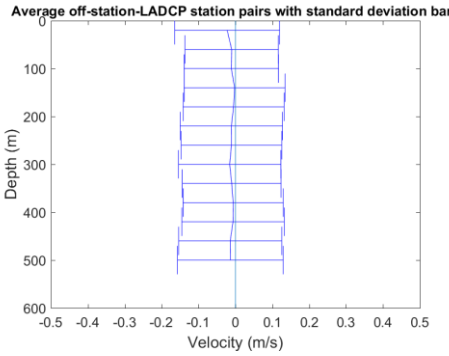
Average off-station-LADCP station pairs with standard deviation bars
Depth (m)
Velocity (m/s)

f.

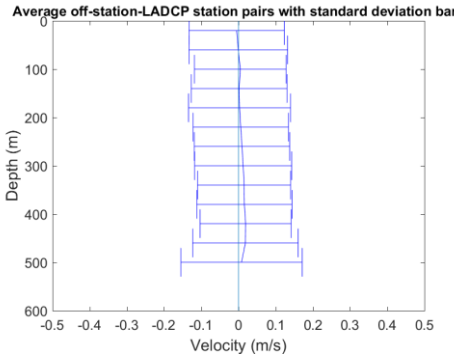
Average off-station-LADCP station pairs with standard deviation bars
Depth (m)
Velocity (m/s)

g.

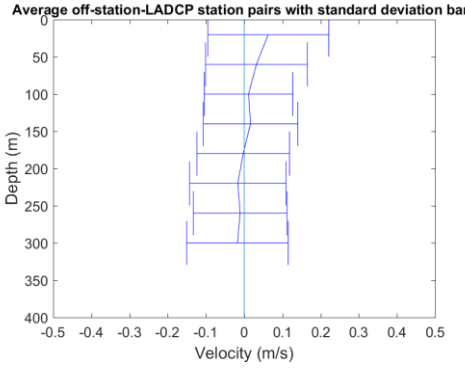
Average off-station-LADCP station pairs with standard deviation bar
Depth (m)
Velocity (m/s)

h.

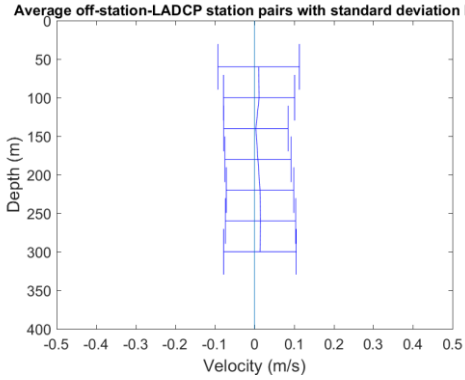
Average off-station-LADCP station pairs with standard deviation ba
Depth (m)
Velocity (m/s)

i. 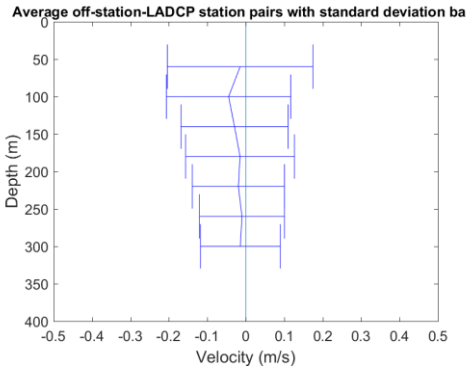


j. 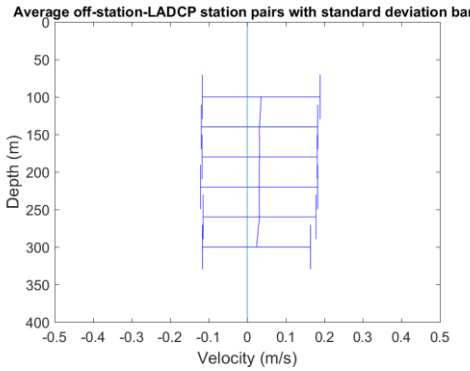


k. 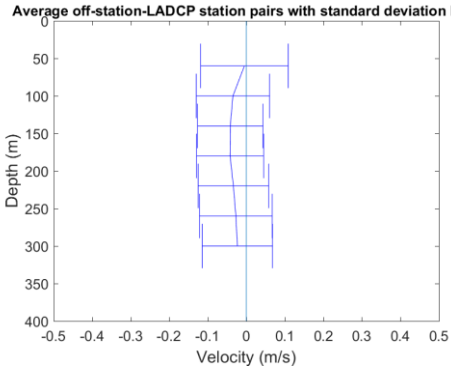


**Figure A.17** Average difference and standard deviation between the SADCP off-station and the LADCP station-pair velocity, across each cruise**. a.-k.** matches the cruise order in **Figure A.1.**

# References


Bacon, S. (1997) 'Circulation and Fluxes in the North Atlantic between Greenland and Ireland', *Journal of Physical Oceanography*, 27(7), pp. 1420–1435. doi: 10.1175/1520-0485(1997)027<1420:CAFITN>2.0.CO;2.

Bacon, S. *et al.* (2015) 'Arctic mass, freshwater and heat fluxes: methods and modelled seasonal variability', *Philosophical Transactions of the Royal Society A: Mathematical, Physical and Engineering Sciences*, 373(2052), p. 20140169. doi: 10.1098/rsta.2014.0169.

Balmaseda, M. A. *et al.* (2007) 'Historical reconstruction of the Atlantic Meridional Overturning Circulation from the ECMWF operational ocean reanalysis', *Geophysical Research Letters*, 34(23), p. n/a-n/a. doi: 10.1029/2007GL031645.

Berx, B. *et al.* (2013) 'Combining in-situ measurements and altimetry to estimate volume, heat and salt transport variability through the Faroe Shetland Channel', *Ocean Science Discussions*. Copernicus GmbH, 10(1), pp. 153–195. doi: 10.5194/osd-10-153-2013.

Booth, D. A. (1988) 'Horizontal dispersion in the northeast Atlantic', *Deep Sea Research Part A. Oceanographic Research Papers*, 35(12), pp. 1937–1951. doi: 10.1016/0198-0149(88)90118-5.

Booth, D. A. and Ellett, D. J. (1983) 'The Scottish continental slope current', *Continental Shelf Research*, 2(2–3), pp. 127–146. doi: 10.1016/0278-4343(83)90012-2.

Bower, A. S. *et al.* (2002) 'Directly measured mid-depth circulation in the northeastern North Atlantic Ocean.', *Nature*. Macmillian Magazines Ltd., 419(6907), pp. 603–7. doi: 10.1038/nature01078.

Bower, A. S. *et al.* (2009) 'Interior pathways of the North Atlantic meridional overturning circulation.', *Nature*. Macmillan Publishers Limited. All rights reserved, 459(7244), pp. 243–7. doi: 10.1038/nature07979.

Brambilla, E. and Talley, L. D. (2008) 'Subpolar Mode Water in the northeastern Atlantic: 1. Averaged properties and mean circulation', *Journal of Geophysical Research*, 113(C4), p. C04025. doi: 10.1029/2006JC004062.

Bryden, H. L. and Imawaki, S. (2001) 'Chapter 6.1 Ocean heat transport', *International Geophysics*. Academic Press, 77(C), pp. 455–474. doi: 10.1016/S0074-6142(01)80134-0.

Buckley, M. W. and Marshall, J. (2016) 'Observations, inferences, and mechanisms of the Atlantic Meridional Overturning Circulation: A review', *Reviews of Geophysics*. Wiley-Blackwell, 54(1), pp. 5–63. doi: 10.1002/2015RG000493.

Burrows, M., Thorpe, S. A. and Meldrum, D. T. (1999) 'Dispersion over the Hebridean and Shetland shelves and slopes', *Continental Shelf Research*, 19(1), pp. 49–55. doi: 10.1016/S0278-4343(98)00082-X.

Chafik, L., Rossby, T. and Schrum, C. (2014) 'On the spatial structure and temporal variability of poleward transport between Scotland and Greenland', *Journal of Geophysical Research: Oceans*, 119(2), pp. 824–841. doi: 10.1002/2013JC009287.

Chelton, D. B. *et al.* (1998) 'Geographical Variability of the First Baroclinic Rossby Radius of Deformation', *Journal of Physical Oceanography*, 28(3), pp. 433–460. doi: 10.1175/1520-

0485(1998)028<0433:GVOTFB>2.0.CO;2.

Childers, K. H., Flagg, C. N. and Rossby, T. (2014) 'Direct velocity observations of volume flux between Iceland and the Shetland Islands', *Journal of Geophysical Research: Oceans*, 119(9), pp. 5934–5944. doi: 10.1002/2014JC009946.

Cokelet, E. D., Schall, M. L. and Dougherty, D. M. (1996) 'ADCP-referenced geostrophic circulation in the Bering Sea Basin', *Journal of Physical Oceanography*, 26(7), pp. 1113–1128. Available at: http://journals.ametsoc.org/doi/pdf/10.1175/1520-0485(1996)026%3C1113:ARGCIT%3E2.0.CO;2.

Daniault, N. *et al.* (2016) 'The northern North Atlantic Ocean mean circulation in the early 21st Century', *Progress in Oceanography*. doi: 10.1016/j.pocean.2016.06.007.

Desbruyères, D., Mercier, H. and Thierry, V. (2014) 'On the mechanisms behind decadal heat content changes in the eastern subpolar gyre', *Progress in Oceanography*, 132, pp. 262–272. doi: 10.1016/j.pocean.2014.02.005.

Donohue, K. A., Firing, E. and Chen, S. (2001) 'Absolute geostrophic velocity within the Subantarctic Front in the Pacific Ocean', *Journal of Geophysical Research*, 106(C9), p. 19869. doi: 10.1029/2000JC000293.

Duchez, A. *et al.* (2016) 'Drivers of exceptionally cold North Atlantic Ocean temperatures and their link to the 2015 European heat wave', *Environmental Research Letters*. IOP Publishing, 11(7), p. 074004. doi: 10.1088/1748-9326/11/7/074004.

Dunstone, N. J., Smith, D. M. and Eade, R. (2011) 'Multi-year predictability of the tropical Atlantic atmosphere driven by the high latitude North Atlantic Ocean', *Geophysical Research Letters*. Wiley-Blackwell, 38(14), p. n/a-n/a. doi: 10.1029/2011GL047949.

Eden, C. and Willebrand, J. (2001) 'Mechanism of interannual to decadal variability of the North Atlantic circulation', *Journal of Climate*, 14(10), pp. 2266–2280.

Egbert, G. D., Bennett, A. F. and Foreman, M. G. G. (1994) 'TOPEX/POSEIDON tides estimated using a global inverse model', *Journal of Geophysical Research*, 99(C12), pp. 24821–24852. doi: doi:10.1029/94JC01894.

Egbert, G. D. and Erofeeva, S. Y. (2002) 'Efficient Inverse Modeling of Barotropic Ocean Tides', *Journal of Atmospheric and Oceanic Technology*, 19(2), pp. 183–204. doi: 10.1175/1520-0426(2002)0192.0.CO;2.

Ellett, D. J. (1978) 'Sub-surface temperatures at the Scottish continental slope', *Internal Report 2*, p. 17.

Ellett, D. J., Edwards, A. and Bowers, R. (1986) 'The hydrography of the Rockall Channel—an overview', *Proceedings of the Royal Society of Edinburgh. Section B. Biological Sciences*. Cambridge University Press, 88, pp. 61–81. Available at: http://journals.cambridge.org/abstract_S0269727000004474 (Accessed: 10 July 2015).

Ellett, D. J. and Martin, J. H. A. (1973) 'The physical and chemical oceanography of the Rockall channel', *Deep Sea Research and Oceanographic Abstracts*, 20(7), pp. 585–625. doi: 10.1016/0011-7471(73)90030-2.

Firing and Gordon, R., E. (1990) 'Deep ocean acoustic Doppler current profiling', *IEEE Fourth Working Conf. on Current Measurements*. Clinton, MD: IEEE, pp. 192–201. Available at:

http://dx.doi.org/.

Fischer, J. and Visbeck, M. (1993) 'Deep Velocity Profiling with Self-contained ADCPs', *Journal of Atmospheric and Oceanic Technology*, 10(5), pp. 764–773. doi: Fischer, Jürgen and Visbeck, Martin (1993) Deep Velocity Profiling with Self-contained ADCPs Journal of Atmospheric and Oceanic Technology, 10 (5). pp. 764-773. DOI 10.1175/1520-0426(1993)0102.0.CO;2 <http://dx.doi.org/10.1175/1520-0426(1993)0102.0.CO;2>.

Flatau, M. K., Talley, L. and Niiler, P. P. (2003) 'The North Atlantic Oscillation, Surface Current Velocities, and SST Changes in the Subpolar North Atlantic', *Journal of Climate*, 16(14), pp. 2355–2369. doi: 10.1175/2787.1.

Fofonoff, N. P. and Millard, R. C. (1983) 'Algorithms for computation of fundamental properties of seawater', *UNESCO Technical Papers in Marine Science = Documents techniques de l'Unesco sur les sciences de la mer*. Available at: http://www.vliz.be/en/imis?refid=7519 (Accessed: 23 November 2015).

Fratantoni, D. M. (2001) 'North Atlantic surface circulation during the 1990's observed with satellite-tracked drifters', *Journal of Geophysical Research*, 106(C10), p. 22067. doi: 10.1029/2000JC000730.

Gill, A. . (1982) *Atmosphere-Ocean Dynamics*. Academic Press.

Hall, M. M., Torres, D. J. and Yashayaev, I. (2013) 'Absolute velocity along the AR7W section in the Labrador Sea', *Deep Sea Research Part I: Oceanographic Research Papers*, 72(0), pp. 72–87. doi: http://dx.doi.org/10.1016/j.dsr.2012.11.005.

Halloran, P. R. *et al.* (2015) 'The mechanisms of North Atlantic CO2uptake in a large Earth System Model ensemble', *Biogeosciences*, 12(14), pp. 4497–4508. doi: 10.5194/bg-12-4497-2015.

Hansen, B. *et al.* (2003) 'The Iceland–Faroe inflow of Atlantic water to the Nordic Seas', *Progress in Oceanography*, 59(4), pp. 443–474. doi: 10.1016/j.pocean.2003.10.003.

Hansen, B. and Østerhus, S. (2000a) 'North Atlantic–Nordic Seas exchanges', *Progress in Oceanography*, 45(2), pp. 109–208. doi: 10.1016/S0079-6611(99)00052-X.

Hansen, B. and Østerhus, S. (2000b) 'North Atlantic–Nordic Seas exchanges', *Progress in Oceanography*. Pergamon, 45(2), pp. 109–208. doi: 10.1016/S0079-6611(99)00052-X.

Hansen, B. and Østerhus, S. (2007) 'Faroe Bank Channel overflow 1995–2005', *Progress in Oceanography*, 75(4), pp. 817–856. doi: 10.1016/j.pocean.2007.09.004.

Hirschi, J. *et al.* (2007) 'Reconstructing the Meridional Overturning Circulation from Boundary Densities and the Zonal Wind Stress', *Journal of Physical Oceanography*, 37(3), pp. 743–763. doi: 10.1175/JPO3019.1.

Holliday, N. *et al.* (2000) 'Water mass properties and fluxes in the Rockall Trough, 1975–1998', *Deep Sea Research Part I: Oceanographic Research Papers*, 47(7), pp. 1303–1332. doi: 10.1016/S0967-0637(99)00109-0.

Holliday, N. P. *et al.* (2015) 'Multidecadal variability of potential temperature, salinity, and transport in the eastern subpolar North Atlantic', *Journal of Geophysical Research: Oceans*, p. n/a-n/a. doi: 10.1002/2015JC010762.

Holliday, N. P. *et al.* (2018) 'Subpolar North Atlantic Overturning and Gyre-Scale Circulation in

the Summers of 2014 and 2016', *Journal of Geophysical Research: Oceans*. Wiley-Blackwell, 123(7), pp. 4538–4559. doi: 10.1029/2018JC013841.

Holliday, P. and Cunningham, S. (2013) 'The Extended Ellett Line: Discoveries from 65 years of marine observations west of the UK', *Oceanography*, 26(2), pp. 156–163.

Houpert, L. *et al.* (2018) 'Structure and Transport of the North Atlantic Current in the Eastern Subpolar Gyre from Sustained Glider Observations', *Journal of Geophysical Research: Oceans*. Wiley-Blackwell. doi: 10.1029/2018JC014162.

Howe, J. A., Stoker, M. S. and Woolfe, K. J. (2001) 'Deep-marine seabed erosion and gravel lags in the northwestern Rockall Trough, North Atlantic Ocean', *Journal of the Geological Society*. Geological Society, 158, pp. 427–438. Available at: http://cat.inist.fr/?aModele=afficheN&cpsidt=1102819 (Accessed: 18 March 2016).

Hughes, S. L. *et al.* (2006) *FLUXES OF ATLANTIC WATER (VOLUME, HEAT AND SALT) IN THE FAROE-SHETLAND CHANNEL CALCULATED FROM A DECADE OF ACOUSTIC DOPPLER CURRENT PROFILER DATA (1994-2005)*. Available at: http://www.gov.scot/Uploads/Documents/Coll0106.pdf (Accessed: 20 October 2015).

Huthnance, J. M. and Huthnance, J. M. (1984) 'Slope Currents and "JEBAR"', *Journal of Physical Oceanography*, 14(4), pp. 795–810. doi: 10.1175/1520-0485(1984)014<0795:SCA>2.0.CO;2.

Johnson, C. *et al.* (2010) 'Wyville Thomson Ridge Overflow Water: Spatial and temporal distribution in the Rockall Trough', *Deep Sea Research Part I: Oceanographic Research Papers*, 57(10), pp. 1153–1162. doi: 10.1016/j.dsr.2010.07.006.

Jónsson, S. and Briem, J. (2003) *Flow of Atlantic water west of Iceland and onto the north Icelandic shelf*, *ICES Marine Science Symposia*. Available at: http://www.ices.dk/sites/pub/Publication Reports/Marine Science Symposia/Phase 2/ICES Marine Science Symposia - Volume 219 - 2003 - Part 38 of 75.pdf (Accessed: 10 July 2015).

Kanzow, T. and Zenk, W. (2014) 'Structure and transport of the Iceland Scotland Overflow plume along the Reykjanes Ridge in the Iceland Basin', *Deep Sea Research Part I: Oceanographic Research Papers*, 86, pp. 82–93. doi: 10.1016/j.dsr.2013.11.003.

Käse, R. H. (2003) 'Structure and variability of the Denmark Strait Overflow: Model and observations', *Journal of Geophysical Research*, 108(C6), p. 3181. doi: 10.1029/2002JC001548.

Khatiwala, S. *et al.* (2013) 'Geoscientific Instrumentation Methods and Data Systems Global ocean storage of anthropogenic carbon', *Biogeosciences*, 10, pp. 2169–2191. doi: 10.5194/bg-10-2169-2013.

Knight, J. R., Folland, C. K. and Scaife, A. A. (2006) 'Climate impacts of the Atlantic Multidecadal Oscillation', *Geophysical Research Letters*. Wiley-Blackwell, 33(17), p. L17706. doi: 10.1029/2006GL026242.

Körtzinger, A. *et al.* (2008) 'The seasonal $p\,CO_2$ cycle at 49°N/16.5°W in the northeastern Atlantic Ocean and what it tells us about biological productivity', *Journal of Geophysical Research*. John Wiley & Sons, Ltd, 113(C4), p. C04020. doi: 10.1029/2007JC004347.

Lankhorst, M. and Zenk, W. (2006) 'Lagrangian Observations of the Middepth and Deep Velocity Fields of the Northeastern Atlantic Ocean', *Journal of Physical Oceanography*, 36(1), pp. 43–63. doi: 10.1175/JPO2869.1.

Lavender, K. L., Brechner Owens, W. and Davis, R. E. (2005) 'The mid-depth circulation of the subpolar North Atlantic Ocean as measured by subsurface floats', *Deep Sea Research Part I: Oceanographic Research Papers*, 52(5), pp. 767–785. doi: 10.1016/j.dsr.2004.12.007.

Lazier, J., Pickart, R. and Rhines, P. (2001) 'Chapter 5.5 Deep convection', *International Geophysics*. Academic Press, 77, pp. 387–400. doi: 10.1016/S0074-6142(01)80130-3.

Lherminier, P. *et al.* (2010) 'The Atlantic Meridional Overturning Circulation and the subpolar gyre observed at the A25-OVIDE section in June 2002 and 2004', *Deep Sea Research Part I: Oceanographic Research Papers*, 57(11), pp. 1374–1391. doi: 10.1016/j.dsr.2010.07.009.

Li, F. *et al.* (2017) 'Calculating the Meridional Volume, Heat, and Freshwater Transports from an Observing System in the Subpolar North Atlantic: Observing System Simulation Experiment', *Journal of Atmospheric and Oceanic Technology*, 34(7), pp. 1483–1500. doi: 10.1175/JTECH-D-16-0247.1.

Li, H. *et al.* (2016) 'Decadal predictions of the North Atlantic CO2uptake', *Nature Communications*. Nature Publishing Group, 7(1), p. 11076. doi: 10.1038/ncomms11076.

Lozier, M. *et al.* (2017) 'Overturning in the Subpolar North Atlantic Program: A New International Ocean Observing System', *Bulletin of the American Meteorological Society*, 98(4), pp. 737–752. doi: 10.1175/BAMS-D-16-0057.1.

Lozier, M. S. *et al.* (2019) 'A sea change in our view of overturning in the subpolar North Atlantic.', *Science (New York, N.Y.)*. American Association for the Advancement of Science, 363(6426), pp. 516–521. doi: 10.1126/science.aau6592.

Marsh, R. *et al.* (2017) 'Large-scale forcing of the European Slope Current and associated inflows to the North Sea', *Ocean Sci*, 13, pp. 315–335. doi: 10.5194/os-13-315-2017.

Mercier, H. *et al.* (2015) 'Variability of the meridional overturning circulation at the Greenland–Portugal OVIDE section from 1993 to 2010', *Progress in Oceanography*, 132, pp. 250–261. doi: 10.1016/j.pocean.2013.11.001.

Olsen, S. M. *et al.* (2008) 'Observed and modelled stability of overflow across the Greenland-Scotland ridge.', *Nature*. Nature Publishing Group, 455(7212), pp. 519–22. doi: 10.1038/nature07302.

Osinski, R. *et al.* (2003) 'ADCP-referenced geostrophic velocity and transport in the West Spitsbergen Current', *Oceanologia*, 45(3).

Østerhus, S. *et al.* (2005) 'Measured volume, heat, and salt fluxes from the Atlantic to the Arctic Mediterranean', *Geophysical Research Letters*. American Geophysical Union, 32(7), p. L07603. doi: 10.1029/2004GL022188.

Palter, J. B. and Lozier, M. S. (2008) 'On the source of Gulf Stream nutrients', *Journal of Geophysical Research: Oceans*. John Wiley & Sons, Ltd, 113(6), p. C06018. doi: 10.1029/2007JC004611.

Pérez, F. F. *et al.* (2013) 'Atlantic Ocean CO2 uptake reduced by weakening of the meridional overturning circulation', *Nature Geoscience*. Nature Research, 6(2), pp. 146–152. doi: 10.1038/ngeo1680.

Pollard, R. T. (2004) 'Water masses and circulation pathways through the Iceland Basin during Vivaldi 1996', *Journal of Geophysical Research*, 109(C4), p. C04004. doi:

10.1029/2003JC002067.

Pujol, M.-I. *et al.* (2016) 'DUACS DT2014: the new multi-mission altimeter data set reprocessed over 20 years', *Ocean Sci*, 12, pp. 1067–1090. doi: 10.5194/os-12-1067-2016.

Raj, R. P. *et al.* (2018) 'Quantifying Atlantic Water transport to the Nordic Seas by remote sensing', *Remote Sensing of Environment*, 5 May. doi: 10.1016/j.rse.2018.04.055.

Read, J. . (2001) 'CONVEX-91: water masses and circulation of the Northeast Atlantic subpolar gyre', *Progress in Oceanography*, 48(4), pp. 461–510. doi: 10.1016/S0079-6611(01)00011-8.

Reverdin, G. (2003) 'North Atlantic Ocean surface currents', *Journal of Geophysical Research*, 108(C1), p. 3002. doi: 10.1029/2001JC001020.

Robson, J. *et al.* (2014) 'Atlantic overturning in decline?', *Nature Geoscience*. Nature Publishing Group, 7(1), pp. 2–3. doi: 10.1038/ngeo2050.

Rosón, G. (2003) 'Carbon distribution, fluxes, and budgets in the subtropical North Atlantic Ocean (24.5°N)', *Journal of Geophysical Research*. John Wiley & Sons, Ltd, 108(C5), p. 3144. doi: 10.1029/1999JC000047.

Rossby, T. *et al.* (2017) 'A direct estimate of poleward volume, heat, and freshwater fluxes at 59.5°N between Greenland and Scotland', *Journal of Geophysical Research: Oceans*, 122(7), pp. 5870–5887. doi: 10.1002/2017JC012835.

Rossby, T. *et al.* (2018) 'A Direct Estimate of Volume, Heat, and Freshwater Exchange Across the Greenland-Iceland-Faroe-Scotland Ridge', *Journal of Geophysical Research: Oceans*. Wiley-Blackwell. doi: 10.1029/2018JC014250.

Rossby, T. and Flagg, C. N. (2012) 'Direct measurement of volume flux in the Faroe-Shetland Channel and over the Iceland-Faroe Ridge', *Geophysical Research Letters*, 39(7), p. n/a-n/a. doi: 10.1029/2012GL051269.

Sabine, C. L. *et al.* (2004) *The Oceanic Sink for Anthropogenic CO 2*. Available at: www.sciencemag.org (Accessed: 14 January 2019).

Sarafanov, A. *et al.* (2012) 'Mean full-depth summer circulation and transports at the northern periphery of the Atlantic Ocean in the 2000s', *Journal of Geophysical Research*, 117(C1), p. C01014. doi: 10.1029/2011JC007572.

Saunders, P. M. (1996) 'The Flux of Dense Cold Overflow Water Southeast of Iceland', *Journal of Physical Oceanography*, 26(1), pp. 85–95. doi: 10.1175/1520-0485(1996)026<0085:TFODCO>2.0.CO;2.

Serreze, M. C., Holland, M. M. and Stroeve, J. (2007) 'Perspectives on the Arctic's shrinking sea-ice cover.', *Science (New York, N.Y.)*. American Association for the Advancement of Science, 315(5818), pp. 1533–6. doi: 10.1126/science.1139426.

Smith, D. M. *et al.* (2010) 'Skilful multi-year predictions of Atlantic hurricane frequency', *Nature Geoscience*. Nature Publishing Group, 3(12), pp. 846–849. doi: 10.1038/ngeo1004.

Straneo, F. *et al.* (2010) 'Rapid circulation of warm subtropical waters in a major glacial fjord in East Greenland', *Nature Geoscience*. Nature Publishing Group, 3(3), pp. 182–186. doi: 10.1038/ngeo764.

Sutton, R. T. and Hodson, D. L. R. (2005) 'Atlantic Ocean forcing of North American and

European summer climate.', *Science (New York, N.Y.)*. American Association for the Advancement of Science, 309(5731), pp. 115–8. doi: 10.1126/science.1109496.

Talley, L. D. (2008) 'Freshwater transport estimates and the global overturning circulation: Shallow, deep and throughflow components', *Progress in Oceanography*, 78(4), pp. 257–303. doi: 10.1016/j.pocean.2008.05.001.

Thurnherr, A. M. (2010) 'A practical assessment of the errors associated with full-depth LADCP profiles obtained using Teledyne RDI Workhorse acoustic Doppler current profilers', *Journal of Atmospheric and Oceanic Technology*, 27(7), pp. 1215–1227.

Turrell, W. R. *et al.* (2003) *Hydrographic variability during the decade of the 1990s in the Northeast Atlantic and southern Norwegian Sea*, *ICES Marine Science Symposia*. Available at: http://www.ices.dk/sites/pub/Publication Reports/Marine Science Symposia/Phase 2/ICES Marine Science Symposia - Volume 219 - 2003 - Part 15 of 75.pdf (Accessed: 10 July 2015).

Visbeck, M. (2002) 'Deep Velocity Profiling Using Lowered Acoustic Doppler Current Profilers: Bottom Track and Inverse Solutions*', *Journal of Atmospheric and Oceanic Technology*, 19(5), pp. 794–807.

Williams, R. G. *et al.* (2014) 'Decadal evolution of ocean thermal anomalies in the North Atlantic: The effects of Ekman, overturning, and horizontal transport', *Journal of Climate*, 27(2), pp. 698–719.

Williams, R. G. *et al.* (2015) 'Mechanisms of Heat Content and Thermocline Change in the Subtropical and Subpolar North Atlantic', *Journal of Climate*, 28(24), pp. 9803–9815. doi: 10.1175/JCLI-D-15-0097.1.

Willis, J. K. and Fu, L.-L. (2008) 'Combining altimeter and subsurface float data to estimate the time-averaged circulation in the upper ocean', *Journal of Geophysical Research*, 113(C12), p. C12017. doi: 10.1029/2007JC004690.

Xu, W. *et al.* (2015) 'Seasonality and interannual variability of the European Slope Current from 20years of altimeter data compared with in situ measurements', *Remote Sensing of Environment*, 162, pp. 196–207. doi: 10.1016/j.rse.2015.02.008.

Xu, X., Rhines, P. B. and Chassignet, E. P. (2016) 'Temperature–Salinity Structure of the North Atlantic Circulation and Associated Heat and Freshwater Transports', *Journal of Climate*, 29(21), pp. 7723–7742. doi: 10.1175/JCLI-D-15-0798.1.

Zhang, R. and Delworth, T. L. (2006) 'Impact of Atlantic multidecadal oscillations on India/Sahel rainfall and Atlantic hurricanes', *Geophysical Research Letters*. Wiley-Blackwell, 33(17), p. L17712. doi: 10.1029/2006GL026267.